Practical Millimetre wave Material Characterisation

By

AINOR KHALIAH BINTI MOHD ISA

Department of Electrical and Electronics
UNIVERSITY OF BRISTOL

A dissertation submitted to the University of Bristol in accordance with the requirements of the degree of DOCTOR OF PHILOSOPHY in the Faculty of Engineering.

JANUARY 2020

Abstract

The rapid growth of the RF spectrum for mobile communication creating a challenge to ensure excellent wireless link quality for high data rate. Therefore, the understanding and modelling of the propagation mechanisms in the environment (including reflection and diffraction) are crucial. Propagation mechanism at higher frequency becomes an issue, due to the short wavelength, features of material cause increased scatter, high propagation loss, directivity and sensitivity to blockage. As such, just knowing the composition of the material may be insufficient to understand the propagation mechanism of any signal incident on that surface, and hence the surface roughness itself may become the more dominant feature.

This thesis mainly focuses on measurement methodologies, calibration and analysis for materials in the range 20GHz to 60GHz and uses small samples (typically around 40cmx40cm) for the extraction of the pertinent material characteristics. Here two practical methods are considered. Sample materials include metal, concrete, wood and ceramic tiles.

The first method uses a transverse measurement technique to identify the diffraction and attenuation of samples. This initial study considered propagation through materials, but it was apparent at an early stage that this is not possible to study material attenuation without an excellent knowledge of the reflection properties of materials. Hence the thesis subsequently concentrates on wideband reflective properties. The transverse measurements helped to yield reflection levels to normal incident signals but do not suitably identify diffuse scatter. The second method considers the angular signal spread with the goal to determine the level of surface reflection and scattering with the different incident signal angle of arrival. Measurements both in an anechoic chamber (5m range at 20GHz) and a shorter range (1m for 60GHz) were performed. Results are able to clearly identify the level of reflectivity and also a good indication of the extent of material scatter.

The thesis also includes indoor propagation measurements as a means of determining the more significant effects when considering propagation between transmitter and receiver. This leads to a discussion of what features (material type, size and construction) may be most useful in inclusion in EM propagation modelling. The measurement methodologies and results presented in this thesis provide a useful guideline to extract material properties but also provide insight as to the level of 'EM details' required for deterministic propagation models at millimetre wave.

Allah have blessed me with a wonderful family
to whom this thesis is dedicated
To my lovely daughter, Alma and my mum, Maimun
and to my late husband, Mahathir
who passed away on 28th May 2017 while I was finishing this thesis
May He Rest In Peace

ACKNOWLEDGMENTS

I would like to express my deepest gratitude to my supervisors Professor Andy Nix and Dr Geoff Hilton for their tremendous knowledge, guidance, encouragement, trust, patience and enthusiasm throughout my journey as PhD student. Their invaluable advice and support have helped shape this thesis and help me become not only a better researcher but a better person, and their passion for research will undoubtedly continue to inspire my career in education.

I would also like to thank the Universiti Kuala Lumpur (UniKL BMI) and Majlis Amanah Rakyat (MARA) of Malaysia for sponsoring this PhD work. I am truly grateful for providing me with this opportunity and financial support throughout my year in Bristol.

I am also thankful to my wonderful friends and colleagues who made my life here an unforgettable experience. Few names worth mentioning are Dr Gaith Al-Juboori, Dr Fatemah Alsewaidi, Dr Amani Alheid, Dr Mohammad Abdullah, Dr Reham amongst others. Furthermore, I am truly grateful to all of my Malaysian friends, who are too many to be named here, for making my stay in Bristol one of the most joyful and exciting periods of my life and help when I am in need. Special thanks to "gengkopibin" beautiful ladies that keep pushing me.

Last but not least, I would like to sincerely thank my late husband Mahathir bin Abdul Rahim, the love of my life, for his never-ending patience and support for all these years. Loves to my only daughter Alma Muzfirah who has kept me going through the worst of times. To my mother and mother in law due to their continuous doa and prayers for my success. Not forgetting my family and in-laws for their advice and support. Without them, the completion of this thesis would not have been possible.

AUTHOR'S DECLARATION

I declare that the work in this dissertation was carried out in accordance with the requirements of the University's Regulations and Code of Practice for Research Degree Programmes and that it has not been submitted for any other academic award. Except where indicated by specific reference in the text, the work is the candidate's own work. Work done in collaboration with, or with the assistance of, others, is indicated as such. Any views expressed in the dissertation are those of the author.

SIGNED: DATE: 23RD JANUARY 2020

TABLE OF CONTENTS

Page

List of Figures **xiii**

List of Tables **xvii**

List of Symbols **xix**

List of Abbreviations **xxi**

1 Introduction **1**

1.1 Overview and Motivation 2
1.2 Challenges and Contribution 5
1.3 Structure of the thesis 7
1.4 List of Publications 8

2 Review of RF Propagation Measurements Studies at K-band and Millimetre wave Frequency **9**

2.1 Review of Propagation Mechanism Measurement Setups 10
2.2 Fixed Position of Transmitter AND Receiver 11
2.2.1 Direct Line of Sight (LoS) and Penetration Investigation 11
2.2.2 Diffraction Analysis 13
2.3 Movable Positions of Transmitter OR/AND Receiver 15
2.3.1 Diffraction Mechanism; The Angular Setup Analysis 15
2.3.2 Reflection from Surfaces 16
2.4 Indoor Azimuth and Elevation Scan 19
2.4.1 Channel measurement campaign at 28GHz 19
2.4.2 Channel measurement campaign at 60GHz 21
2.4.3 Propagation modelling at millimetre wave 22
2.5 Summary and Future Challenges 23

3 A study of transverse propagation and material characterisation measurements 25
3.1 Transverse Measurement Setup for Diffraction Analysis 26
3.1.1 Procedure of measurement and data collections 27
3.1.2 Knife Edge Diffraction (KED) 29
3.2 Material Characterisation Based on Diffraction and Attenuation Propagation Analysis 32
3.2.1 Material under Test (MUT) 32
3.2.2 Received Signals and Regions Identification 33
3.2.3 Material comparison 36
3.3 Reflection model: a single port model 39
3.3.1 Model validation to analyse the measurement results 44
3.4 Transverse Wideband Measurement for Surface Reflection Analysis 46
3.4.1 Procedure of Measurement and Data Collections 46
3.4.2 Results and Discussions 49
3.5 Conclusion 58

4 Angular Based Measurement for Material Scatter Characterisation 61
4.1 Angular Measurement Setup: Reflection and Material Properties Analysis 63
4.1.1 The measurement setup 64
4.1.2 Metal plate as calibrated reference 66
4.1.3 Material comparison 72
4.2 Short Range Angular Measurement 76
4.2.1 Material comparison in short-range measurement 77
4.2.2 Metal Plate Size Comparison 80
4.2.3 60GHz Material Comparison in Short-Range Measurement 85
4.3 Conclusion 89

5 Indoor Scanning; Objects Identification and Propagation Mechanism 91
5.1 Radar Cross Section of Material 93
5.1.1 Theoretical validation with Radar Cross Section 94
5.2 Object identifications measurement 96
5.2.1 Measurement setup 96
5.2.2 Object Identification: Metal pole 97
5.2.3 Object identifications analysis; various object classification 101
5.2.4 Beamwidth refinement 103

5.2.5 Outside Anechoic Chamber 106
5.3 Indoor Laboratory Environment Measurements 109
5.3.1 AoA Measurement Results for the Laboratory Environment 111
5.4 Conclusion 116

6 Conclusion and Future Works **119**
6.1 Thesis overview 119
6.2 Material Characteristic 121
6.3 Future Works 123

A Appendix A: Antenna Radiation Patterns **125**

B Appendix B: 3D Indoor Laboratory Plots **127**

Bibliography **129**

List of Figures

Figure **Page**

1.1 Propagation Mechanism 2
1.2 Specular and Diffuse Reflection 4
1.3 Propagation Model: Ray Tracing 5
1.4 Small sample versus larger sample propagation 6

2.1 Fixed Tx AND Rx: Transmission Measurement Setup 11
2.2 Movable Tx OR Rx: Corner Measurement Setup 15
2.3 Movable Tx OR Rx: Arc Measurement Setup 16

3.1 Transverse Measurement setup 27
3.2 Photo of Transverse Measurement setup 28
3.3 The path geometry of Knife Edge Diffraction (KED) 29
3.4 Diffraction Gain, Gd of material 31
3.5 Material under test (MUT) 32
3.6 Signals and regions identification 33
3.7 Regions Identification with concrete as MUT at 45GHz 35
3.8 Transmission measurement at 45GHz 36
3.9 Material versus KED at 45GHz 37
3.10 Transmission between 2 materials 39
3.11 Schematic diagram for model development 40
3.12 Signal flow graph for one-port network analysis 41
3.13 Network analysis up to Face 1 (assuming no internal material reflections) . . 42
3.14 Signals flow graph derivation 43
3.15 Final diagram to solve the SFG 43
3.16 Linear positioner with platform to hold MUT 46
3.17 Additional samples (MUT) 47
3.18 Photos of Different Types of Concrete Surfaces 48

3.19 Metal plate at centre frequency 55GHz 49
3.20 Concrete Surface Comparison at centre frequency 55GHz 50
3.21 Tiles at centre frequency 55GHz 51
3.22 M11 of materials at centre frequency 55GHz 53
3.23 Metalplate at wide frequency of 45GHz to 65GHz 54
3.24 Concrete (smooth surface) at wide frequency of 45GHz to 65GHz 54
3.25 Concrete (rough surface) at wide frequency of 45GHz to 65GHz 55
3.26 Tiles at wide frequency of 45GHz to 65GHz 56
3.27 3D plots of M11: Materials at wide frequency of 45GHz to 65GHz 57

4.1 Measurement setup in anechoic chamber 63
4.2 Schematic diagram of reflections and direct transmission path between transmitter and receiver (diagram not to scale) 64
4.3 Three setup positions of angular measurement as seen from the receiver . . . 65
4.4 Schematic diagram of fixing the sample and moving the transmit and receive antennas in all incident angles (diagram not to scale) 66
4.5 Chamber measurement: Metal plate frequency comparison (raw data) 68
4.6 Calibration Process 69
4.7 Metal plate frequency comparison (normalised data) 70
4.8 Chamber measurement: Material comparison at 20GHz (raw data) 72
4.9 Chamber Measurement: Material reflectivity at 20GHz (normalised data) . . 73
4.10 Chamber Measurement: Material comparison at 20GHz (normalised data) . . 74
4.11 Short range measurement setup 76
4.12 Short range measurement: Material comparison at 20GHz (raw data) 78
4.13 Short Range Measurement: Material reflectivity at 20GHz (normalised data) 78
4.14 Short Range Measurement: Material comparison at 20GHz (normalised data) 79
4.15 Short range measurement: Metal size comparison at 20GHz (raw data) 81
4.16 Short Range Measurement: Metal size comparison at 20GHz (normalised data) 82
4.17 Short range measurement: Metal shape comparison at 20GHz (raw data) . . 83
4.18 Short Range Measurement: Metal shape comparison at 20GHz (normalised data) 84
4.19 Short range measurement: Material comparison at 60GHz (raw data) 85
4.20 Short Range Measurement: Material Reflectivity at 60GHz (normalised data) 86
4.21 Short Range Measurement: Material comparison at 60GHz (normalised data) 87

5.1 Chamber 96

5.2 The skirt dipole antenna . . . 97
5.3 Three configurations of the metal pole in the anechoic chamber . . . 98
5.4 Metal pole as reference . . . 99
5.5 Two metal poles configuration . . . 99
5.6 Two metal poles (0.45m apart) . . . 100
5.7 Azimuth scans at 22GHz for the four reflective materials . . . 102
5.8 All 3 configurations at 22GHz: beam refinement . . . 104
5.9 Circular metal sheet with different angle of configuration . . . 105
5.10 Polar plot of circular metal sheet with different angle configuration at 22GHz 105
5.11 Dipole antenna configurations . . . 106
5.12 Dipole at position A for both configurations at 22GHz . . . 107
5.13 Dipole at position B for both configurations at 22GHz . . . 108
5.14 Layout of the laboratory and adjacent office space . . . 110
5.15 3D: Location 4 . . . 111
5.16 Location 4 . . . 112
5.17 3D: Location 5 . . . 112
5.18 Location 5 . . . 113
5.19 3D: Location 6 . . . 114
5.20 Location 6 . . . 114

A.1 Radiation pattern of rectangular horn antenna at 22GHz . . . 125
A.2 Radiation pattern of circularly polarised antenna at 22GHz . . . 126
A.3 Radiation pattern of dipole antenna at 22GHz . . . 126

B.1 3D: Location 1 . . . 127
B.2 3D: Location 2 . . . 128
B.3 3D: Location 3 . . . 128

List of Tables

Table		Page
2.1	Categories of Propagation Measurement Setup	10
2.2	Summary of attenuation/penetration loss (dB) at 28GHz, 38GHz and 40GHz	13
2.3	Summary of Comparison of reflectivity for different material at 28GHz as reported in [1]	17
3.1	Material under test (MUT)	32
3.2	Parameters of the model	41
3.3	Material under test (MUT)	47
3.4	Edge detection and length estimation of sample material at centre frequency 55GHz	52
3.5	Average M11 of materials at centre frequency 55GHz	53
4.1	Material Reflectivity Level at 20GHz	74
4.2	Chamber Measurement at 20GHz: Average diffraction/diffuse scatter level of materials	75
4.3	Material under test (MUT)	77
4.4	Short Range Measurement: Material Reflectivity Level at 20GHz	79
4.5	Short range measurement: Average diffraction/diffuse scatter level of materials at 20GHz	80
4.6	Various sizes of metal plate	81
4.7	Short range measurement: Material Reflectivity Level at 60GHz	86
4.8	Short Range Measurement: Average diffraction/diffuse scatter level of materials at 60GHz	87
5.1	Radar Cross Section (RCS) of simple target object [2]	94
5.2	Metal poles Gain, Gs and RCS, σ	100
5.3	List of objects for identification measurement	101

5.4 Object Gain, Gs and RCS, σ 102
5.5 Metal poles Gain, Gs and RCS, σ 103
5.6 Measurement in the laboratory configurations 110
5.7 Summary of propagation mechanism involved 115

List of Symbols

λ	wavelength
R	distance between the transmit and the receive antenna
f	frequency
d1	distance between transmitter to MUT
d2	distance between MUT to receiver
ds	thickness of MUT
τ	reflection coefficient
h	effective height
Δ	path difference
Gd	diffraction gain
v	Fresnel diffraction parameter
Ei	incident field
Et	transmitted field

List of Abbreviations

5G	5th Generation
AoA	Angle of Arrival
AoD	Angle of departure
CSN	Communication and System Network
DoA	Direction of Arrival
EM	Electromagnetic Wave
FSL	Free Space Loss
H	Horizontal
HPBW	Half Power BeamWidth
LoS	Line of Sight
KED	Knife edge diffraction
NA	Not available
NLoS	Non Line of Sight
RCS	Radar Cross Section
RF	Radio Frequency
RT	Ray Tracing
Rx	Receiver
SGH	Standard Gain Horn
SNR	Signal to Noise Ratio
Tx	Transmitter
UTD	Uniform theory of diffraction
V	Vertical
VNA	Vector Network Analyser

CHAPTER 1

INTRODUCTION

With the ever-increasing expansion of the RF spectrum for mobile communications systems (i.e. 5G) and the need to ensure an excellent wireless link quality for high data rate, the understanding and modelling of the propagation mechanisms in the environment (including reflection and diffraction) is essential. While at lower frequencies, sub 6GHz, these are relatively-well understood, this becomes more of a challenge at millimetre wave frequencies where, due to the short wavelength, features of, say, walls cause increased scatter.

As such, just knowing the composition of the material (glass, brick, concrete) may be insufficient to understand the propagation mechanism (angle of departure and polarisation) of any signal incident on that surface, and hence the surface roughness itself may become the more dominant feature. Therefore, in order to insert material characteristics into EM propagation modelling tools (i.e. ray tracing) not only the conductivity/permittivity/permeability of the 'smooth' material needs to be known, but its scattering properties.

This significant interest means determining the material characterisation with respect to reflection (specular and diffuse scatter), diffraction and attenuation to insert the data into propagation modelling are being considered in this research.

1.1 Overview and Motivation

Propagation Mechanisms

The same physics governs millimetre waves as for all the radio spectrum. Therefore, they have limitations related to their wavelength. The shorter the wavelength as the frequency increases, the higher the path loss (for given antennas gains) and probably higher material attenuation loss, the propagation mechanisms are greatly different from those the sub-6 GHz, therefore have to be particularly studied and modelled to describe the millimetre wave channel.

K band that lies between 18GHz to 27GHz and millimetre wave in the range of 28GHz to 60GHz will be the main frequency of operations that will be reviewed. In these frequency range, wavelength of 16mm to 5mm will be the major concern for material characterisation. How large the material sample or obstacle and how far the transmitter to the receiver with respect to the material target will be the focal point. Furthermore, the millimetre wave communication system will be primarily employed in hot spots (short range indoor environment) instead of longer-range coverage in outdoor scenarios.

Radio propagation is the technique of how radio waves travel or propagate (transmitted from one point to another) and affected by the medium travelled. The main mechanisms behind the radio wave propagation can be categories as: Line of Sight (LoS) and multipath due to reflection, diffraction and attenuation as shown in Figure 1.1.

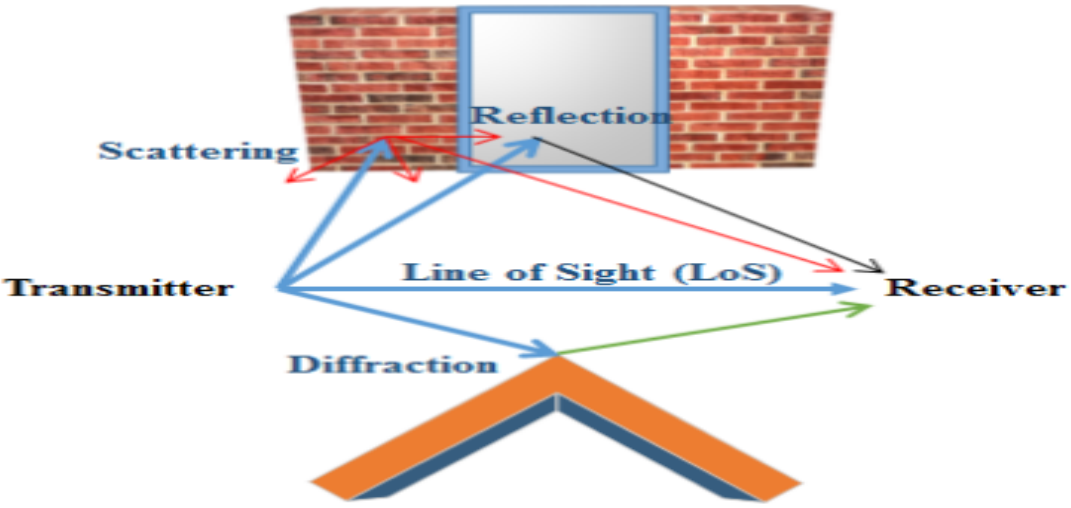

FIGURE 1.1. Propagation Mechanism

Many factors affect how the radio signals or radio waves propagate. These are define

by the medium through which the radio waves travel and the various objects that may present along the path. The level and quality of the received signal are depending on the properties of the path of which the radio signals propagated.

Several different types of radio propagation are used in practical radio transmission systems. The **line of sight propagation** indicates the state of radio waves as it travels from the transmitter to the receiver in a straight line without any obstruction. For this line of sight propagation, the free space loss (FSL) is given by Equation 1.1:

$$L_{FSL} = (\frac{4\pi R}{\lambda})^2 \tag{1.1}$$

where R is the distance between the transmit and the receive antennas, and λ is the operating wavelength.

and in dB, the equation becomes:

$$L_{FSL}[dB] = 92.4 + 20logf + 20logR \tag{1.2}$$

where f is the frequency in GHz and R is the line-of-sight (LOS) range between antennas in kilometres.

When including the multipath propagation, this term in Equation 1.2 is often modified to take the effect of other losses into account. This multipath components come from reflection, diffraction and attenuation either in indoor or outdoor environments.

The **reflection** of a wave is a process by which a wave hits an object and bounces off it. For radio wave, reflection defines an electromagnetic wave hits upon an object which has very large dimensions when compared to the wavelength [3]. When a signal is reflected there is usually some loss of the signal, either through absorption or as a result of some of the signal penetrates into the medium. There are many factors that influence the attenuation of the signal strength of the reflected wave; such as wavelength (frequency) of the wave, incident and reflected angle and the characteristics of the object, including its material properties, thickness, surface roughness, etc.

There are two general types of reflection: specular and diffuse, as shown in Figure 1.2 . A specular reflection, such as what you see in a mirror or a polished surface, occurs when wave is reflected away from the surface at the same angle as the incoming wave,Äôs angle. A diffuse reflection, sometimes called Lambertian scattering or diffusion, occurs when a rough surface reflects the wave at many different angles. These signals are generated because of gaps and sharp changes in the surface for example a wall of a building that have windows, balconies, brick or stone decorations or beams.

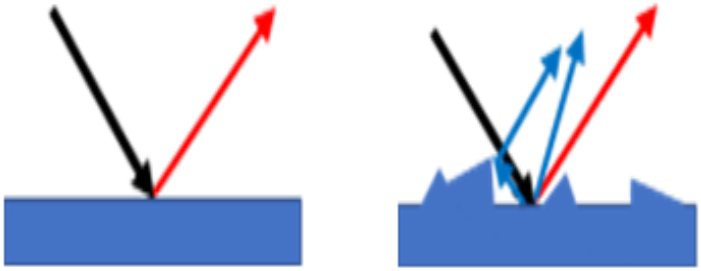

(a) Specular reflection (b) Diffuse reflection

Figure 1.2: Specular and Diffuse Reflection

Diffraction occurs when a radio wave travels meets an obstacle, it tends to bend around the obstacle. The bending or change in direction makes it possible to receive energy around the edges of an obstacle [4]. At millimetre wave frequency, diffraction has a small effect on the received power compared to direct LoS, reflected or scattered wave, however in [5] diffraction was reported to be significant propagation mechanism in non-line-of-sight (NLOS) environments.

Consequently, a radio signal may be received behind the obstacle even if it is impenetrable. At frequencies up to a few GHz, it is significant to consider diffraction for outdoor propagation to predict the field strength accurately since the diffracted field around objects and building edges can contribute substantially to the total received power.

Propagation Modelling

In order to fully understand the radio propagation characteristics in higher frequency band, it is necessary to develop its particular channel model. At millimetre wave frequency, a detail propagation modelling is a crucial in order to design an adequate communications system operating at this frequency band [6]. The propagation modelling can be characterise as Figure 1.3.

Ray-Tracing (RT) techniques [7, 8] are best method for characterising deterministic models. RT is generally carried out using an independent software package to simulate the proper channel scenario, where all environmental/scenarios features and parameters are known and stored in the system. Ray tracing models are really useful when there are no measurements available for a specific environment, this is an added advantage and reduce the cost of measurement. At millimetre wave frequencies, several studies involved the ray tracing model [6, 9, 10] are use to predict the propagation behaviour of the channel in various scenarios. The disadvantage of the ray tracing software is that it does not always include all of the relevant propagation mechanisms, such as

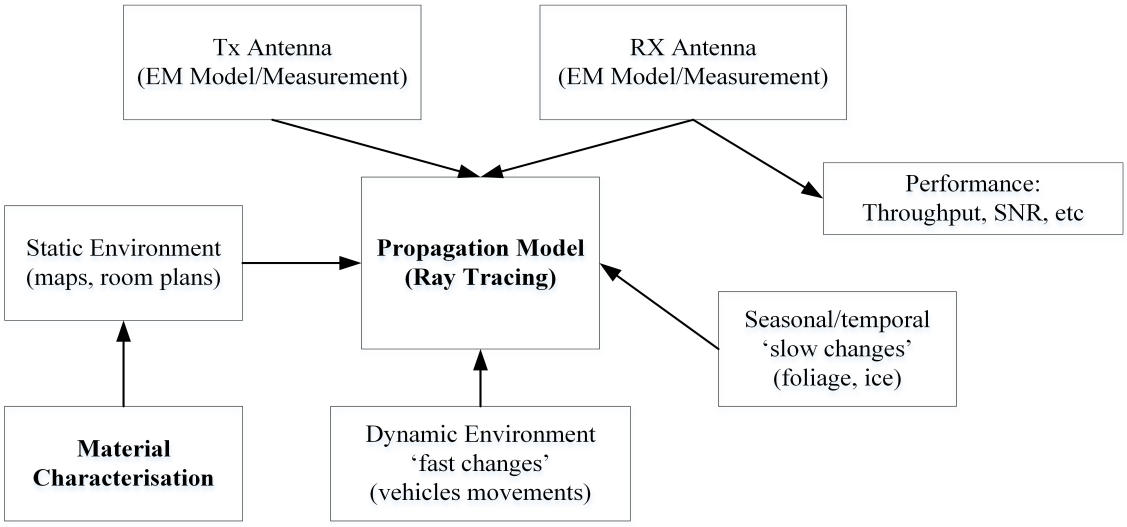

FIGURE 1.3. Propagation Model: Ray Tracing

non-specular scattering effects and this leads to the geometry data-base errors. However, [11–13] have been successfully used ray tracing to model wireless radio propagation. .

One of important input towards the building a propagation model is a material characterisation that contributes to the static environment parameters. A review on the electromagnetic characterisation of building materials at microwave and millimetre wave frequencies was presented in [14]. The hypothesis was the building material should produce the permittivity values which are frequency dependent, and conductivity is indirectly related to the absolute value of the material permittivity as it only affects its imaginary part (complex values). The complex permittivity of a material, its thickness and surface roughness, polarisation and incident angle, determine the total amount of energy that is reflected or transmitted through the material. Characterisation of building material has been done quite a lot over a range of frequencies [15–18]. Practical predictions of the channel properties/parameters require the measurement of angle-dependent reflection coefficients for common building material over a wide frequency range.

1.2 Challenges and Contribution

As increased interest in K-band and millimetre wave frequency due to the expansion of communications systems, increased data rates etc. were reported in [19–23]. How accurate do the new propagation models need to be? Do building specific materials really

matter or is an 'average' reflectivity good enough?

There is a need to have a better understanding of propagation loss mechanisms; reflection, scatter, diffraction and attenuation. The demand to be able to focus on particular materials to see how sensitive the measurements are and hence how accurate any propagation model will be using high material parameter tolerances.

The need to compare a large scale studies with laboratory-based reliable, repeatable measurements to allow full material characterisation including scatter and also determine the variation in parameters from sample to sample. The need, therefore, is to the able to scale the problem from knowing the small-size material characteristics to those for large scale and to remove the small-scale artefacts, i.e. diffraction effects will be different, as will the illumination of the object etc. as illustrated in Figure 1.4.

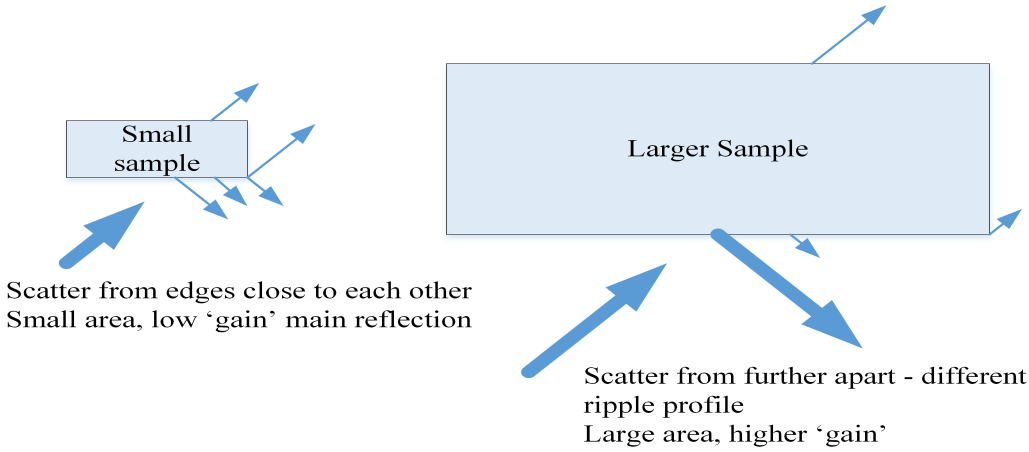

FIGURE 1.4. Small sample versus larger sample propagation

This thesis does not answer all these questions but puts forward some practical and repeatable measurement methods start to allow relative and absolute characterisation using small-scale material samples. The thesis will first review the state of the art in the propagation mechanism in the millimetre wave band. The thesis will then concentrate on the determination of material parameters with the small sample orientation normal to the transmit antenna and develop a finer resolution transverse measurement for wideband frequency and investigation of reflection from surface material.

The thesis will explore and propose different analysis techniques including the calibration of the measurement range and processing of the data in indoor laboratory measurements.

1.3 Structure of the thesis

- Chapter 2 presents a comprehensive literature review of RF propagation and material characterisation measurements for the K-band (18GHz to 27GHz) and millimetre wave (28GHz to 60GHz) frequency range for various indoor and outdoor scenarios. The transmission and reflection measurement with respect to small sample materials and building for indoor scenarios will be presented. The review of full indoor azimuth and elevation scan and clutter identification will also be discussed and propagation modelling at millimetre wave. At the end of this chapter, the thesis will summarise the reviews studies and relate it to the main contribution of this thesis.

- In Chapter 3, two methods will be presented that concentrate on determination of material parameters with the sample orientation normal to the transmit antenna, and hence the material broadside reflection and transmission through the material will be examined, and the other method concentrates on the development of a comprehensive model of the normal reflection of a material taking into account the transmit antenna, path between the material and antenna and the thickness of the sample, with method of system calibration suggested. The chapter will end with challenges and realisation towards measurements at higher frequency bands.

- Chapter 4 will present the angular measurement both in anechoic chamber and in indoor laboratory area. Measurement will be conducted at frequency of 20GHz and 60GHz (for short range indoor laboratory area). The calibration of the measurement range and processing of the data is presented with the means to identify the reflectivity versus angle (scatter) at frequency of 20GHz and a number of samples are considered: metal, concrete and wood. The level of reflectivity with respect to metal plate are useful for propagation model for future works.

- In Chapter 5, an intensive azimuth-elevation scan measurement in the anechoic chamber and indoor laboratory and adjacent office environment at the lower band of millimetre-wave frequencies, 22GHz were presented. The work in this chapter focus on object identification and their perceived size as seen at a receiver. This chapter will conclude with significant findings that will be further used for future research in propagation mechanism area.

- This chapter concludes the contributions and impact of this work, particularly the prospects for further research in the field.

1.4 List of Publications

- A.K.M.Isa,A.Nix, and G.Hilton,"Material Characterisation for Short Range Indoor Environment in the Millimetre Wave Bands", 2015 IEEE 81st Vehicular Technology Conference (VTC Spring), 11-14 May 2015, Glasgow, United Kingdom.
- A.K.M.Isa,A.Nix, and G.Hilton,"Impact of diffraction and attenuation for material characterisation in millimetre wave bands", 2015 Loughborough Antennas Propagation Conference (LAPC), 2-3 November 2015, Loughborough, United Kingdom.

CHAPTER 2

REVIEW OF RF PROPAGATION MEASUREMENTS STUDIES AT K-BAND AND MILLIMETRE WAVE FREQUENCY

This chapter presents a comprehensive literature review of RF propagation and material characterisation measurements for the K-band (18GHz to 27GHz) and millimetre wave (28GHz to 60GHz) frequency range for various indoor and outdoor scenarios. The aims are to identify the motivation for a practical material characterisation measurements, the current state of the art for the research and review the relevant published research.

The chapter sets out as follows: Section 2.1 will reviewed the measurement techniques and categories it into three methods based on the measurement setup of the transmitter and the receiver antenna. In Section 2.2, the fixed antenna position will be reviewed. The investigation will consider the type of antenna used, the distance between the antenna and the sample material and the propagation mechanism. In Section 2.3 will focus on the movable transmitter or receiver antenna. Section 2.4 concentrates on the indoor and outdoor scanning both for azimuth and elevation angles.

This chapter will end with a summary and challenges that this thesis focus on.

2.1 Review of Propagation Mechanism Measurement Setups

In considering the measurement of the RF characteristics of materials, the number of degrees of freedom in terms of transmitter position and receiver position with respect to the material under test together with polarisation (co-co and co-cross) deems the complete analysis of the material in terms of its reflection and attenuation properties with frequency an extremely complex task. The material properties will include its bulk conductivity, permittivity and permeability, compactness (i.e. density), material texture (i.e. surface roughness) and shape (i.e. curvature). At low frequencies, say sub 6GHz, surface roughness may not necessarily impact on material properties however with increased frequency (or size of material 'features') the potential scatter may start to compete in dominance with the bulk material characteristics and general shape. In this review, methods to determine material characteristics are identified. Table 2.1 provides the outline on how transmitter and receiver setting related to RF propagation mechanism. The categories are based on the positioning of the transmitter and receiver either fixed or moved position.

Table 2.1: Categories of Propagation Measurement Setup

		Transmitter (Tx)	
Receiver (Rx)		**Fixed**	**Moved**
	Fixed	Transmission and Diffraction	Reflection and Diffraction
	Moved	Reflection and Diffraction	Scanning

The overall discussion in this chapter will be based on this Table 2.1. There are basically three main setups of interest. Based on these setups, the measurement methodologies, calibration and analysis are the main concern that will be adopt in this thesis.

2.2 Fixed Position of Transmitter AND Receiver

The first setup to be discussed is when the transmitter and receiver antennas are at the fixed position. The line of sight (LoS), attenuation through material (penetration) and diffraction will be observed and studied. This section will cover review of both indoor and outdoor environments, concentrating on the frequency range 20GHz to 60GHz. Figure 2.1 shows the typical setup for fixed transmission measurement. In this setup, transmitter and receiver are kept fixed at a certain distance (d1 and d2) and material under test (with thickness, ds), was placed in between the two antennas. Reviews will cover the details setup, observation and results obtained and the challenges that arose.

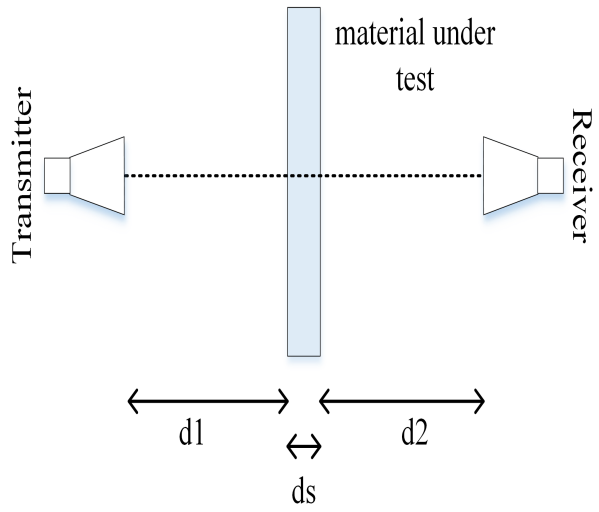

FIGURE 2.1. Fixed Tx AND Rx: Transmission Measurement Setup

2.2.1 Direct Line of Sight (LoS) and Penetration Investigation

The first review for this fixed position of antennas setup will cover the direct line of sight and penetration mechanism. In this section, transmission across obstacles and building material either in an indoor environment or from indoor to outdoor or vice-versa will be analysed. Transmission and attenuation loss through various material that commonly uses in building construction will be presented. This section aims to demonstrate that the results from this transmission and diffraction measurements cannot be neglected for the considered frequency band.

Transmission: direct line of sight

The line of sight propagation describes as signal travel in a straight line from the transmitting antenna to the receiving antenna. Loss in this direct transmission is known as free-space loss. This free-space path loss is defined [24] as:

$$FSL[dB] = 92.4 + 20logf[GHz] + 20logd[km]. \tag{2.1}$$

where two communicating antennas operating at a frequency f in GHz and separated by d in kilometres (km). Based on this equation, the free-space loss is proportional to both frequency and distance between the antennas. Therefore, higher free-space loss is expected when it is in millimetre wave frequency band.

Attenuation/Penetration

Penetration loss is an essential factor which determines the ability of the indoor signal to pass through interior walls or furniture and the outdoor signal to penetrate into buildings wall. This ability for common building materials are vital for the planning and design of millimetre wireless system. Common relative permittivity and conductivity for different building materials are presented by [25] and [26].

At higher frequency bands, penetration loss study of various materials have been conducted for single frequency of 20GHz [27], 28GHz [1, 28], 40GHz [29, 30], 60GHz [31–33] and wide range of frequency such as [34] from 2GHz to 74GHz, [35] in the range of 800MHz to 18GHz, [36] for 8GHz to 37GHz. In general, mechanisms such as attenuation or penetration are becoming significant problems that limit the quality of radio wave link. Alternatively, in [29], this problem makes possible by using this effect to shield the radio station sides. This idea is to take advantage of the attenuation to minimise the interference in and from other communication systems.

Measurement campaign in an indoor environment to study the penetration loss for various material have been conducted in [29, 34]. Wall materials made of wood and glass have been measured. Measurement setups are as Figure 2.1 with a distance of 3m between the antenna in [34] while [29] was not specified. Results from both measurements are tabulated in Table 2.2.

Noted that both measurements did not specify the dimension of the material even though the antenna illuminated the materials sufficiently.

Investigation of outdoor to indoor wall penetration for a different type of wall and window are reported in [1, 28, 32, 37]. At 28GHz, path loss through both standard window glass and coated glass were measured in [28], and at the same frequency, measurement was extended for a different type of material (brick, concrete and drywall) in [1]. At a

Table 2.2: Summary of attenuation/penetration loss (dB) at 28GHz, 38GHz and 40GHz

References	Material	Thickness (mm)	Attenuation/penetration loss (dB)
[1] at 28GHz	Tinted glass	38	40.1
	Brick	1850	28.3
[37] at 38GHz	Modern window	NA	25
	Modern door	NA	40
[29] at 40GHz	Glass	4	3.1
	Chipwood	16	7.9
	Wood	7	2.6
	Plasterboard	15	2.7
	Concrete	100	174.95

lower frequency of 800MHz to 18GHz, comparison of modern building material versus old building material was conducted in [37].

2.2.2 Diffraction Analysis

In wireless communications especially the wedge and edge diffraction measurements are of interest because building corners, both indoors and outdoors, are the main objects causing diffraction [38–40]. In addition, diffraction for cylindrical and rectangular shapes of obstacles [29, 41–43] at 40GHz and 60GHz also essential. Accurate characterisation of diffraction at higher frequency is crucial for the understanding of rate of change of signal strength in mobile communication systems (the reduction in strength as the signal becomes more in 'shadow' has bigger impact at higher frequencies, since the the millimetre wave system will have to rely less on diffraction as a dominant propagation mechanism [20], [44], [45].

This diffraction analysis will start with discussion based on the fixed antenna measurement setup, then a review of the results before finding the suitability of this setup for material characterisation at higher frequencies.

A building corner diffraction measurement campaign at 28GHz [46] were conducted at three separate buildings with 90° sharp corners. A 2.5° parabolic antenna was used at the transmitter and a horn antenna with a 17° HPBW at the receiver. The path lengths were set from 39m to 50m. Typical building materials of brick and concrete block were considered. The measurement results showed that as diffraction angle increased (moved to shadowed region) , the diffraction loss increased. The concrete block corner attenuated the signal by 3dB more than the brick corner for the shadowed region.

Diffraction measurement as comparison between frequencies was conducted in [47] for 2GHz, 11GHz, and 38GHz. It was discovered that the diffraction loss increased as frequency increases, and decreased with RX antenna height. Another frequency comparison for diffraction loss measurement was conducted in In [19]. Frequency of 10GHz, 20GHz, and 26 GHz measurement was conducted in indoor and outdoor environment. In the indoor measurements, 90° wall corners made of drywall, wood, and semitransparent plastic board with 2cm thickness and outdoor measurements investigate one rounded stone pillar corner and one marble building corner.

Diffraction over the rooftop at 28GHz was conducted in [48]. The distance range was limited between 12m to 150m and diffracted angle of 0° to 50°. Based on the measurement results, they conclude that the diffraction losses are proportional to a diffraction angle, and the slope varies with the propagation lengths of the diffracted waves.

At 60GHz, investigation of attenuation by diffraction caused by metallic and wooden edges and wedges in the indoor environment have been conducted by [38]. Follow the fixed setup(the transmitter and receiver at a fixed position and the object moved across them); the measurements were conducted with a Rohde & Schwarz ZVA50 vector network analyser (VNA) in combination with 20dBi WR-15 and WR-3 fed standard gain horns (SGH) antenna as transmitter and receiver for both horizontal and vertical polarisation. The object moved in steps of 1mm, but the distance between both transmitter and receiver was not stated. A metal cylinder of the 45mm radius and 250mm height and metallic cuboid with quadratic area cross section (80x80mm^2) was used.

Another diffraction analysis measurement at 60GHz was conducted in [42] with a metallic circular cylinder vertically placed at the intersection (radius was not stated). The purpose of their works is to evaluate the influence of the deflecting objects (DO) in broadband propagation characteristic at the NLOS (T-shaped) intersection. Two identical pyramidal horns with mid-band gain of 23.4dBi were used for transmitter and receiver with vertical polarisation at 20m apart.

2.3 Movable Positions of Transmitter OR/AND Receiver

Positions of transmitter and receiver have a major contribution in determining an exact propagation mechanism involve in propagation studies. In this second setup, movable positions of either transmitter or receiver will be reviewed. From this setup, diffraction can still be determine but the main observation will be the reflection both from smooth (specular) and rough (diffuse) materials.

2.3.1 Diffraction Mechanism; The Angular Setup Analysis

The diffraction effect occurred or being observed when the wave is approaching the tip or the corner of any obstruction. There are measurements of corner diffraction being undertaken in the frequency range of 20GHz to 60GHz both indoor and outdoor environments [29, 30, 37, 46, 49–57]. Isolated corner measurement setup for diffraction analysis was observed as parallel and angular measurement. Parallel measurement describes as either the transmitter or receiver moved in a straight line with respect to the nearest wall, while angular measurement describes as the antenna moved in angular motion as shown in Figure 2.2.

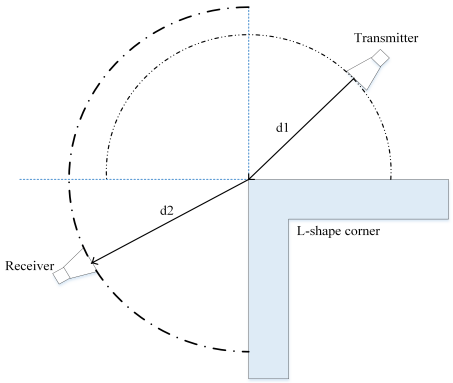

FIGURE 2.2. Movable Tx OR Rx: Corner Measurement Setup

In parallel measurement [49], the transmitter was located 5m from the corner with 1m away from the nearest wall, and the receiver was moved along the 6m route with parallel tracks from the wall; measurement was taken every 4mm while the trolley being pulled along the track. Meanwhile, in [37], the receiver was moved to 3m and 6m deeper to NLOS area, and measurement was taken in azimuthal range scanned (180° to of

360°). For [37] measurement, the analysis focused not only on reflection and scattering but also on diffraction. There are some drawbacks in using the setup: The placement of the antenna on the handle or trolley may include vibration hence the data reading will be varying. Repeatable measurements also will be not accurate in [49] because of the manual movement of the trolley.

In the angular measurement, the transmitter and receiver antenna was held at a certain distance away from the rotation axis; 2m for both transmitter and receiver in [51], 3.75m [50] and 0.6m for transmitter and 1.2m of receive antenna in [29], in contrast [46] not specified the distance between the corner and the antennas. For all the setups, limitation of angular movement in degree rotation and distance depth in NLOS area is crucial. The receiver was moved in an arc and measurement was recorded for intervals of 10° in [29, 50, 51].

2.3.2 Reflection from Surfaces

Reflection, in this case, is surface dependent and frequency dependent. If the waves hit the smooth surface, all the energy will get reflected back, and this case is known as specular reflection, whereas if the waves hit the rough surface, the energy will reflect back but in all other direction, and this case is called diffuse scattering. Furthermore, measurement setup as Figure 2.3 also being observed of reflection existence.

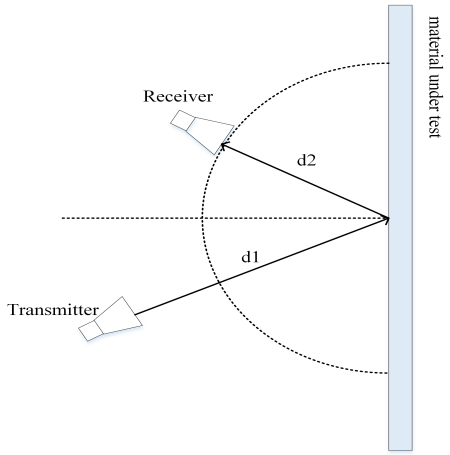

FIGURE 2.3. Movable Tx OR Rx: Arc Measurement Setup

Reflection loss in and around buildings in New York city at 28GHz have been presented in [1]. Reflected power was measured from a a variety of materials (tinted glass, clear glass, concrete and dry wall) based on the following this setup; the transmitter and

receiver antenna was placed at a distance of 2.5m from the material with the antenna oriented at two different incident angle (10° and 45°). Both the transmitter and receiver are horn antennas with 24.5dBi gains with 10° half power beamwidth. The materials under test are tinted glass, clear glass, concrete and drywall. Reflection coefficient for stated building materials were tabulated in Table 2.3, comparing the results for indoor and outdoor materials.

Table 2.3: Summary of Comparison of reflectivity for different material at 28GHz as reported in [1]

Environment	Material	Angle (∘)	Reflection coefficient (Γ)
Outdoor	Tinted Glass	10	0.869
	Concrete	10	0.815
		45	0.623
Indoor	Clear Glass	10	0.740
	Drywall	10	0.704
		45	0.628

With regards to the results, reflection coefficient for outdoor materials was as large as 0.869, showing that it has a high value of reflectivity and a very small transmitivity.

Another outdoor measurement campaign to determine reflection and scattering was conducted in [37] at 38GHz in urban scenarios. A commercial 38GHz backhaul equipment was installed at both the transmitter and receiver. The antennas have a maximum gain of 40.5dBi (vertical) and 39dBi (horizontal) with a highly directional pencil beam shaped with half power beamwidth of 1.45°. The transmitter antenna was pointed towards the building facade. For specular reflection, incidence angle is equal to reflected angle with respect to the normal plane of incidence of the building wall. Measurements were done for both (V-V and H-H) polarisations. Reflection loss, in this case, is defined as the difference between the line of sight (LOS) power and the received power measured at the same particular distance travelled. They also observed that the reflection loss decreases with increasing of incident angle or the reflected component is stronger for the larger incident angle.

Setup that is the same as shown in Figure 2.3 for the arc movement have been used in [58, 59] for parameterisation procedure of diffuse scatter at 60GHz. A directive lens antenna acts as a transmitter (51.5GHz to 75GHz) was placed at a distance of 1.4m and points to the centre of the material, while the receiver (omnidirectional antenna), moved in semi-circular motion around the material (at 10°, 50°, 90°, 130° and 170°). For each

receiver position, the relative received power that comes from the area of the material that received a maximum level of energy was measured.

The goal of their research was to find the best diffuse scattering model for typical building materials; glass, plasterboard, chipboard, cardboard of a box and bricks used both indoor and outdoor walls. A time gating techniques were applied to the measured data to distinguish the received power of the diffuse scattered components. For modelling purposes, the Lambertian and directive model has been chosen to investigate the existence of diffuse scatter and to characterise the building materials.

Reflection scattering and bistatic reflection measurements have been conducted in [17] at 60.2GHz using the same setups. For reflection scattering measurement, the transmitter was kept fixed and illuminating a test material at a particular angle, the receiver moved in angular position and recording the reflected power. As for bistatic reflection measurement, both the transmitter and receiver antennas were moved in angular motion so that the incident angle is as identical as receiving angle.

From these measurements campaign, only the materials with a standard deviation of roughness equal to or greater than 0.3mm exhibit more significant influence on the received power of the scattered material. Whereas from bistatic reflection measurements, they have derived a material complex permittivity and material thickness relationship with respect to reflection scattering measurements.

Analysis of this scattering caused by various building elements in [60] was conducted using a Millimeter-Wave Scale Model Measurements and Ray Tracing [61] and reflection coefficient for house flooring materials measurement was also conducted in [62] at 57GHz-64GHz.

2.4 Indoor Azimuth and Elevation Scan

This last section will investigate the measurement setup that involved the movement of the transmit and receive antenna. The movement of the antenna, in this case, includes the rotation of the antenna itself either in azimuth or elevation plane. Reflection and scattering mechanism are the propagation mechanism being evaluated from this measurement. In addition, this indoor azimuth and elevation scan investigates path loss characteristics based on both angle orientation and distance.

In recent years, the propagation characteristics of indoor radio channels have been studied through extensive channel measurement campaign in higher frequency bands such as 20GHz [63], 26GHz [64], 28GHz [65–78] and at 60GHz [5, 11, 26, 68, 79–89]. Comparative studies between lower frequency versus high frequency also can be reviewed in [90] at 2.9GHz and 29GHz, at 14GHz and 22GHz indoor [91], [71, 92] at 28GHz and 73GHz, [93] at four different frequencies of 28GHz, 39GHz, 60GHz and 73GHz and [94, 95] at 19GHz, 28GHz and 38GHz.

Even though the focus of work in this project is for indoor scanning, the outdoor channel propagation also become the interest of researchers due to larger multipath propagation in that scenario. At 28GHz [96–99] and at 60GHz [31, 100] outdoor channel measurement campaign were actively conducted.

The aim of this section is to analyse the setup not only the positioning of the antennas but also on how the result being evaluated from the measurement and factors that contribute to the channel measurement itself.

2.4.1 Channel measurement campaign at 28GHz

Conducting well-planned and detailed measurement campaigns is an extremely valuable method to investigate the millimetre wave channel. Many researchers have performed channel sounding and channel characterisation for the 28GHz frequency band in indoor scenario. This subsection will looks into the 28GHz channel measurements that were conducted indoor in terms of the size of the measurement space, the channel sounder and VNA used and the results based on rotation angles.

At 28GHz, the wavelength is approximately 10.7mm, therefore the size or space of where the measurement was conducted was crucial. Measurements were performed in smaller room [71], for maximum range of 30m [70] or in the laboratory environment (7m x 10m x 3.5m area; equipped with chairs, table, computers and electronics devices) [65]. [92] conducted the measurements in a modern building of (65.5m x 35m x 2.7m) with

common office partitions (such as cubicles, desks, chairs, metal shelves, wood closets, concrete walls, glass and elevator doors). All the clusters in the indoor environment need to be specified in order to determine the source of multipath signals. At a wider space such as Seoul railway station (170m x 45m x 21m) and Incheon International Airport (650m x 82m x 20m) in Korea [66, 69] measurement were conducted considering population density or hot spot areas.

Based on the review, most of the measurement were conducted in a rectangular size of room. This is probably the best geometric shape for modelling the propagation mechanism as been used in ray tracing simulation [76], but this thesis will not go in depth regarding this issue.

In this multiple measurement campaigns, antenna with narrow half power beam width (HPBW) were used. Details of gains, beamwidth and rotation either in azimuth or elevation plane need to be specified to investigate the effect of illumination by the antenna itself and the angle of rotations. Horn antennas (18.52dBi gain and 20° (3dB beamwidth)) that rotated in the entire azimuth plane (0° to 360° with 15° step) while using a VNA to measure the channel was conducted in [65]. [70] only describe their measurement using a VNA and a pair of 26dBi gain horn antennas for distances up to 30m.

The same configurations were used both in [96] and [69] for measurement in the larger room. They used a 60° HPBW horn antenna of 10dBi gain as a transmitter, and 24.4dBi horn antenna with 10° HPBW as a receiver. The height of the transmitter and receiver were set at 8m and 1.5m respectively. At the receiver side, the azimuthal rotation step size was 10° and ranging from 0° to 360°, while in the co-elevation scan, ranging from $-10°$ to 10°.

The empirical results of path loss, RMS delay spread, PAP are believed by [**?**] to provide a reference for the design of communication systems in the near future. Path loss characteristic in term of angle orientation were focused in [69] and Saleh-Valenzeula model for extra cluster parameters [65].

In this channel measurement campaign, LOS path plays the dominant role, however, abundant multi-paths were generated during these propagation. Received signal can be detected from different directions. The method of detecting and receiving these signals effectively with directional antennas is highly significant for further investigation.

2.4.2 Channel measurement campaign at 60GHz

Channel measurement campaign at 60GHz will be more crucial compared to 28GHz because the wavelength now is only 3mm. The same points of interest as in 28GHz will be reviewed,

The 60GHz indoor channel measurement using a directional horn antenna with 7° HPBW in the azimuth plane and 29dBi of gain at the RX, and an open-ended waveguide with 90° HPBW in the azimuth plane and 6.7dBi of gain at the TX was conducted in [84]. A sliding correlator channel sounder was utilised and channel impulse responses captured at discrete pointing angles while Rx rotates. LOS measurements resulted in a PLE less than 2 (theoretical FSPL), using a 1m close-in free space reference distance. These findings were similar to those at lower frequencies in indoor environments, where ground and ceiling bounce reflections and a waveguide effect are known to increase power at the receiver such that the measured path loss is less than theoretical FSPL.

A 60GHz propagation measurements in various indoor environments in continuous-route (CR) and direction-of-arrival (DOA) measurement campaigns were conducted in [5]. The propagation mechanisms were studied based on DOA measurements, indicating that the direct wave and the first-order reflected waves from smooth surfaces were significant in LOS propagation environments, while in NLOS cases, diffraction was a substantial propagation mechanism, and the transmission loss through walls was very high. A 60GHz measurements in the corridor, LOS hallway, and NLOS hallway environments, and the measured PLEs were 1.6 in LOS corridor, 2.2 in LOS hallway, and 3.0 in NLOS hallway environments were also conducted by the same researcher in [79].

An indoor 60GHz radio channel measurements by recording power delay profiles using a direct RF pulse technique with a 10ns repetitive square pulse, modulated up to the 60GHz carrier having a bandwidth of 100 MHz and 10dBm of transmit power while using identical 21dBi vertically polarised horn antennas at the TX and RX was performed in [82]. The extracted power delay profiles were found to be less in hallways (up to 8.18ns) compared to offices (up to 14.69ns). The measurements also discovered that the office environment did not experience large channel variation over local areas.

How the radiation patterns and antenna polarisations at remote terminals affect multipath propagation characteristics at 60GHz, in a conference room was investigated by [88]. Four types of antennas were used to examine the effects of radiation patterns of RX antennas: an omnidirectional antenna and three directive antennas with wide, medium, and narrow HPBWs. The use of a directive antenna at the remote terminal was an effective method to reduce the effects of multipath propagation. Further reduction in

multipath effects was achieved with the use of circularly polarised directive antennas instead of linearly polarised directive antennas.

Channel sounder have been widely used in these 60GHz channel measurements. Channel sounding hardware equipment's is expensive especially at millimetre wave frequency bands. Furthermore, extensive channel sounding measurements campaign in various propagation scenarios at many potential millimetre wave frequency bands is time-consuming and stored a relatively large data. This thesis will take to face the challenge by setting up the scanning measurement in an indoor scenario with less expensive but repeatable measurements.

2.4.3 Propagation modelling at millimetre wave

Channel models are essential for system performance evaluation and comparison especially at higher frequency band. It should depends on a profound knowledge of the basic radio channel. Deterministic model (ray- tracing) is one of the approaches/method that describing the channel model [21]. In ray tracing, exact information of geometry and parameters of materials are important.

There are a lot of thing to consider in order to develop such an efficient ray tracing model, for example; free space loss, foliage and atmospheric attenuation and propagation mechanism (reflection, diffraction, scattering and attenuation) [6, 101]. The ray tracing model should be extended to include the probability of diffuse scatter in materials, because due to the smaller wavelength, presence of small roughness on the surface should be more visible compared at lower frequency. In directly, the small objects or clutter in and around the environment also need to be taken care of.

2.5 Summary and Future Challenges

This chapter has presented a detailed review of the current state of the art for the various measurement campaign, and propagation mechanism observed based on the positions of a transmitter (Tx) and receiver (Rx) with respect to a material surface.

Section 2.1 contained a review of measurement campaigns that has been conducted based on the fixed position of Tx and Rx and considered direct line of sight (LoS) propagation, penetration, and diffraction effects. Based on the reviewed results, it was found that attenuation was influenced by the frequency of operation and thickness of materials. The diffraction effect from small sample materials such as wedges and edges have also been studies. The challenges in this category are the distance between Tx and Rx to the sample materials, the dimensions of material under test and the attenuation with respect to the frequency and thickness of the materials. In Chapter 3 an initial study at 40GHz to 50GHz of the transmission and reflection properties based upon this configuration has been undertaken.

Movable Tx or Rx have been presented in Section 2.2. Diffraction again was observed from this setup, but it focuses more on building corner diffraction, with the receiver being moved in an arc around the corner feature. Based on the reviewed results, it was found that the attenuation increase as the receiver moved into a shadow region. Results indicated several trends concerning diffraction angle, building materials, and antenna polarisations. The challenge in this categories is the angle precision, how many degrees of movement are adequate to capture the diffraction and reflection. The challenge also arises from the beamwidth of the transmitter and receiver antenna. How wide the beam that falls onto the material under test or the corner of the building. The setup in this category is modified and presented in Chapter 4 and become the main contribution of this thesis.

Section 2.3 highlighted the case when Rx is moved in azimuth and elevation plane. In this category, indoor azimuth and elevation scan is the main focus. Propagation mechanism, in this case, covers all type of propagation mechanism such as a line of sight (LoS), diffraction and reflection (diffuse and scattering). The multipath propagation has been observed and several techniques been used to identify the mechanism separately. The challenge in these categories is the size of indoor scenarios that can be covered in these higher frequency bands and how are the clutter and human blockage in the environment affect the propagation mechanism. The technique to identify the specific propagation mechanism based on the raw data can be a challenge too. This scanning

mechanism will be presented in Chapter 5 for indoor laboratory and adjacent office area cases and will focus on object identification in the controlled environment before further investigation of propagation path in larger scenarios.

Overall, the challenges are to identify whether the practical methods to produce material parameters for inclusion in propagation models are repeatable and accurate, and over what frequency range. Are there enough or suitable data or parameters as an input to that propagation modelling, especially indoor environment?

CHAPTER 3

A STUDY OF TRANSVERSE PROPAGATION AND MATERIAL CHARACTERISATION MEASUREMENTS

Chapter 2 has presented the reviews of several types of measurement setup to identify propagation mechanism in, primarily an indoor scenario. The first method is presented in this chapter concentrates on determination of material parameters with the sample orientation normal to the transmit antenna, and hence the material broadside reflection and transmission through the material will be examined.

This initial investigation was carried over a range of frequencies from 40GHz to 50GHz on samples of maximum dimension 40cm by 40cm and both reflection and transmission properties are considered for a number of materials. Antennas are placed either side of the sample and the distance to the sample and the size of the sample affect the level of reflection back to the transmit antenna and the signal received by the second antenna placed behind the sample. The effects of both the signal reflection from and transmission through the material as well as diffraction effects are considered in the method shown.

In section 3.1 a laboratory-based transverse measurement is introduced, and the initial investigation described. This measurement process identifies three possible signal components: direct line of sight, attenuation through the material and diffraction effects. Basic Knife Edge Diffraction (KED) theory is therefore described here to help understand diffraction mechanism.

In section 3.2, data from the initial transmit to receive antenna measurements are

presented. It is important with attenuation measurements that a clear distinction between effects due to attenuation as not confused with those arising from diffraction around the material and hence incorrect levels of attenuation recorded. Arising observations and challenges for this measurements are discussed, and these lead to the new approaches and analysis.

Section 3.3 concentrates on the development of a comprehensive model of the normal reflection of a material taking into account the transmit antenna, path between the material and antenna and the thickness of the sample, with method of system calibration suggested. Section 3.4 then describes the approach to undertake repeatable wideband measurements using an automated test set up. The calibration process is described for real data and results are presented for sample materials.

3.1 Transverse Measurement Setup for Diffraction Analysis

In this study, the setup is as follows; the transmitter and receiver were kept fixed while material under test is moved in transverse motion between the two antennas. The transverse movement has therefore been used to investigate both the effect of diffraction of the small material sample and the sample attenuation.

The movement of the material across the path has three propagation phenomena: direct Line of Sight (LoS), diffraction and attenuation. The diffraction is evident in all aspects of the measurement: when the material is approaching the intersection or crossover between the transmitter and receiver position, while attenuation at its highest when the material is in the middle of the transmitter-receiver path. This means that it is important to establish its part in the determination of attenuation through the material in order to remove it from the data. This would not be evident (in the same way) in a large sample and hence scaling this analysis to allow inclusion in propagation modelling tool would require only the true attenuation.

The closest similarity of using this type of measurement to the author's knowledge has been presented in a previous study [38] as translation measurement. In their paper, measurements were taken for a single frequency of 60GHz and 300GHz and with only copper cuboid and metal cylinder as the sample material. This is therefore a study of diffraction around metal and rather than attenuation and other material attenuations do not appear to account for the combined effects of attenuation and diffraction as noted in Chapter 2.

The objectives of this measurement campaign are to investigate the effect of diffraction and attenuation on small sample material in a range of less than 1m in an indoor laboratory environment and compare the diffraction results with Knife Edge Diffraction (KED) theory and establish a level of attenuation for some sample materials.

3.1.1 Procedure of measurement and data collections

The transverse measurement campaign was conducted in University of Bristol Communication System and Network (CSN) laboratory area. Figure 3.1 and Figure 3.2 show the transverse measurement setup.

An area in front of the vector network analyser was selected as a measurement area to avoid use of long cables that needed to be fixed in position after calibration to minimise measurements errors. The area was also relatively free from clutter and hence multipath from clutter was not seen to be an issue.

The 2-port 37397C Anritsu Vector Network Analyser (VNA) was connected to two identical 20dBi directional standard gain horns. The 20dBi gain antenna has a half power beamwidth (HPBW) of approximately 23° at mid-band frequency of 45GHz. Both antennas were mounted on fixed poles and pointed towards each other at 1m apart.

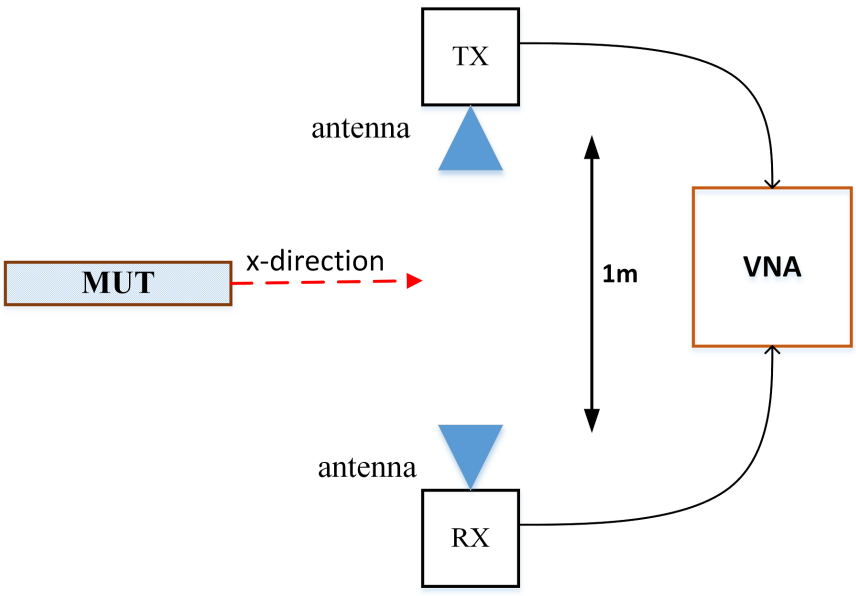

FIGURE 3.1. Transverse Measurement setup

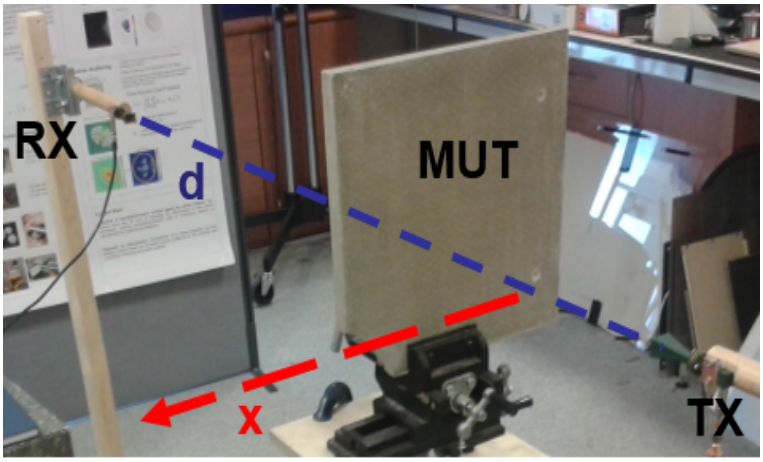

FIGURE 3.2. Photo of Transverse Measurement setup

Measurements were taken over the range 40GHz to 50GHz. All measurements were carried out with vertical transmit to vertical receive (V-V) and horizontal transmit to horizontal receive (H-H) polarisations to determine the influence of polarisation on the extracted parameters. Cross-polarisation was not considered for this study.

The material under test is placed on a translation stage and moved across transmitter and receiver in the x- direction using a positioner as depicted in Figure 3.1. The procedures of measurements are as follows:

At the beginning, the material was positioned well away from the centre of transmitter and receiver. In this position, the transmitter and receiver are at the line of sight (LoS) between each other. This unobstructed case or line of sight acts as a propagation reference. Subsequently, the material under test is moved in 20mm steps in x-direction using a manual positioner. From then on, the material moved across and passed the transmitter and receiver position in a straight line. This positioner is equipped with a stand and adjustable vice to hold different thickness of material in place as shows in Figure 3.2.The S21 measurement readings were therefore taken every 20mm along the track using Matlab based software to control the VNA and record the data.

3.1.2 Knife Edge Diffraction (KED)

As the measured data is a combination of diffraction and attenuation through the material, it is necessary to identify both individually and the effect based on the overall data collected. Therefore Knife Edge Diffraction (KED) is discussed here as a possible means of representing the diffraction effect seen in the sample data.

The KED theory is a commonly used model to validate the diffraction effect. Knife edge diffraction assumes a single sharp object edge separates the transmitter and receiver. In [38], the researcher describe the KED as to provide an approximation formula for the edge of diffraction at the semi-infinite half plane. KED theory also has been applied in [49] to validate the measurement results.

Figure 3.3 shows the KED model geometry. A transmitter and a receiver separated in free space, with a material as an obstructing screen which has an effective height of h placed at a distance of d_1 and d_2 from transmitter and receiver respectively. From this geometry, there are two propagation paths from transmitter to receiver; a direct line of sight path and diffraction path.

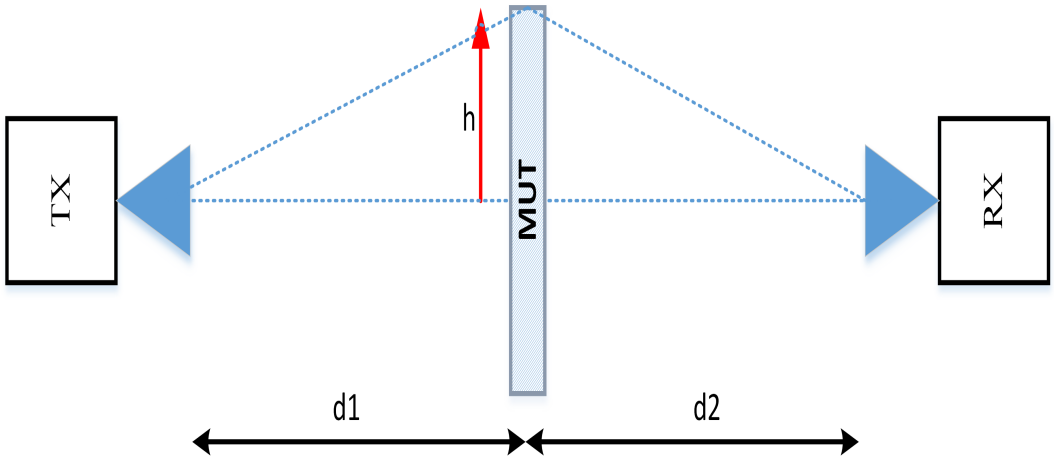

FIGURE 3.3. The path geometry of Knife Edge Diffraction (KED)

The received electric field characteristics depend on the path difference $\triangle$ between the length of the diffracted path and the length of the line of sight path. Using the geometry shown, $\triangle$ is easily found as follows:

$$\triangle = \sqrt{d_1^2 + h^2} + \sqrt{d_2^2 + h^2} - (d_1 + d_2) \tag{3.1}$$

$$\triangle = d_1\sqrt{1 + \frac{h^2}{d_1^2}} + d_2\sqrt{1 + \frac{h^2}{d_2^2}} - d_1 - d_2 \tag{3.2}$$

$$\triangle \approx d_1(1+\frac{h^2}{2d_1^2}+d_2(1+\frac{h^2}{2d_2^2}-d_1-d_2 \tag{3.3}$$

$$\triangle = \frac{h^2}{2}(\frac{1}{d_1}+\frac{1}{d_2}) \tag{3.4}$$

$$\triangle = \frac{h^2}{2}(\frac{d_1+d_2}{d_1 d_2}) \tag{3.5}$$

$$\triangle \approx \frac{h^2}{2}\frac{(d_1+d_2)}{d_1 d_2} \tag{3.6}$$

This Equation 3.6 will then be normalised using the dimensionless Fresnel diffraction parameter v which is given by Equation 3.7, which measures how deep the receiver is within a shadowed region.

$$v = h\sqrt{\frac{2}{\lambda}(\frac{1}{d_1}+\frac{1}{d_2})} \tag{3.7}$$

Based in [102]; consider a receiver, located in the shadowed region, the electric field strength at that particular receiver is given by Equation 3.8:

$$\frac{E_d}{E_o} = F(v) = \frac{(1+j)}{2}\int_v^\infty exp((-j\pi t^2)/2)dt \tag{3.8}$$

Where Eo is the free space field strength and F(v) is the complex Fresnel integral. The Fresnel integral F(v) is a function of the Fresnel diffraction parameter v which is given by equation 3.7 previously. The diffraction gain due to the existence of a knife edge, as compared to the free space E-field, is given by:

$$G_d(dB) = 20log|F(v)| \tag{3.9}$$

With this, an approximate solution for equation 3.9 is provided as:

$$G_d(dB) = 0 \qquad v \leq -1 \tag{3.10}$$

$$G_d(dB) = 20log(0.5-0.62v) \qquad -1 \geq v \leq 0 \tag{3.11}$$

$$G_d(dB) = 20log(0.5exp(-0.95v) \qquad 0 \geq v \leq 1 \tag{3.12}$$

$$G_d(dB) = 20log(0.5-\sqrt{0.1184-(0.38-0.1v^2)}) \qquad 1 \geq v \leq 2.4 \tag{3.13}$$

$$G_d(dB) = 20log(\frac{0.225}{v}) \qquad v \geq 2.4 \tag{3.14}$$

Based on these equations(3.10 - 3.14),three conditions can be assumed;

- if the Fresnel diffraction parameter v is a negative value, it shows that the obstruction is below the line of sight.
- a value of 0 means that the transmitter, receiver and the tip of the object are all in line, at this position the electric field strength is reduced by half or the power is reduced to 1/4 of the value at the line of sight or without obstruction (i.e. a loss of 6dB).
- when the value of v increases on the positive side, the path loss rapidly increases.

The measurement setup as in Figure 3.1, replicate the geometry path of KED as in Figure 3.3 accordingly. Based on this geometry, the movement of material in 20mm steps is known as h (effective height); from this, the Fresnel diffraction parameter, v and the estimated value of diffraction gain, G_d can be obtained from Equation 3.7 and Equation 3.9. The results were plotted in Figure 3.4.

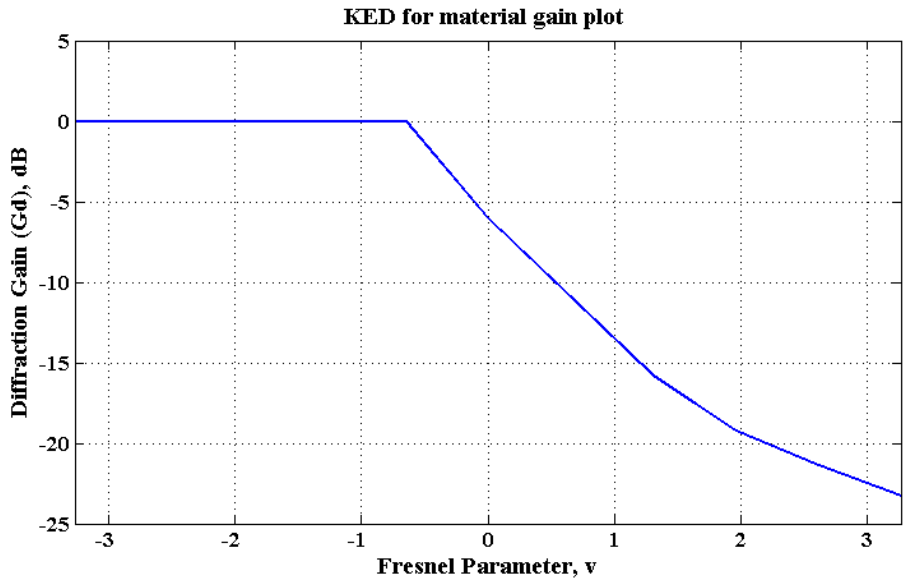

FIGURE 3.4. Diffraction Gain, Gd of material

Figure 3.4 only show that the measurement setup in this section follows the geometry that valid for diffraction effect analysis at the edge. Further analysis based on material comparison will be discussed in the next section.

Note that, KED only limited to the height of the obstacle, h and distance from transmitter and receiver to obstacle, d_1 and d_2. Even though the material is not assembled the knife edge shaped, it follows the approximate solution calculation closely.

3.2 Material Characterisation Based on Diffraction and Attenuation Propagation Analysis

In this section, S21 data (signal from the transmit antenna to the receive antenna) for the the transverse measurements campaign is analysed. The analysis covers three main propagation mechanism that involve or arise from this measurement setup. The first propagation is Line of Sight (LoS); the situation when transmitter and receiver are aligned to point towards each other (this serve s a distance reference). The second propagation mechanism is diffraction; when the sample material starts to move across the transmitter and receiver and the third propagation is attenuation; when the materials are in the middle and blocked both transmitter and receiver.

3.2.1 Material under Test (MUT)

For this initial investigation three materials of the same length were investigated. Table 3.1 shows the material under test with respect to dimension and photographs of all the materials are showed in Figure 3.5.

Table 3.1: Material under test (MUT)

Material under Test (MUT)	Size/cm	Thickness/cm
Concrete slab	40x40	3.0
solid wood	40x40	2.0
laminated wood	40x28	2.0

(a) A concrete slab (b) A laminated wood (c) A wood

Figure 3.5: Material under test (MUT)

Based on the tabulated dimension and picture of the materials, general descriptions of material under test are as follows;

The first material is a concrete slab; it is a common structural element of modern building construction either in internal or external walls. Concrete is a material that can be manufactured with a variety of different specifications, and this may influence its electromagnetic response. Concrete may be different in its structure, mixture, moisture content, and in the size of grit used in the reinforce mixture. It is also may be internally reinforced with a metallic grid arrangement, and the method in which it is treated that will influence its internal porosity.

There are two types of wood that are tested in this measurement, the differences between these two is the surfaces and densities; one with the regular wood surface and the other one coated with the smooth and reflective surface. It is an important study to realise how the same type of material with different surface and densities gives different results for diffraction, attenuation and reflection in an indoor environment.

3.2.2 Received Signals and Regions Identification

The analysis identifies three regions as depicted in Figure 3.6 as LoS, diffraction and attenuation.

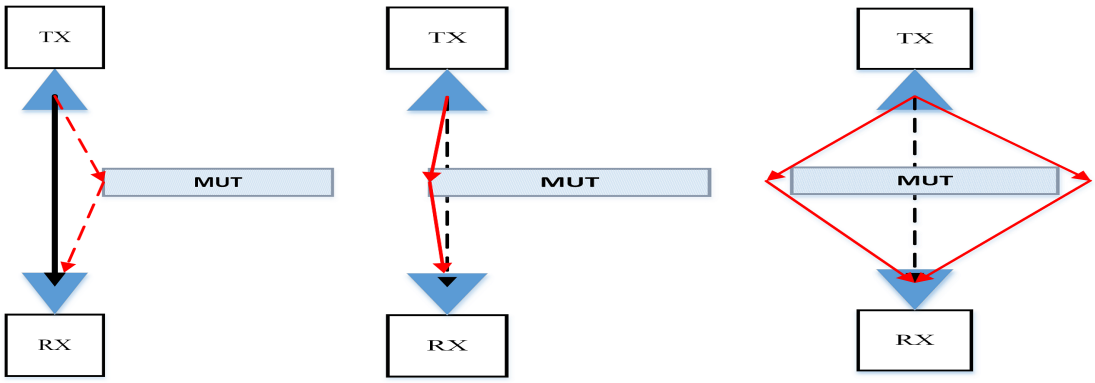

(a) LOS (b) Diffraction (c) Attenuation

Figure 3.6: Signals and regions identification

The first key observation from this transverse set of measurement setup is region identification. As the material under test travels from one side of transmitter and receiver, across the transmitter and receiver and passed the transmitter and receiver, three distinct regions are identified.

The second key observation is based on the type and strength of the received signal. The received signals are categorised into the dominant and secondary signal. As there were three regions detected, the received signal also will be further explained based on these regions. The three areas and the received signal are described in Figure 3.6. In the figure, the bold lines are the dominant signal, and the dashed lines are the secondary signal.

The three distinctive regions are identified as Line of Sight (LoS) region (Figure 3.6(a)): region when the material is out of the path between transmitter and receiver. During this region, the dominant signal is a line of sight. The signals surrounding are assumed to be negligible.

The second region is Penumbra (diffraction) regions (Figure 3.6(b)):this area occurs when the material is approaching the direct sight of transmitter and receiver and when the material started to block the view between the transmitter and receiver. Throughout this phase, the dominant signal is diffraction, and direct path signal become the secondary signal.

The third region is Umbra (attenuation) regions (Figure 3.6(a)): this phenomenon occurs when the material is totally blocked the direct transmission path between transmitter and receiver. The dominant signal at this point is attenuation and penetration signals.

A results of the concrete measurement can be seen in Figure 3.7. The results were plotted as S21 (dB) versus distance (mm). In the figure, 0mm is the point where where both antennas are aligned with the tip or edge of the MUT, and the material starting point is -100mm from the origin and will end at 100mm from the origin. This is the limitation of the setup as the manual positioner can only cover 200mm of total distance.

The first region; LoS occurred when concrete is away from the transmitter and receiver (at the distance of -100mm only up to nearly -20mm from the tip of the material). In this area, LOS and diffraction from the edge (and possibly some reflection due to material thickness) are noted that increases the signal level slightly.

The second region; From -20mm to 20mm, there is a drop of the signal observed as the concrete enter penumbra region, and it is known as diffraction loss.

The third region; In umbra region, which started after 20mm from the edge (0mm), the signals start to oscillate. It is expected that the signal will continue to oscillate until it reaches the other end of the material. This is because of the interaction between the attenuated signal and the diffracted signal. Depending on material size, this may just be diffraction from only from one edge, but if the sample is small this may be from more

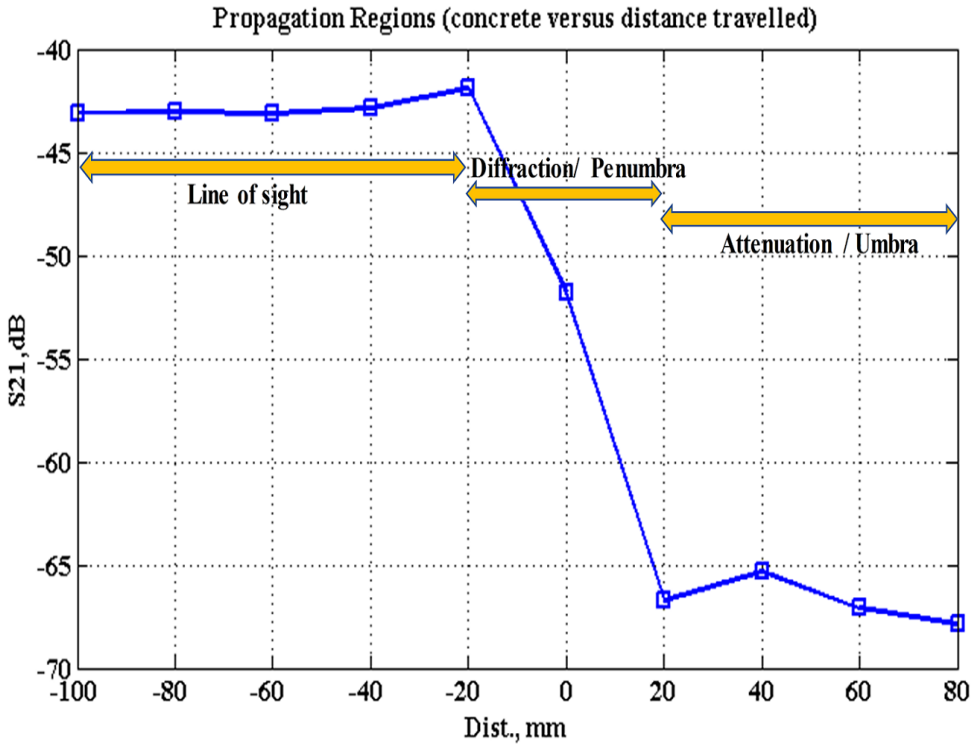

FIGURE 3.7. Regions Identification with concrete as MUT at 45GHz

edges, and hence the sample size and distance from the sample is important here.

The value of LoS signal, diffraction loss and attenuation loss for a different type of materials will be further discussed in the next section.

3.2.3 Material comparison

In this subsection, three materials are examined and analysed in terms of diffraction and attenuation as shown in Figure 3.8. All data have been normalised to LoS since cables, antenna gains and path loss need to be removed from the analysis. Figure 3.8 shows S21 transmission data for three types of materials at the centre frequency of 45GHz. Three distinct regions that have been discussed in previous section; can be observed at this frequency plot.

The rate of change in dB of the penumbra region, which is from -20mm to 20mm can be deduced from the figure itself. Concrete has the highest changes of the received signal in that region; the signal drops approximately 24dB. Wood and laminated wood have a slight decrease in signal at around 4dB to 6dB in this penumbra region.

In umbra region it can be seen that concrete had the highest attenuation and that there is similar attenuated rate for both types of wood.

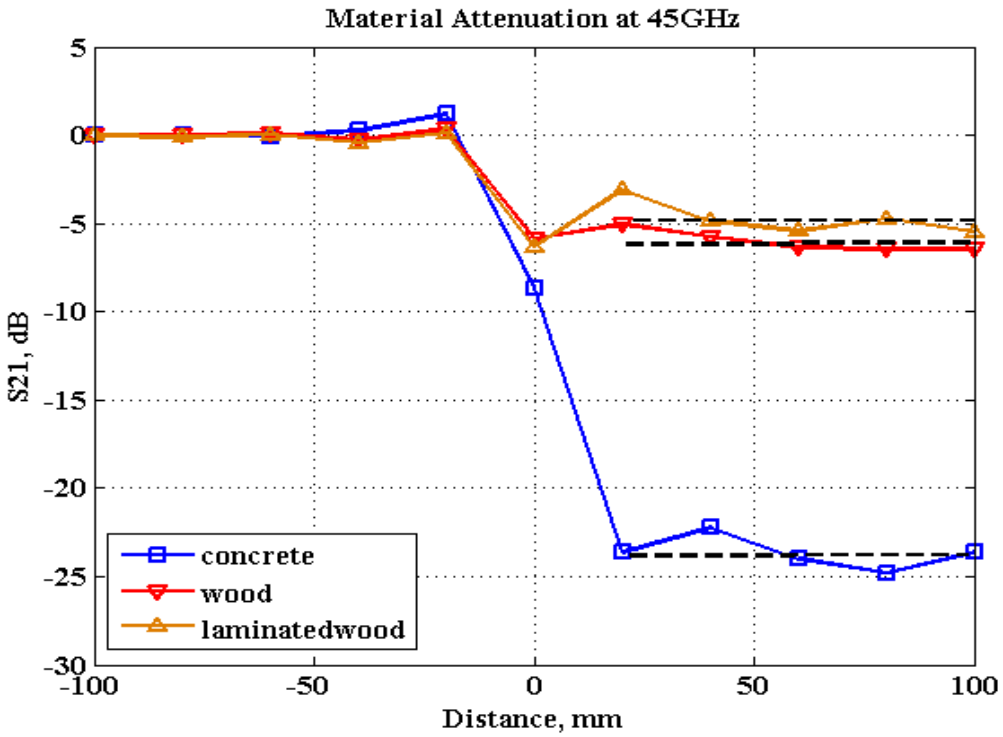

FIGURE 3.8. Transmission measurement at 45GHz

In the same figure, the average values of attenuation in umbra region was shown (black dotted lines). From these average values, laminated wood has the lowest value of

attenuation (-4.7dB) since the it has a smooth and reflective surface compared to concrete (-23.6dB) that have rougher surface.

A comparison has also been made between the materials with KED, as shown in Figure 3.9. In this figure, the horizontal axis was standardised to Fresnel parameter,v as Equation 3.7. The figure shows a very good fit of diffraction gain signal between the measured results and the calculated KED theory. The diffraction signal is crucial at v=0 where the edge or tips of the materials are. From the previous section, diffraction gain for this measurement setup is -6.02dB based on the calculation. At the same point of v, concrete has -8.65dB, while wood and laminated wood have -5.83dB and -6.34dB. Note also the concrete is thicker and less likely to follow KED as there is more of a double diffraction from the edges of the (thick) material.

to add: comparison with Tom and Alberto

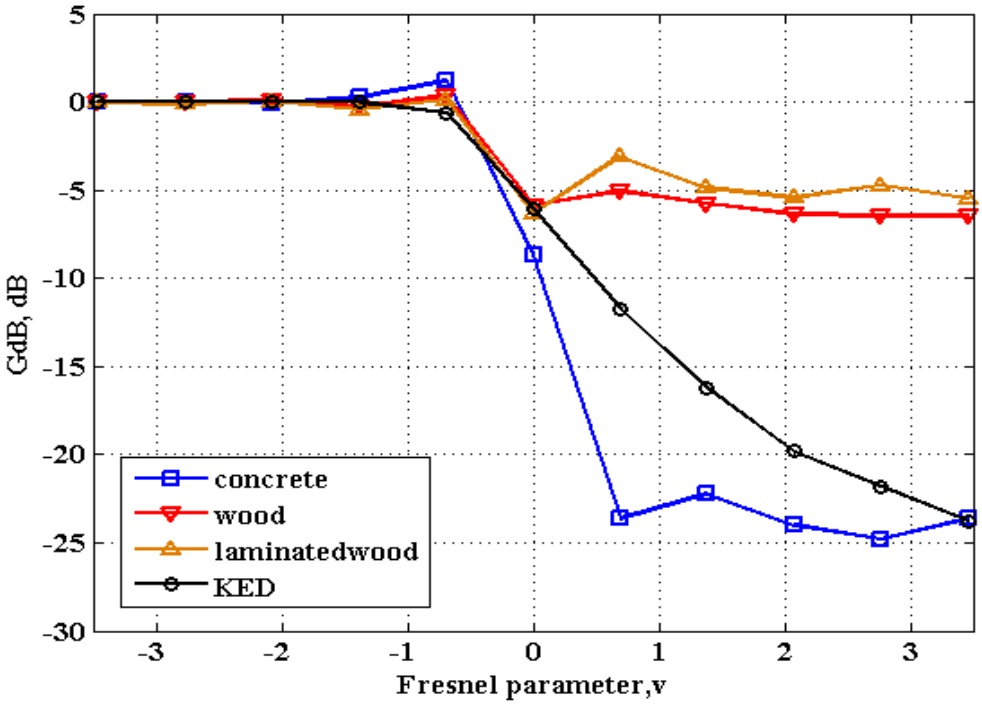

FIGURE 3.9. Material versus KED at 45GHz

Diffraction and attenuation values presented were significant in observing the propagation mechanism for small sample materials. However, there were some limitation and drawbacks identified from this measurement.

Firstly, the measurement setup, the positioner track only 200mm long, therefore it is

not enough length to cover the transition from the direct line of sight, diffraction at the edge, direct transmission and direct line of sight again for the full cycle of detection and data collections.

Secondly, the data collection. The positioner was manually operated. Consequently, the data collections also were manually recorded. The data collected and discussed in this section were agreeable but, the precision especially the resolution of the data was not certainly accurate.

As a solution, a new track was assembled (a one-metre linear track with stepper motor and fully automated). This new track will increase accuracy and repeatability of future measurements. The new track and data collections will be further discuss in the next section.

Thirdly, results presented. S21 data in this measurement was denoted as attenuation through the material. The physical meaning of S21 is the forward transmission (from port 1 to port 2) while S11 is the input reflection coefficient with the output of the network terminated by a matched load [103]. S21 is not the attenuation since any reflection will not appear in the S21 data set. Therefore it is necessary to take a step back and to measure the S11 data. However, S11 data includes antenna and sample (with distance to sample) parameters. The next section will look into this matter in depth.

3.3 Reflection model: a single port model

The fundamental knowledge of propagation mechanism is the behaviour of the plane wave as it approaches the boundary or surfaces [103]. In practical scenarios of wireless and mobile communications, radio wave will partly transmitted and partly reflected from surfaces or other obstacles on its path, as in Figure 3.10. The percentage of the incident wave that is transmitted or reflected depends on constitutive parameters of the two medium involved or in this case, the properties of the materials. From these parameters, the transmission and reflection coefficient of multipath propagation mechanism can be deduced.

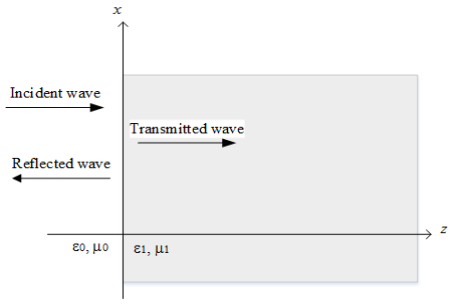

FIGURE 3.10. Transmission between 2 materials

In this case of normal incidence, the incidence wave propagation vector is along the normal to the interface between two media. In general, for smooth surfaces, radio wave will be reflected, for rough surfaces, the wave will be scattered, and for edges of surfaces, the wave will be diffracted.

Incident wave

For a general medium, with no loss of generality we can assume that the incident plane wave has an electric field vector oriented along the x-axis and is propagating along the positive z-axis. The incident fields can then be written, for z<0 as;

$$E_i = E_0 e^{-jk_0 z} \tag{3.15}$$

Transmitted wave

The transmitted fields for z>0 in the lossy medium can be written as:

$$E_t = E_{t0} e^{-jk_2 z} \tag{3.16}$$

Reflected wave

In the z<0 region, a reflected wave may exist with the form:

$$E_r = E_{r0} e^{-jk_1 z} \tag{3.17}$$

From these equations of incident, transmitted and reflected wave, the reflection r and transmitted coefficient t can be deduces as:

$$r = \frac{E_r}{E_i} \tag{3.18}$$

$$t = \frac{E_t}{E_i} \tag{3.19}$$

In this study, the reflection measurement for small sample materials can be modelled as a single port or one-port network. The input of the one-port network of a transmitting antenna is connected to a wireless channel or free space and followed by a small sample material and follow the same path for its output. The schematic diagram of the model is shown in Figure 3.11.

In general, a network has two ports; one port is represented as the input terminals, and the other denoted as the output terminals. Such networks are very beneficial in the design of transmission systems, a control systems, communications systems, and others where electric energy or a signal enters the input ports, it is altered by the network, and it exits through the output ports.

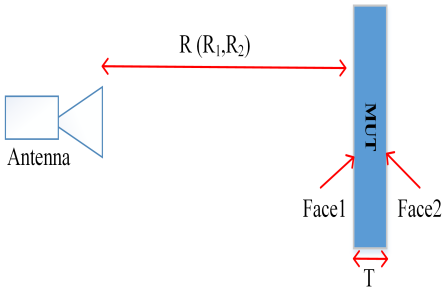

FIGURE 3.11. Schematic diagram for model development

Based on the schematic diagram, a transmission line circuit network symbolise all the parameters are being established as shown in Figure 3.12. A signal flow graph (SFG) has been deduced to solve the network [103]. The SFG is introduced as a graphical means to visualise how waves propagate in an RF network. A generalised parameter has been assigned to the port and the nodes.

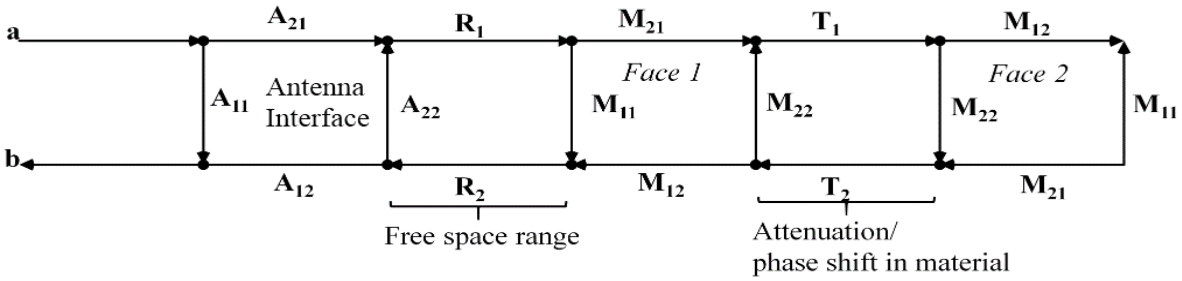

FIGURE 3.12. Signal flow graph for one-port network analysis

A signal flow graph is a graphical presentation that consists of nodes that are connected by branches. The main advantage of using signal flow graph is that it provides a method for simplifying or reducing any network, in this case, microwave network to more fundamental form or transfer function [103].

The scattering parameters are set for the antenna and small material accordingly. The parameters are as follows:

Table 3.2: Parameters of the model

Parameters	description
A_{11}	antenna input response
$A_{12} = A_{21}$	antenna reciprocity
A_{22}	antenna scatter
$R_1 = R_2$	range/distance from antenna to MUT (free space)
$T_1 = T_2$	thickness of MUT (attenuation in the sample)
M_{11}	Face 1 of MUT
M_{22}	Face 2 of MUT
$M_{12} = M_{21}$	signal at the boundary (air to sample)

*Face 2 is mirror image of Face 1

The model will consider the propagation from the transmit antenna to a line of sight towards the sample material for both surfaces (Face 1 and Face 2) then reflected back with the same path. The analysis will focus up to Face 1 to show how the complex circuit can be reduced to a simpler network using signal flow graph decomposition rules to determine the input reflection coefficient τ_{in} as shown in Figure 3.13.

In this model, each port is represented by two nodes,“a” and “b”;“a” node represents the value of incident wave on that port, and “b” represents the value of exiting wave from that port.

The input reflection coefficient τ_{in} is defined as Equation 3.20:

$$\tau_{in} = \frac{b}{a} \tag{3.20}$$

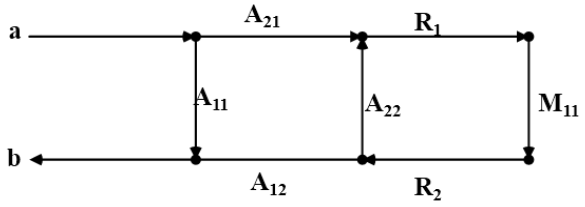

FIGURE 3.13. Network analysis up to Face 1 (assuming no internal material reflections)

Figure 3.14 shows how the signal flow graph being reduced using the decomposition rules. There are four rules to reduce the signal flow graph; series rule, parallel rule, self-loop rule and splitting rule [103]. In Figure 3.14(a) and 3.14(d), series rules has been used solve two in-series paths, while, the self-loop rule has been applied in Figure 3.14(b) and 3.14(c) to simplify the feedback loop.

Figure 3.15 shows the final flow graph after decomposition. From the figure, the final Equation 3.21 can be deduced.

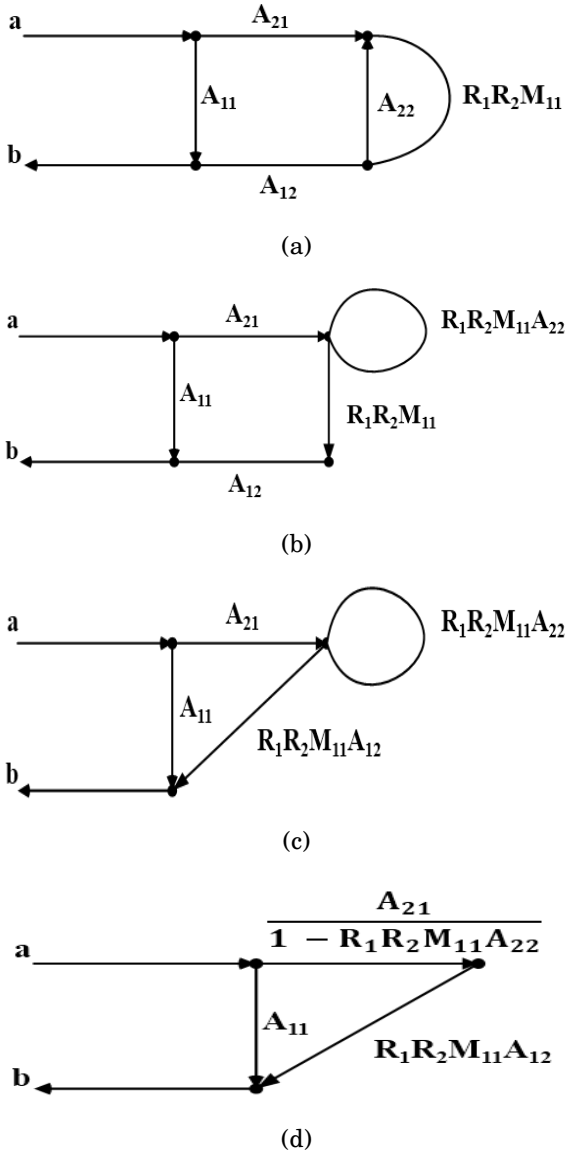

Figure 3.14: Signals flow graph derivation

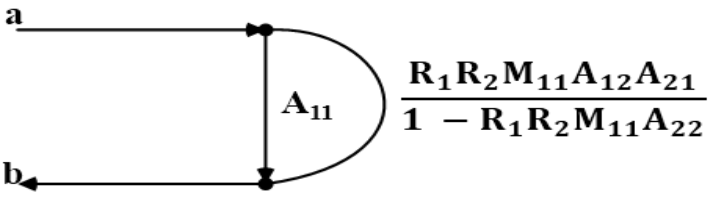

FIGURE 3.15. Final diagram to solve the SFG

From the last diagram, τ_{in} can directly be solved as:

$$\tau_{in} = \frac{b}{a} = A_{11} + \frac{R_1 R_2 M_{11} A_{12} A_{21}}{1 - R_1 R_2 M_{11} A_{22}} \tag{3.21}$$

Equation 3.21 infer that, reflection coefficient τ is directly proportional to antenna input response (A_{11}) and with the influence of other parameters.

3.3.1 Model validation to analyse the measurement results

Based on the collected S11 data, Equation 3.21 can be written as Equation 3.22; where reflection coefficient τ can suited to be S11 as represent in equation 3.22. S11 is now given as the S11 parameter of the network analyser.

$$S_{11} = A_{11} + \frac{(R_1 R_2)(A_{12} A_{21}) M_{11}}{1 - (R_1 R_2) M_{11} A_{22}} \tag{3.22}$$

From the transmitter or input side, it shows that the reflection coefficient is proportional to the distance apart, antenna reciprocity and reflection at Face 1 of MUT. The calibration process starts with rearranging the equation or group the S11 with A11 (the antenna input response) as in equation 3.23

$$S_{11} - A_{11} = \frac{(R_1 R_2)(A_{12} A_{21}) M_{11}}{1 - (R_1 R_2) M_{11} A_{22}} \tag{3.23}$$

A_{22} is assumed to be negligible and reduced to zero to allow a first simple reordering of the equation. In reality this is the related to the radar cross section of the antenna structure and its inclusion may introduce some frequency-dependent ripple into the results.

Since metal plate will be the reference MUT, therefore two conditions need to be investigated.

The first condition when direct transmission between transmitter and receiver, M_{11} = 0 when is no sample and therefore only the antenna is giving rise to a non-zero S11, hence;

$$S_{11} = A_{11} \tag{3.24}$$

The second condition when metal plate is the MUT, M_{11} = -1 (short circuit), hence:

$$S_{11(sc)} - A_{11} = -\frac{(R_1 R_2)(A_{12} A_{21})}{1 - (R_1 R_2) M_{11} A_{22}} \tag{3.25}$$

$$S_{11(sc)} - A_{11} \approx -R_1 R_2 A_{12} A_{21} \tag{3.26}$$

The assumption to be made is $R_1 R_2 A_{22} \ll 1$; this is the condition where the material distance between transmitter and receiver are kept constant R1=R2 and antenna scatter A_{22} is ignored.

The equation aims to prove that the reflection at the face of MUT is proportional to the S11 of the signal with the elimination of the metal plate reflection signal. Rearranging the equations, resulted in:

$$S_{11} = A_{11} - (S_{11(sc)} - A_{11}) M_{11} \tag{3.27}$$

$$M_{11} \approx -\frac{S_{11} - A_{11}}{S_{11sc} - A_{11}} \tag{3.28}$$

Equation 3.28 shows that the surface reflection at face 1 of the material is comparative to the S11 received signal with a background subtraction of received signal of the metal plate.

The actual M11 will depend upon the size of the metal plate since diffraction, distance to sample and antenna beamwidth may all be expected to have an impact here.

In the next section, the new transverse measurement setup will be discussed and the results obtained will be matched with the equation 3.28 of reflection model.

3.4 Transverse Wideband Measurement for Surface Reflection Analysis

In this section, the aim is to use the same concept setup as in the previous section to investigate the surface reflection propagation. This study focuses on the wideband frequency range of 45GHz to 65GHz. Material under test in this section will concentrate on a metal plate, concrete (two different surfaces) and ceramic tiles supported on a plasterboard backing. In this measurement, metal plate is used as a reference material for MUT. A new automated movable platform that clamps the MUT was designed to create an easy method to scan the surface of MUT with minimal supervision. Although wideband measurements have been undertaken, a single frequency will be used to show the measurement, calibration process and the initial data analysis , before the full distance-frequency data is presented.

3.4.1 Procedure of Measurement and Data Collections

In this measurement, the manual operated track was replaced with a linear positioner. The linear positioner, as shown in Figure 3.16 is 1 metre long with a platform to hold the vice capable of 100mm opening. The positioner and the platform are connected to a stepper motor at the end of the track. A 0.01 degree per step stepper motor was used with an ESP301 Motion Controller to achieve the precision needed. Matlab scripts were written to ease the procedures and data collection. The Matlab code controls the movement of the ESP301 motor and synchronously recording the VNA data at specific position programmed.

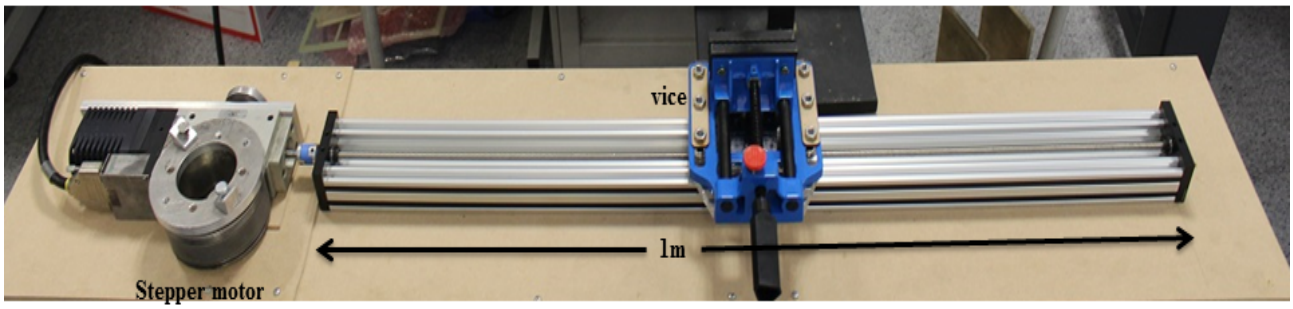

FIGURE 3.16. Linear positioner with platform to hold MUT

This new setup was assembled at the same area as the previous measurement; the

small area in front of Vector Network Analyser (VNA) in CSN laboratory. In this setup, only port 1 is connected to the antenna (antenna details are given previously). In this measurement, S11; the reflection coefficient were recorded at every stop points of 2mm.

Two new materials were introduced; metal and ceramic tiles as in Figure 3.17. Since in this section, the main observation will be the reflected signal on the surface material, the selections of these two materials are appropriate. Metal is also a common material for modern building. There is increased use of metal shielded materials (aluminium foils) in modern constructions to provide thermal isolation and fulfil with the new energy-regulations [35].

Ceramic tiles are common construction material, especially for indoor use. Ceramic tile is made from natural clay, water and sand and moulded to form a square or rectangular tiles. In this measurement, four tiles (plus two strips) are pasted onto 1cm thick plasterboard so here both tiles and grouting are a factor in the measurements. Hence both the effect of the tiles themselves and the grouting joint between the tiles will be featured in the measurement. Noted that there also some cracks (scratches) on the surface of the tiles that may contribute to the reflection measurement.

Table 3.3: Material under test (MUT)

Material under Test (MUT)	Size/cm	Thickness/cm
Metal plate	40x40	<1.0
Ceramic Tiles	40x40	2.0

(a) metal plate (b) tiles

Figure 3.17: Additional samples (MUT)

In addition to these two new materials, a concrete slab that been used in the previous measurement will be further analysed. This concrete slab has two different types of surface, one with a rougher side compared to the other side as shown in Figure 3.18.

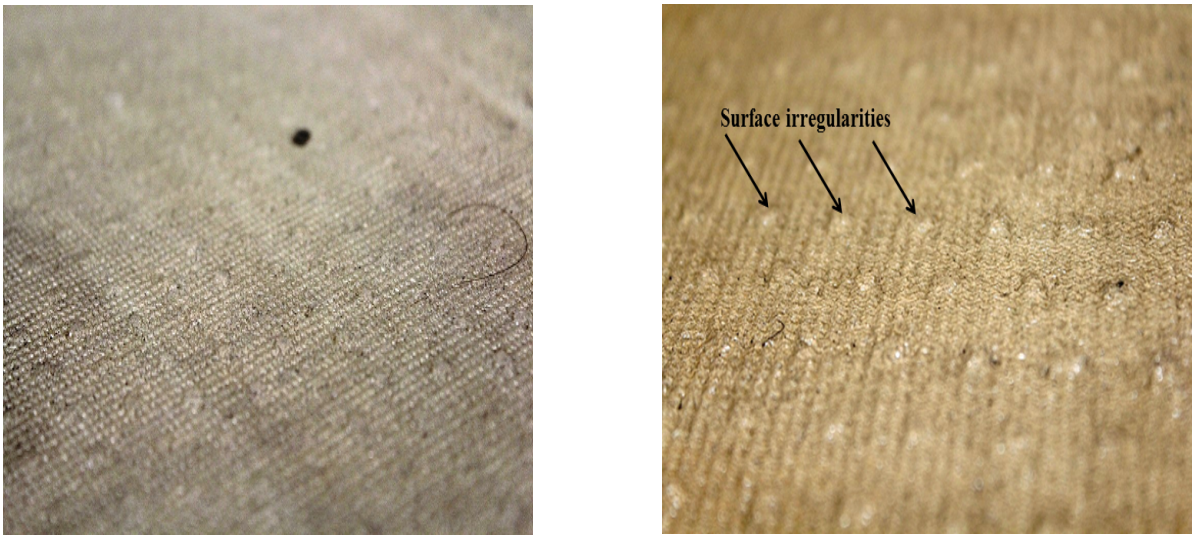

(a) Smooth Surface (b) Rough Surface

Figure 3.18: Photos of Different Types of Concrete Surfaces

3.4.2 Results and Discussions

The platform that holds the MUT was programmed to move a total distance of 500mm along the track and data was collected at every 2mm. As the platform moves pass the antenna, the reflected power changes. As the edge of the material moving closer towards the antenna, the signal increase as it reflected onto the edge and back to the antenna. The signal will stabilise when it is reflecting at the main surface area of the MUT and will decrease when it moves away from the antenna.

Single frequency analysis

Based on the collected data set, the analysis will first be presented in two dimensional (2D) figures of the received signal of S11 versus distance travel for a single frequency (centre frequency) of 55GHz. The discussion will cover sample size prediction based on the observed received signals and the calibration process to determine the reflection coefficient of the sample materials.

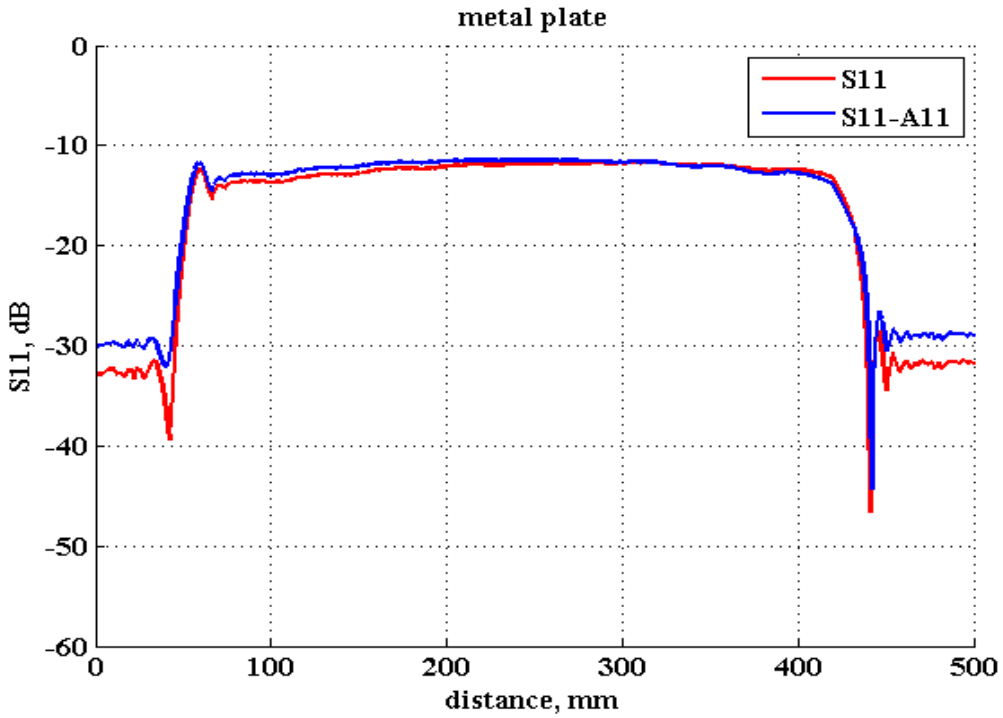

FIGURE 3.19. Metal plate at centre frequency 55GHz

First, data collected for the metal plate was presented for the metal plate reference. The calibration process will be based on equation 3.24 and 3.25. Figure 3.19 shows the

raw data (S11) and the normalised data (S11-A11). This data was normalised to the reference data set (the line of sight data); a condition where there is no sample material on the platform. From this, the same procedure will then be used for other sample materials in order to determine the respective reflection coefficient of the materials.

Based on the same figure, the predicted dimension of the metal plate can be deduced. This was done by taking the first edge at 60mm and the last edge at 420mm. The calculated dimension was tabulated in Table 3.4. This is slightly higher than actual dimensions as this is based upon an approximation of the 'diffraction curve' at the edge of the metal plate.

Figure 3.18 show two different surfaces of the concrete slab (smooth and rough). Based on these differences, there will be a variation of the received signal over distance travel for both surfaces. Figure 3.20 shows the irregularities of the signals. The irregularities are significant on the rougher surface. There are approximately 3dB drops or variation of the signal between both surfaces.

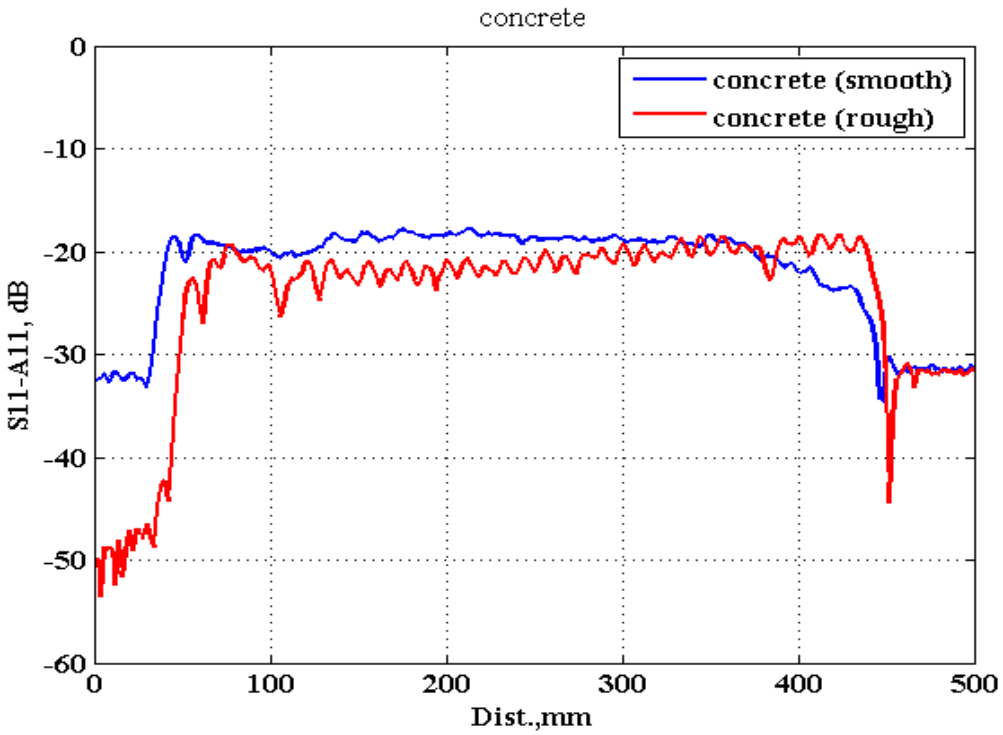

FIGURE 3.20. Concrete Surface Comparison at centre frequency 55GHz

The edges detection were made separately for both surfaces. For the less rough surface, the first edge is at 46mm, while the rougher surface starts at 76mm. Their

last edge ends at 430mm while the rougher surface ends at 436mm. There is a slight difference in the dimension of approximately 2cm of length. The rough surface of the concrete has the shorter edges as the peak/edge tends to delay as tabulated in Table 3.4.

The reflected signal for tiles is depicted in Figure 3.21; there are six edges detected (equivalent to three tiles) as for how the tiles being glued on. The low dips in the data set show the positions of the grouting between tiles. Note that the received signal varies probably as a function of the separation of the tiles, the edge distortions of the individual tiles and the thickness of the grouting. Furthermore, the scratch that appeared on the surface of the tiles as in Figure 3.17 also contributes to the irregularities of the signal received.

The second tile, as expected will be the perfect size tiles as the placement is in the middle, while the first tile and the third tile strip will be smaller because of the first and the last edges. The predicted dimension is 30cm while the dimension from Table 3.1 is 40cm. The difference of approximately 10cm maybe because of the placement of plasterboard at the back of the tiles that not evenly placed and diffraction at the edges of the tiles.

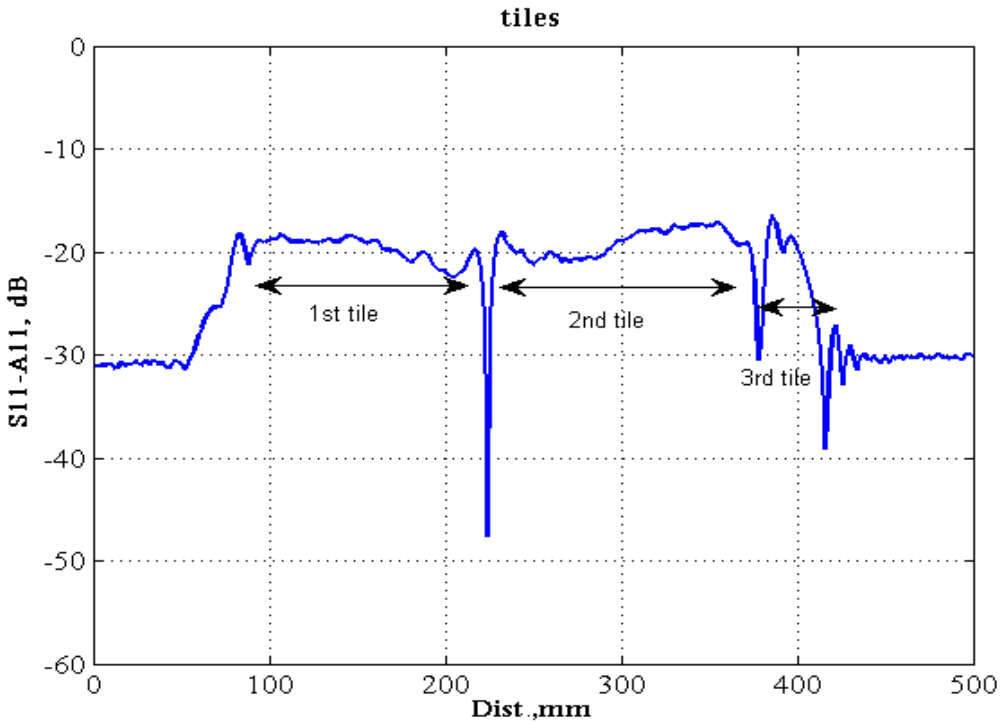

FIGURE 3.21. Tiles at centre frequency 55GHz

The edge detection for all materials was determined using the identification of the first highest data point(signal) as the sample moved, and on the other end at the point where the signal starts to drop. The difference in length of these two edges was then compared with the dimension of the sample as Table 3.17. The differences of a few centimetres in all sample materials assumed to be because of the signal be diffracted instead of reflected. Noted that Figure 3.20 and Figure 3.21 show the S11 - A11 values.

Table 3.4: Edge detection and length estimation of sample material at centre frequency 55GHz

Material	**1st edge**	**2nd edge**	**predicted dimension (cm)**	**dimension as Table 3.1 and Table 3.3 (cm)**
Metal plate	dist = 60	dist = 420	36	40
	-11.19dB	-14.02dB		
Concrete	dist = 46	dist = 430	38.4	40
	-18.49	-23.39dB		
Concrete with rough surface	dist = 76	dist = 436	36	40
	-19.31	-18.59		
Tiles: 1st tile	dist = 92	dist = 216	12.4	40
	-18.38	-21.15		
Tiles: 2nd tile	dist = 232	dist = 372	14	
	-17.31	-19.6		
Tiles: 3rd tile	dist = 386	dist = 422	3.6	
	-16.46	-27.17		

For further analysis, normalisation to the maximum value of metal plate was conducted for all materials. This is the condition where the metal plate levels are around 0dB (and its average value taken across the region where the diffraction is small (200mm to 300mm) and all other materials data is referenced to this value. This to satisfied Equation 3.28. Figure 3.22 shows all sample materials with background subtraction of metal.

From this figure, the average values of M11 between the distance range of 200mm to 300mm (where diffraction ripple has settled down) were calculated and tabulated in Table 3.5. Based on the table, tiles have the highest reflection coefficient compared to concrete for both surfaces. The irregularities of the concrete surface (rough) that make the signal tends to reflect in random order that may cause the lower value of the reflected signal.

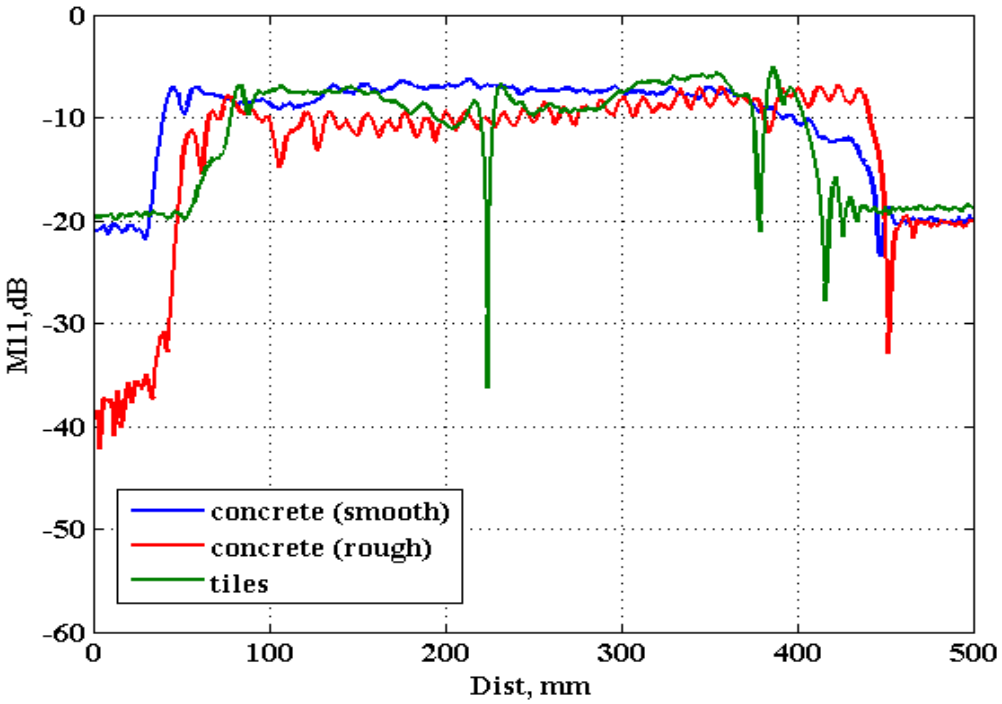

FIGURE 3.22. M11 of materials at centre frequency 55GHz

Table 3.5: Average M11 of materials at centre frequency 55GHz

Material	Average of M11
Concrete	-6.3
Concrete with rough surface	-6.9
Tiles	-5

Wideband frequency analysis

The analysis shown so far has just concentrated on the processing of one frequency set of data. These measurements were for the range 45GHz to 65GHz and hence the processing describe was applied to the whole of the frequency data set. This analysis aims to observe how reflectivity changes over a wide frequency range. The 3D figures presented here are the raw data, S11 (dB) and normalised to the direct line of sight, S11-A11 (dB) over a travelling distance of 500mm. Changes in colour represent the changes in relative received power over the distance travel.

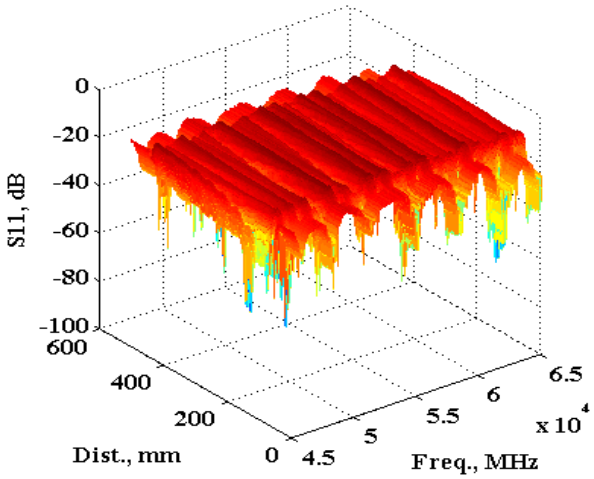

(a) S11 - Metalplate

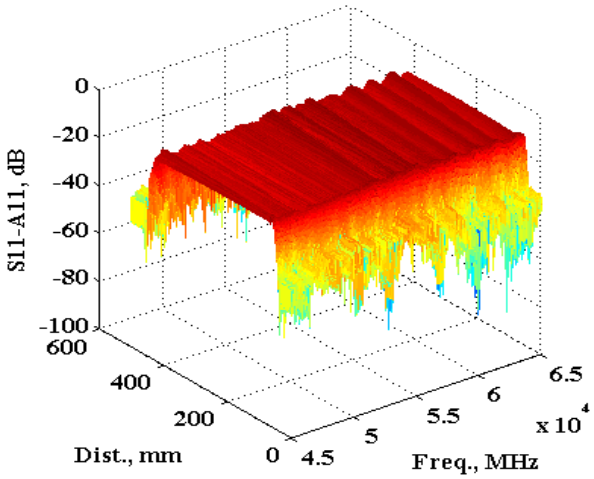

(b) S11-A11 - Metalplate

Figure 3.23: Metalplate at wide frequency of 45GHz to 65GHz

Figure 3.23 shows the raw data of the metal plate. The 2D figures from the previous analysis show the edges based on the first maximum signal appeared and the last peak signal before its start to drop. In these 3D figures, that features still can be observed and its constant throughout the wideband frequency range.

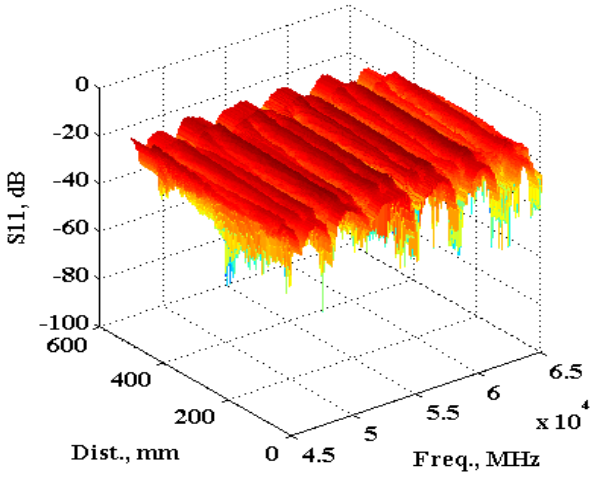

(a) S11 - concrete

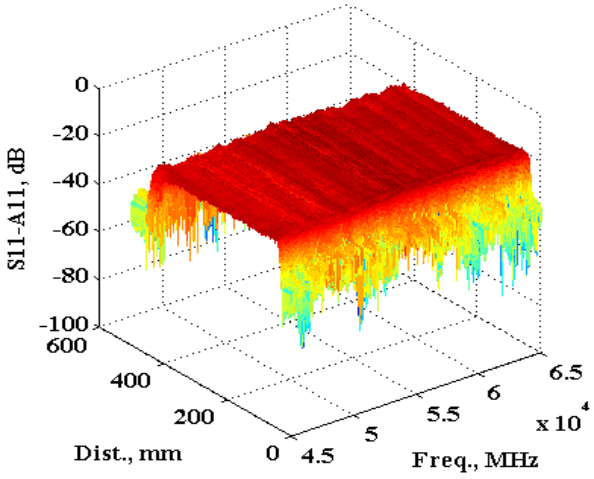

(b) S11-A11 - concrete

Figure 3.24: Concrete (smooth surface) at wide frequency of 45GHz to 65GHz

Figure 3.24 and Figure 3.25 show the S11 and S11-A11 data for both surface of the

concrete slab. Amount of ripples in concrete with a rough surface are more significant throughout the frequency and appear as sinusoidal random ripples. In the rough surface, the signal reflected and transmitted in several different directions compared to the less rough surface. The amount of directions that the signal reflected depends on the degree of roughness or the dimension of the irregularities itself.

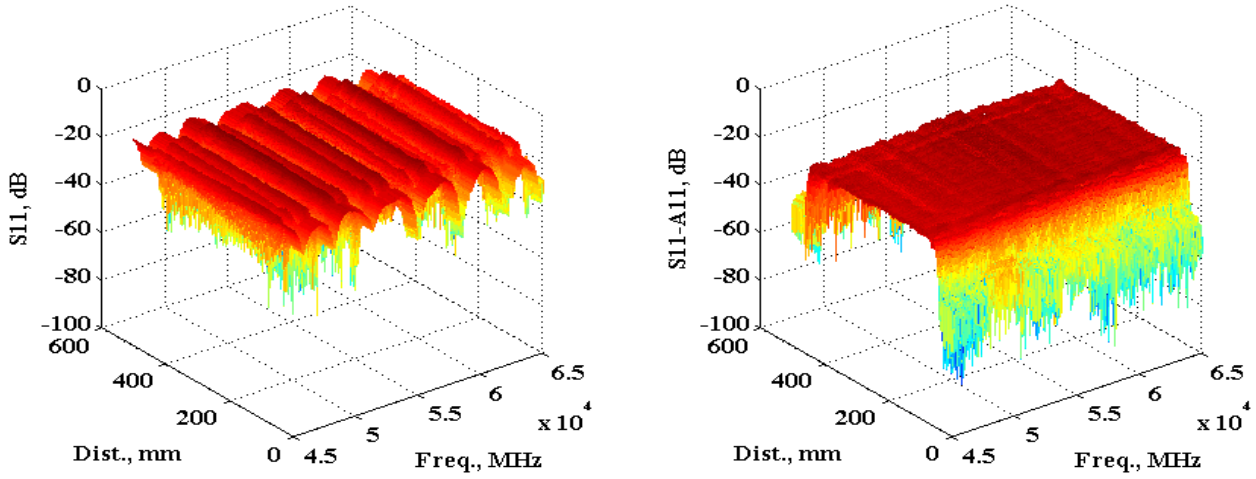

(a) S11 - concrete rough

(b) S11-A11 - concrete rough

Figure 3.25: Concrete (rough surface) at wide frequency of 45GHz to 65GHz

Figure 3.26 shows raw data of tiles over a wideband frequency. The same effect in 2D figure for single frequency can still be observed.

The 3D data set for materials reflectivity with respect to metal plate are shown in Figure 3.27. It can be clearly seen even from this small set of material samples that the material surface roughness and construction as well as the material bulk properties affect the (normal) reflectivity of the material. Average values and variants (upper lower levels depending upon frequency and roughness) will therefore be required in material description for deterministic model.

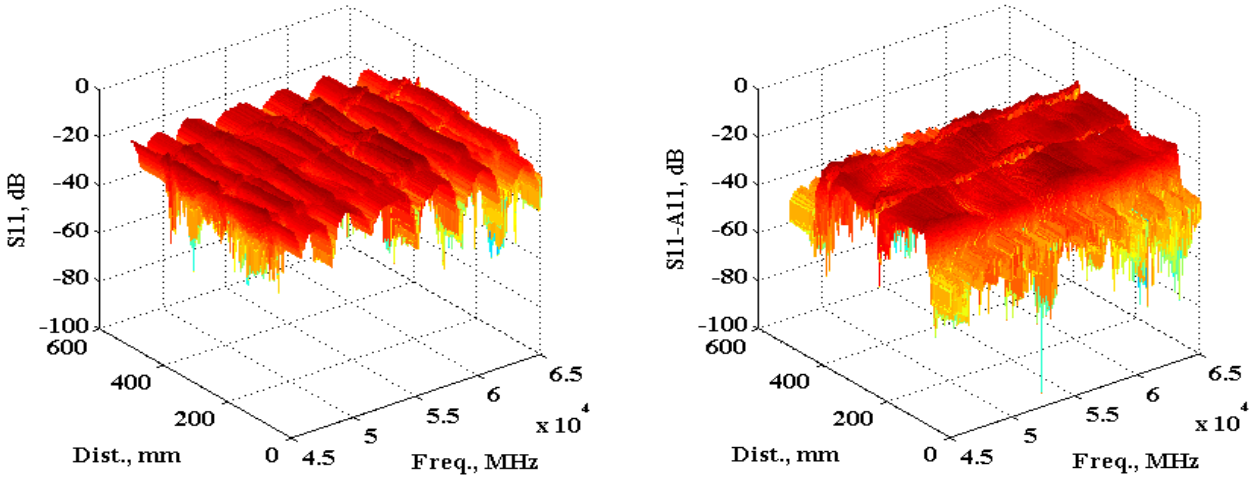

(a) S11 - tiles

(b) S11-A11 - tiles

Figure 3.26: Tiles at wide frequency of 45GHz to 65GHz

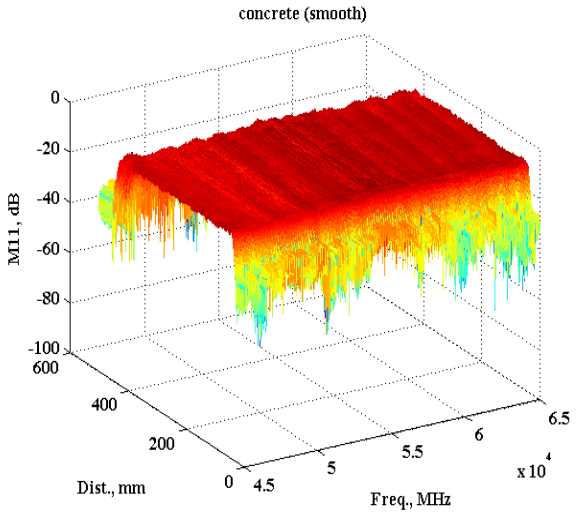

(a) M11: concrete (smooth)

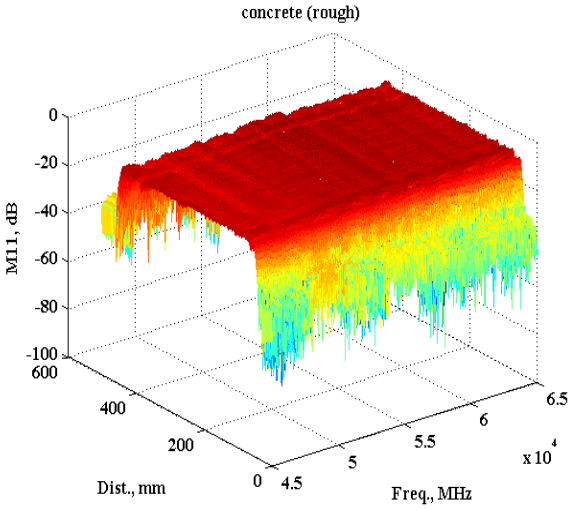

(b) M11: concrete rough

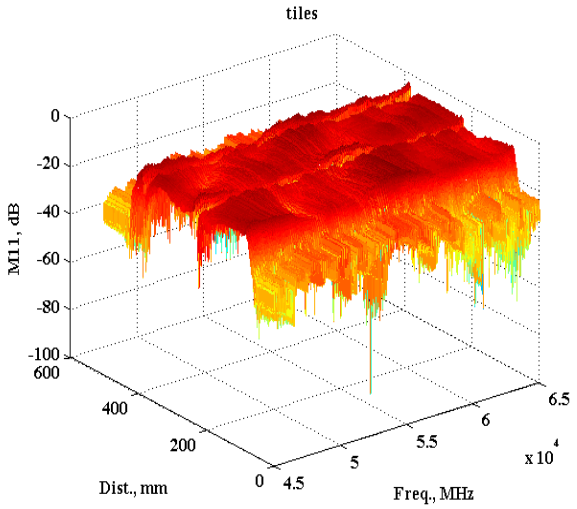

(c) M11: tiles

Figure 3.27: 3D plots of M11: Materials at wide frequency of 45GHz to 65GHz

3.5 Conclusion

This chapter has presented the short-range transverse propagation measurements for material characterisation analysis in the indoor laboratory area at a frequency range of 40Hz to 50GHz. The Knife-edge diffraction (KED) is a suitable method to model the diffraction observed in the material sample measurements at the penumbra region before entering the umbra region.

Three sample materials have been used for the initial measurement with 20mm resolution, and additional two materials were used in the wide band measurement with a finer resolution of 2mm. Outcomes from these materials showed success with diffraction and attenuation, but in order to fully understand attenuation, reflection of the materials need to be acknowledge first.

A further measurement study using a programmable finer-resolution material surface scanner for detailed reflectivity measurements has been conducted. This wideband frequency measurement (45GHz to 65GHz) shows that the reflected signal was dependent on surface roughness. When a wave hits on a rough surface, waves scattered in all directions. This reduces the reflection directly back to the receiver but does not identify the direction of the scatter. Furthermore, the reflected signal contains frequency-varying diffraction ripple that has to be taken into account in the data processing. Average of the reflection coefficient, M11, with respects to metal; results in approximately 6dB difference for concrete of both surfaces and 5dB different for tiles. Differences between surface irregularities of a concrete slab also contributed to the value of reflection coefficient (0.6dB different). Average of M11 over a wideband frequency provides the outcomes of reflection coefficient as the frequency increases.

The wideband measurement used a metal plate as reflector references (short circuit), but this is not an ideal condition because of this of size limitation (40x40cm). The observation did not account for material thickness and the signal travel in the material (attenuation), and hence the latter work focused on reflectivity. For future works, the larger size of metal needed to eliminate the effect of diffraction especially at the edges.

This study has only identified the benefits (and limitations) of the technique to determine material properties from small samples. Additional measurements with various type of materials (and thickness) are needed to increase the reliability and validity of surface materials towards the received signals. For future works, the larger size of metal needed to eliminate the effect of diffraction especially at the edges. Development of the deterministic model needs to take into account the average reflectivity across the

material.

CHAPTER 4

ANGULAR BASED MEASUREMENT FOR MATERIAL SCATTER CHARACTERISATION

The previous chapter has identified that an understanding of the reflective properties of materials is essential before factors such as material attenuation can be considered, simply because the amount of signal penetrating the sample material (air-sample interface) must be accurately known. The study only considered the normal incidence signal at millimetre wave frequencies and materials surface features can be responsible for scattering away from the normal. Hence the level of signal penetrating the sample cannot be completely measured from the normal-incident measurements as performed in Chapter 3.

As reviewed in Chapter 2, the setup when either the transmitter or receiver is fixed, or the other one is movable (in angular form) was the common measurement setup for the detection of reflection mechanism both specular and diffuse scatter either indoor or outdoor scenario in higher frequency bands.

However, to fully characterise a sample, all angles of departure from a sample for all possible angles of arrival (in both θ and α) needs to be undertaken, Furthermore, the irregular nature of most materials and the frequency-dependent of the scatter needs to be taken into account with wide-band measurements of a number of samples of over a wide area of one sample to produce average values of scatter and some idea of limits of scatter of a sample. This is clearly a mammoth task since the data may also be dependent upon the size of the sample (i.e. diffraction as highlighted in Chapter 3).

This chapter provides the different setup and procedures of angular measurement

for material reflection characterisation. The material under test rotates (angular) while the transmitter and the receiver are kept stationary.

Section 4.1 will starts with angular measurement in a controlled environment of the anechoic chamber. Measurements were conducted at a frequency of 20GHz. However, measurement at lower frequency also has been conducted to observe the trends in beamwidth as the frequency increases.

The method consists of illuminating a sample material and using a second antenna to receive the signal from the sample that is positioned 90° with respect to the transmit antenna. The calibration of the measurement range and processing of the data is presented with the means to identify the reflectivity versus angle (scatter) at frequency of 20GHz and a number of samples are considered: metal, concrete and wood. This 'raw' data is then processed further in Section 4.2, and the relative features with respect to the metal reflector are established as a means to remove range path loss (for the chamber's 5m range).

Section 4.3 presents the measurements for a much shorter range and without the need for the anechoic chamber. The same measurement process was used for samples materials at 20GHz and 60GHz, though with here smaller samples sizes were used. Samples here included metal plates, concrete, wood and ceramic tiles. The tiles were actually a number of tiles (approximately 2x2) with grouting in between and mounted on the plasterboard.

The analysis continues for a different type of materials and comparison between the various size of the metal plate. The results will be calibrated, analysed and presented and measurement validation based on the comparison from the anechoic chamber measurement was performed before the chapter ends with a summary of contributions.

4.1 Angular Measurement Setup: Reflection and Material Properties Analysis

This section will describe the angular measurement process. These angular measurements are conducted in a controlled environment of an anechoic chamber at a frequency range of 5GHz to 22GHz. This section aims to examine the reflection (normal and diffuse scatter) effect for material under test as the material rotates.

The measurements are performed over a 5m range with two antennas located at either end of the 5m range and placed at 90° to each other pointing towards the sample. Measurements of metal, wood and concrete were undertaken at varies frequencies with metal plate primary acting as (perfect reflector) reference for the other samples. Measurements are a performance for 'azimuth only', though samples could potentially be rotated so that other planes could be analysed.

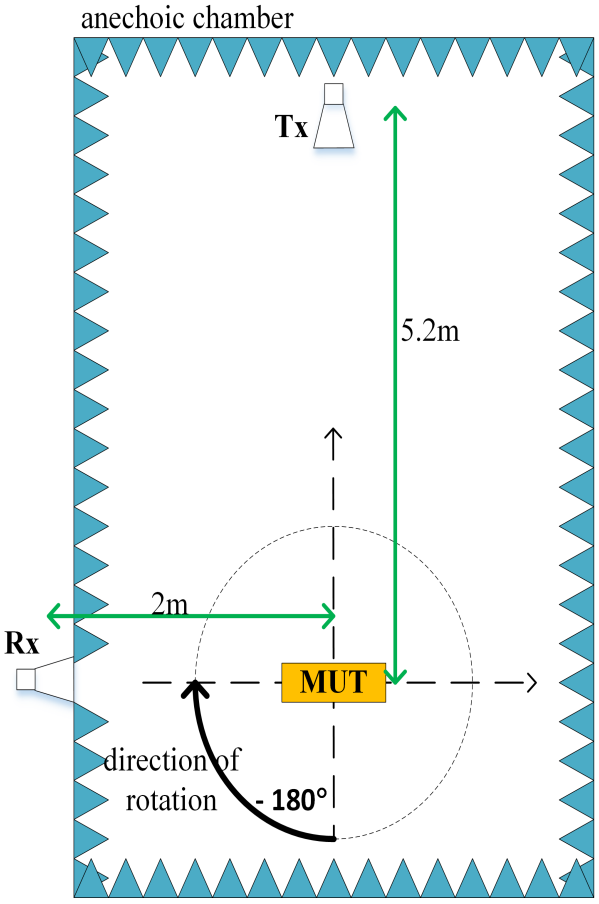

FIGURE 4.1. Measurement setup in anechoic chamber

4.1.1 The measurement setup

The angular measurement was conducted in the University of Bristol's pyramidal-cone anechoic chamber. The chamber was designed and certified by Emerson Cuming with a dimension of 8m (long) x 5m (wide) x 4m (high) [104]. The anechoic chamber provides a controlled environment where both the antenna and measurement devices are isolated from outside multipath signals and interference.

The transmit and receive antennas are identical wideband horn antennas that can transmit separately two polarisations and are connected to the ports on VNA. The wideband antenna is the circular horn with 3dB beamwidth of 10° at 18GHz and aperture diameter of 135mm.

The material under test is placed at a distance of 5.2m from the transmit antenna and is fixed on a rotating stand. The rotating stand of 1.5m high is mounted on a turntable, which can be automatically rotated from −180° to 180° by the use of motors. The transmit antenna mounted on the pole of 1.3m high and at a right angle to the receiving antenna. The receiver antenna is placed at the chamber door, 2m away from the rotating stand pointing directly to the centre point of material under test. Figure 4.1 illustrate the setup as in the anechoic chamber.

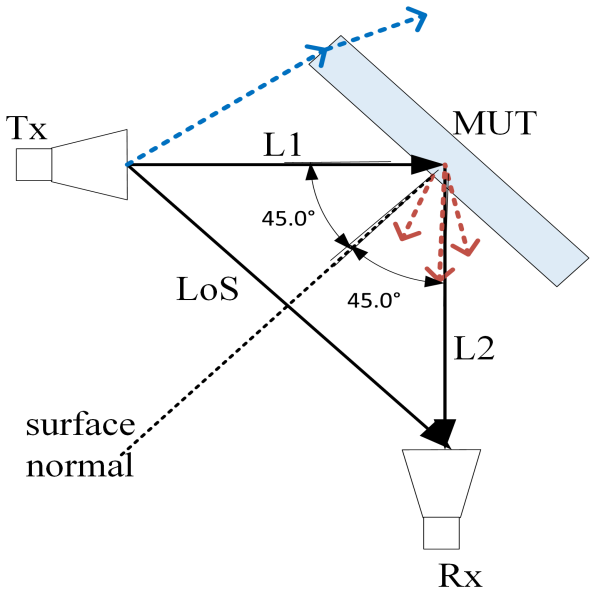

FIGURE 4.2. Schematic diagram of reflections and direct transmission path between transmitter and receiver (diagram not to scale)

Figure 4.2 shows the schematic of the setup with possible reflection and illumination

on the MUT. Based on this figure, there are three main paths of LoS, reflected from MUT (main body) and diffraction from all edges. The reflected is therefore subject to diffuse scatter. LoS is the direct transmission path between the transmitter and the receiver antennas. L1 is the incident path, while L2 is the reflected path. The black arrows shows the ideal condition when the incident and reflected angle at 45°; while the red arrows indicate the possible reflections for diffuse scatter reflections and the blue arrows indicate the possible diffraction at the edge of the material.

Figure 4.3 show the setup of the three setup positions of angular measurement as seen from the receiver position. In the figures, as an example; 4 concrete slabs were fixed onto the rotating stand and rotated from $-180°$ to $180°$ in a counter clock-wise direction. The stand is 1.5m high and was designed to hold a maximum of four blocks of concrete slabs with the total size of 80cm x 80cm.

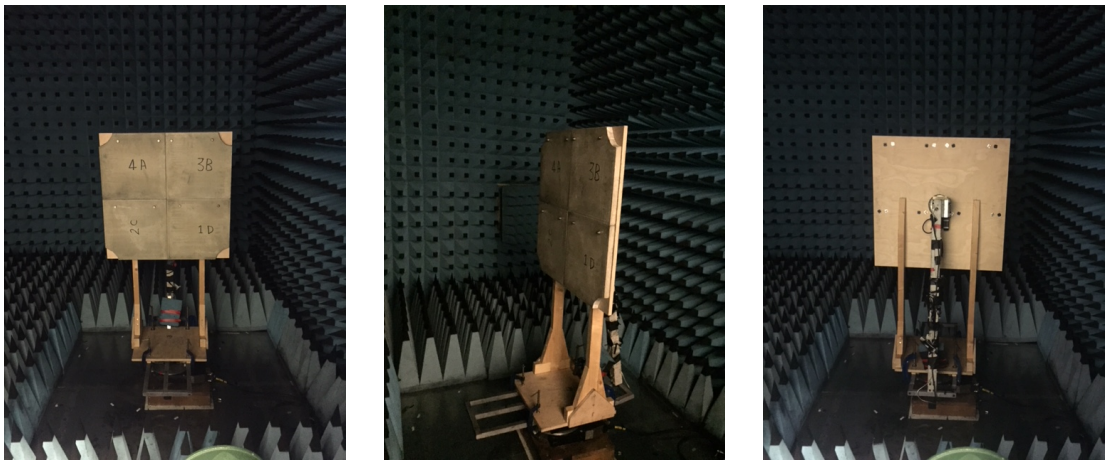

(a) $-90°$ (b) $0°$ (c) $90°$

Figure 4.3: Three setup positions of angular measurement as seen from the receiver

It can be seen in Figure 4.3 that by keeping the antennas fixed and moving the sample, the angle of arrival (illumination) normal to the material surface and the angle of departure of the 'main' signal normal to the surface add up to the 90° orientation of the two antennas.

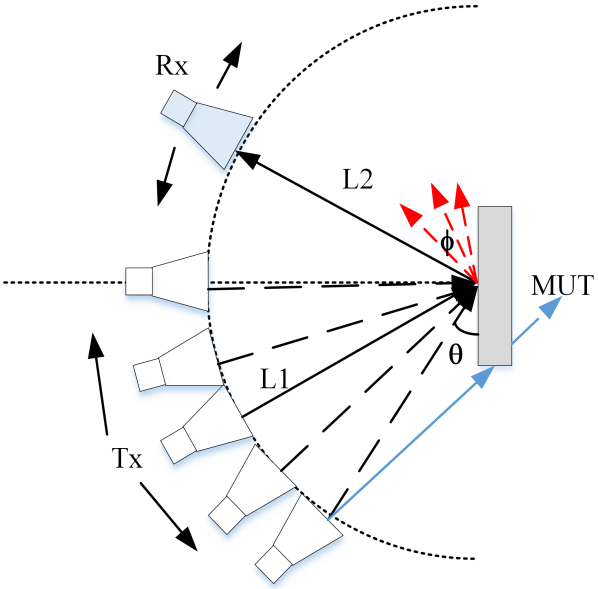

FIGURE 4.4. Schematic diagram of fixing the sample and moving the transmit and receive antennas in all incident angles (diagram not to scale)

This is not the same as fixing the sample and moving the transmit and receive antennas in all incident angles as in Figure 4.4. It is therefore clear that only a sub-sample of all possible angles for the transmit and receive antennas are possible here. Here 'azimuth' only is considered, though the reality is that the material characteristics will depend upon its area and hence a 3D version would be required (with elevation) for complete material characterisation. So only azimuth is considered in this work. The drawback is that not all angles can be determined, though enough can be in order to suitably understand the nature of the material reflectivity. However, keeping the antennas fixed, as with the method described in the previous chapter, means that cable movement is not an issue that will result in signal level fluctuations.

4.1.2 Metal plate as calibrated reference

The issue with all practical measurements is the ability to produce robust (repeatable) measurements and to be able to calibrate to remove measurement uncertainly or for range/equipment calibration. The calibration of the range therefore requires the use of a reference sample material (in the same way that for VNA calibration a short circuit is used to identify distance). Ideally the sample should have infinite area (clearly not possible), but should be sufficiency large to be illuminated by the transmit antenna and

its reflectivity suitable focussed to the receive antenna with sufficient power to give a good dynamic range for the material comparisons.

In this section, the analysis of metal plate for various frequencies was conducted. A metal plate of size 70cm x 70cm was placed on the rotating stand and rotated in 1° step from −180° to 180° as in Figure 4.3. Four different frequencies of 5GHz, 15GHz, 20GHz and 22GHz have been chosen for comparison, and several features can be identified from these data.

Although ideally the work would concentrate on the K band 18-27GHz, the limitations of the horn antenna available and losses due to cabling and amplification requirements dictated the actual frequencies chosen, though the range allowed useful comparison of the frequency-dependent effects of the sample (physical and electrical) size and the surface roughness.

The 5GHz measurement is outside the range of interest for this thesis but was considered as a useful comparison for the technique since the antenna has a much wider beam at this frequency and hence a more uniform illumination of the MUT.

Figure 4.5 shows the raw data for the metal plate that includes the reflection from the plate and the LoS from the transmit antenna. It can be clearly seen that the sample position where the range of illumination equals the angle of reflection is around −45° and also repeated at 135° as this is the 'back' of the sample. Ideally the peaks should be exactly at −45° and 135° if the transmits and receive antennas are exactly 90° - the small offset is a result of the difficulty in setting this up completely accurately, though does not significantly affect the outcomes of the measurements (reflectivity and scatter).

Differences between maximum levels can be attributed to antenna gains (increasing with frequency) and cabling losses (increasing with frequency). The reflected levels away from the peaks depend upon the LoS signal (higher at 5GHz due to the wider beamwidth) and the diffraction from the edges of the samples (ripples). The LoS has the effect of reducing the 'reflecting' dynamic range, while the sample size will influence the level of reflection and distribution of ripple (peaks and nulls).

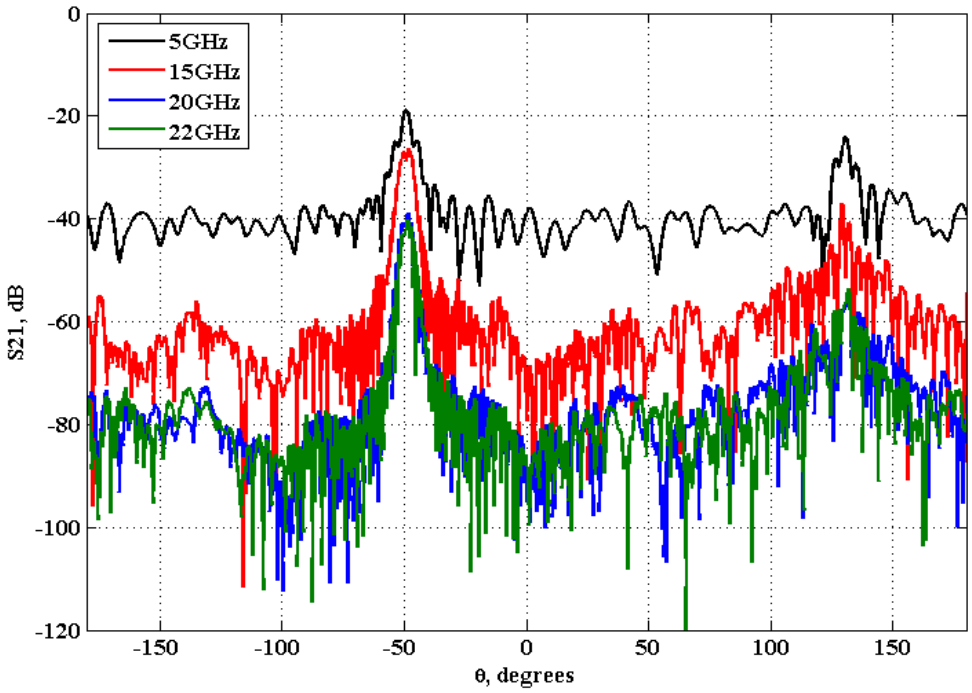

FIGURE 4.5. Chamber measurement: Metal plate frequency comparison (raw data)

There is therefore a need to systematically process this data to remove the LoS signal and hence allow the effect of the reflection-only to be analysed. Figure 4.6 therefore shows this process in detail. The flow diagram summarises the calibration procedure that will be used for the whole analysis in this chapter.

In this flow diagram, two methods of data processing are shown with an example based on this frequency comparison measurement results.

1. The first process removed the line of sight data from the raw data by applying the background subtraction to extract the reflected or attenuated signals. This method will reduce the ripple in the data set.

2. The second process normalised to the maximum at 0dB. This normalisation shifted and scaled the data to the maximum value with the intention to ease the comparison between the data.

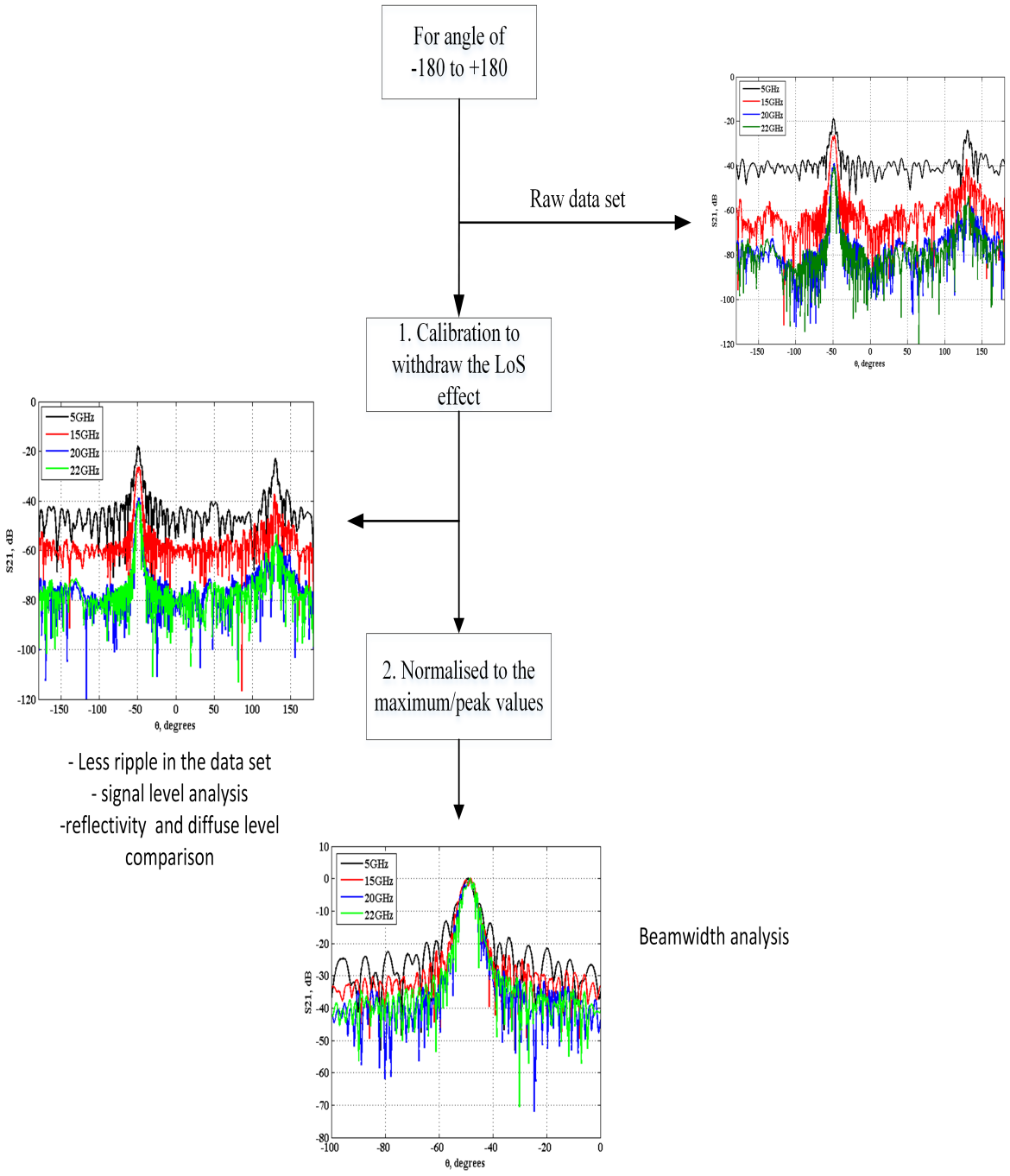

FIGURE 4.6. Calibration Process

After LoS removal it can clearly be seen that for the 5GHz data set especially, the ripples away from the 45° reflected path are not significantly deeper as these were 'filled in' by the LoS signal. There is less impact with the higher frequencies as the LoS is lower due to a more directive antenna beam.

The final stage is the normalisation of the data sets with respect to the peak values. The purpose of this normalisation is to allow comparisons of beam shape, ripple regularity and levels and comparison of reflectivity and scattering from other material samples. Here the path loss, cabling, amplifier and antenna gains are 'removed'. The gains are frequency-dependent so the relevant metal calibration has to be applied and also the sample sizes will yield different 'reflective gains' so other material samples should be of a similar size or else results adjusted to compensate for this. In these measurements, the samples were almost identical in size.

Both the data processing procedures has been applied in Figure 4.7 to have a better understanding of how the rotation affects the received signal as the material rotates. In this figure, a sample of the signal between the range of $-100°$ to $0°$ where the first highest peak occurred was selected to be further discussed.

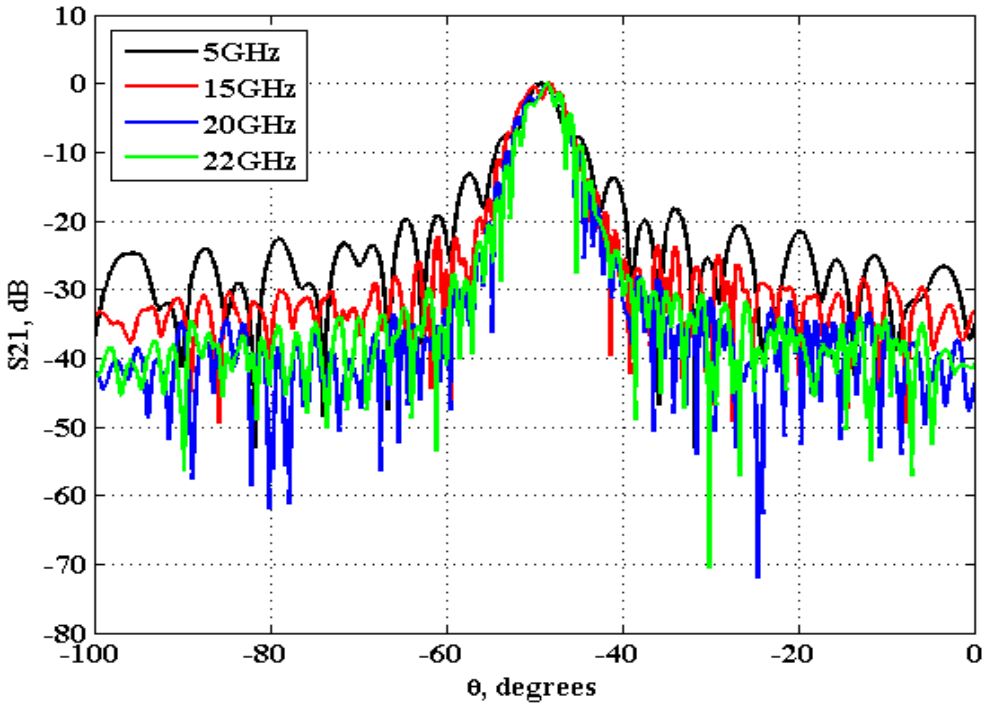

FIGURE 4.7. Metal plate frequency comparison (normalised data)

As wavelength concern, an increase in frequency leads to a decrease in wavelength. At 5GHz the wavelength is 0.06m, 15GHz of 0.02m, 20GHz of 0.015m and 22GHz of 0.013m. The metal plate that been used in this measurement is 0.7x0.7m in size which indicates 11 times to 50 times larger than the wavelengths. The fundamental analysis is to count the ripple or number of null points in a certain range of ($-60°$ to $-40°$) where the peak occurred for all the frequencies measured. This is the maximum reflection area or at the main beam that the signal produced as it hit the metal plate. Based on this calculation, the ripples or number of null points at 15GHz, 20GHz and 22GHz are three times more than ripples points at 5GHz. The ripple of the beam increases as frequency increases.

The 3dB half-power beamwidth (HPBW) also be deduced from this normalised figure. 5GHz frequency only have a $3°$ angle of beamwidth, while $5°$ at 15GHz, $4°$ at 20GHz and $3°$ at 22GHz. Even beamwidth or roll off at the range of ($-60°$ to $-40°$) wider as frequency increases, but the beams tend to converge at the peak of the signal.

The antenna used is a wide-beam antenna. Therefore the wider beam would illuminate the metal plate better, and this would give a narrow-reflected beam. The aperture is the same, but the field illumination will be different. Increasing in frequency will lead to reducing in distance range; thus; the area of cross section being illuminated will be less, resulting in the narrower beam as the material rotated in Figure 4.7. The following measurements will continue using the 20GHz as a tested frequency.

4.1.3 Material comparison

In this subsection, the material comparison at 20GHz in the anechoic chamber will be presented. The materials involved are a square metal plate (70x70 cm), concrete (four slabs of concrete, each of 40x40cm with a thickness of 3cm - arranged in to form 80x80cm) and a wood of 80x80cm. The angular measurement setup in the anechoic chamber as Figure 4.3 shows that the samples were all about the same size and placed on the rotating stand.

The analysis will first present the raw data as in Figure 4.8. The figure shows the comparison based at 20GHz in the range of $-180°$ to $180°$ for all the three material under test. There are a few observations from this figure;

- Firstly; the reflected signal. The metal plate has the highest reflected signal compared to a concrete and wood.
- Secondly; the dynamic range of the observed signal. Metal plate has 30dB dynamic range; concrete has 20dB and wooden stand of approximately 10dB dynamic range.
- Thirdly; the VNA noise floor can be seen at signal below -90dB.

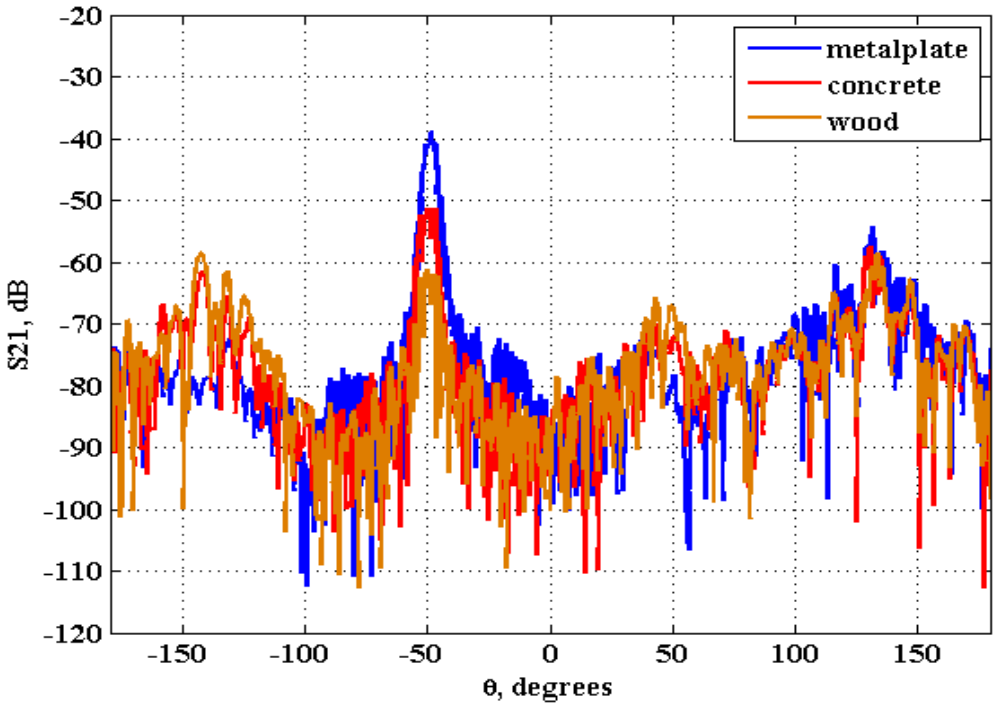

FIGURE 4.8. Chamber measurement: Material comparison at 20GHz (raw data)

To compare the reflectivity of material with respect to metal plate, the normalisation to the maximum value of metal plate was conducted.

In Figure 4.9, the data for the concrete and the wood are shown with respect to the (maximum) level of the metal plate. Hence the normal incidence reflectivity of the two samples can be determined. Both contain ripples (due to surface effect as well as the sample diffraction), though the latter can be clearly observed in the off-axis ripples. Therefore the peak value may not necessarily be the most accurate way of identifying the sample reflectivity and an average based upon an angular spread that takes in a number of ripples (around 8°) will give a more realistic value.

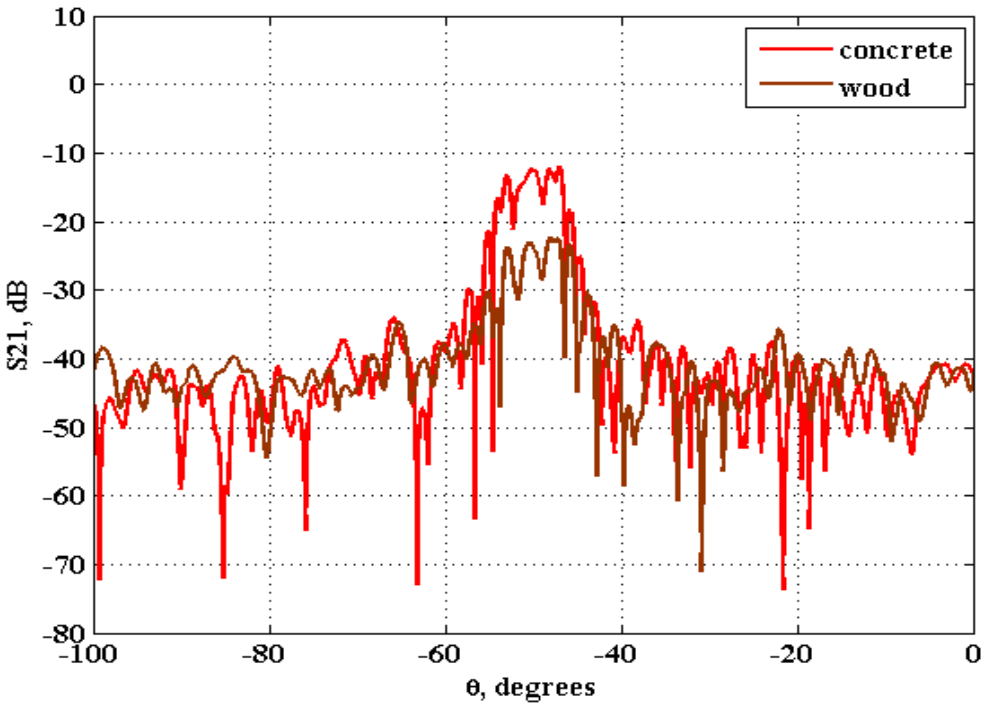

FIGURE 4.9. Chamber Measurement: Material reflectivity at 20GHz (normalised data)

Table 4.1 therefore summarises the material reflectivity in terms of peak and average values.

Table 4.1: Material Reflectivity Level at 20GHz

Material	**Peak value, dB**	**Average reflectivity "peak value" for 8° beamwidth, dB**
Concrete	-12.0	-16.3
Wood	-19.1	-26.6

Subsequently, another data processing (normalised to the maximum values of each material) was applied to the raw data and produce the results as Figure 4.10. The reflected signal mainly distributed in the range of $-60°$ to $-40°$ angle and produce approximately -30dB signal range.

This analysis concentrates on the relative shape of the beams. It can be clearly seen that the metal plate has by far the narrower beam there should be no diffuse scatter) and the beam is only affected by the size of the material (shown here as ripples) and the extent of the illumination (antenna pattern and range). The material will not therefore be uniformly illuminated, and this will influence beamwidth and peak reflectivity levels. Beamwidths for samples are different and additional ripples can be observed.

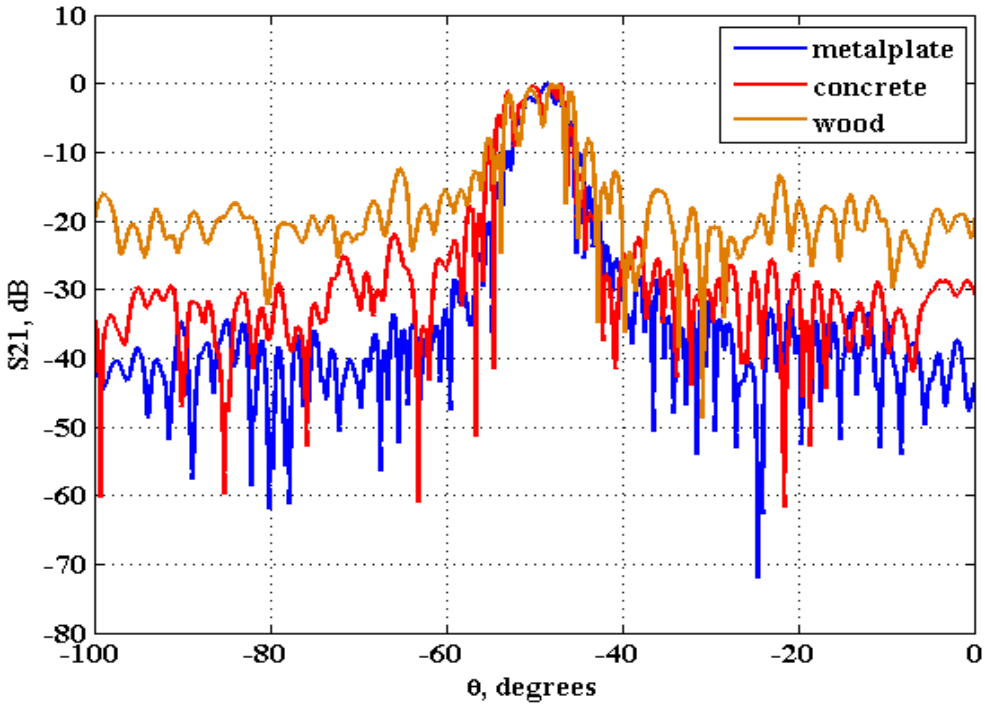

FIGURE 4.10. Chamber Measurement: Material comparison at 20GHz (normalised data)

The surface material for metal plate, concrete and wood are different, therefore averaging between $-100°$ to $-60°$ and $-35°$ to $0°$ from the normalised data will determine the additional ripples (probably diffraction or diffuse scatter level) that raised from the surface of these materials.

Table 4.2: Chamber Measurement at 20GHz: Average diffraction/diffuse scatter level of materials

Material	**Average Diffraction/Diffuse scatter level at the range (dB):**		**3dB HPBW**
	$-100°$ to $-60°$	$-30°$ to $0°$	
Metal plate	-41.9	-40.58	5°
Concrete	-33.59	-33.3	7°
Wood	-23.34	-23.05	7°

Table 4.2 tabulated the average value for the range of interest and summarises the outcomes from the beamwidth analysis. Due to these average data, concrete yield a higher diffuse scatter level compare to metal plate because of different surface structure of the material.

4.2 Short Range Angular Measurement

The issue with cable attenuation and range 'losses' mean that extending the angular measurement to include 60GHz frequency band was not possible with the aforementioned set up. The technique was useful to extract relive reflectivity and diffuse scatter properties, and hence a shorter range version was tested. In order to reduce cable losses while maintaining a suitable signal level above the noise floor of the VNA the set up was positioned close to the VNA ports and used the VNA high specification cables only (no additional amplification). Outside the chamber could results in more spurious reflections not associated with the sample, but given the distances to possible reflective surfaces, these would be minimal and also absorber was placed in front of obvious surfaces. In this set up the range is therefore significantly reduced and this meant reduce size samples. Measurements at 60GHz were then possible with comparison made at the lower 20GHz to allow comparison with the previous chamber measurements.

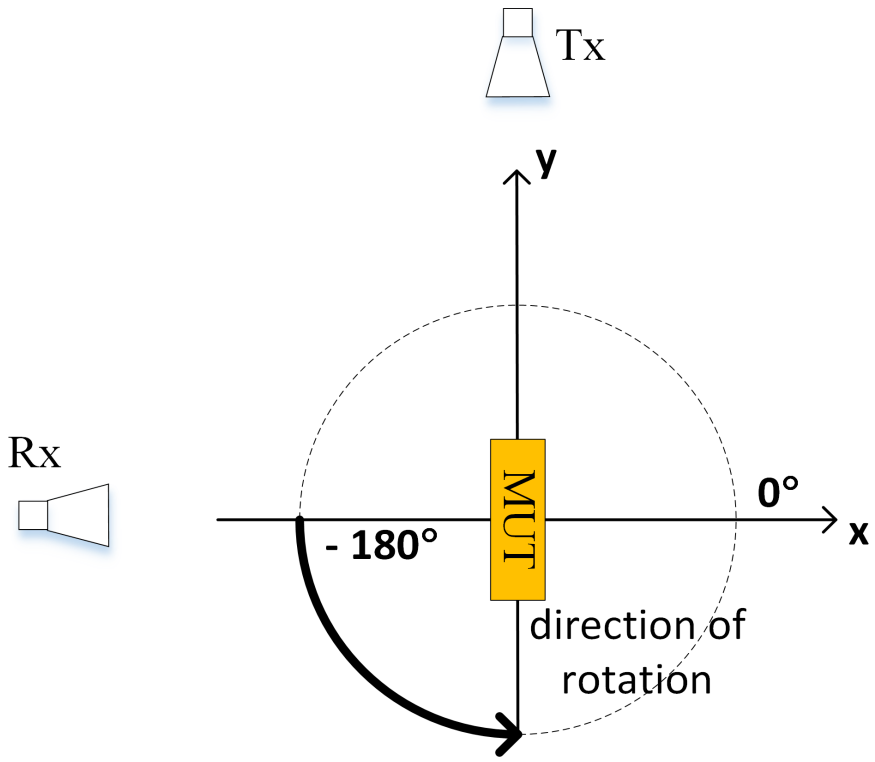

FIGURE 4.11. Short range measurement setup

The angular measurement was conducted in a smaller area in front of the VNA. The distance between both the transmitter and receiver antenna to the centre of the material

was fixed at 50cm. The material under test (MUT) was placed on the positioner that was fixed on top of the rotating platform. Standard gain horn antenna of the frequency range between 17.6GHz to 26.7GHz with approximately 19° of 3dB beamwidth and an aperture width of 52mm was used for both the transmitter and the receiver. Figure 4.11 shows the short-range measurement setup in the laboratory area.

4.2.1 Material comparison in short-range measurement

The material under test (MUT) and dimension are tabulated in Table 4.3. The reflected and diffracted signals from these materials will be observed and analysed.

Table 4.3: Material under test (MUT)

Material under Test (MUT)	Size/cm	Thickness/cm
metal plate	40x40	<1.0
concrete slab	40x40	3.0
wood	40x40	2.0
tiles	40x40	2.0

The first set of results refer to measurements at 20GHz. The raw data is shown in Figure 4.12 with the maximum occurring at 45° and 135° as previous. The observation was made based on comparing the peak signals of all the materials. Metal plate has the highest peak at -25dB, concrete slab of -27dB, tiles of -33dB and lastly wood with approximately -38dB of reflected signal.

The analysis of the samples then followed the same process. Comparison of sample levels with respect to the metal plate to yield maximum reflectivity levels and normalisation with respect to each sample maximum to yield beamwidth and diffraction ripple.

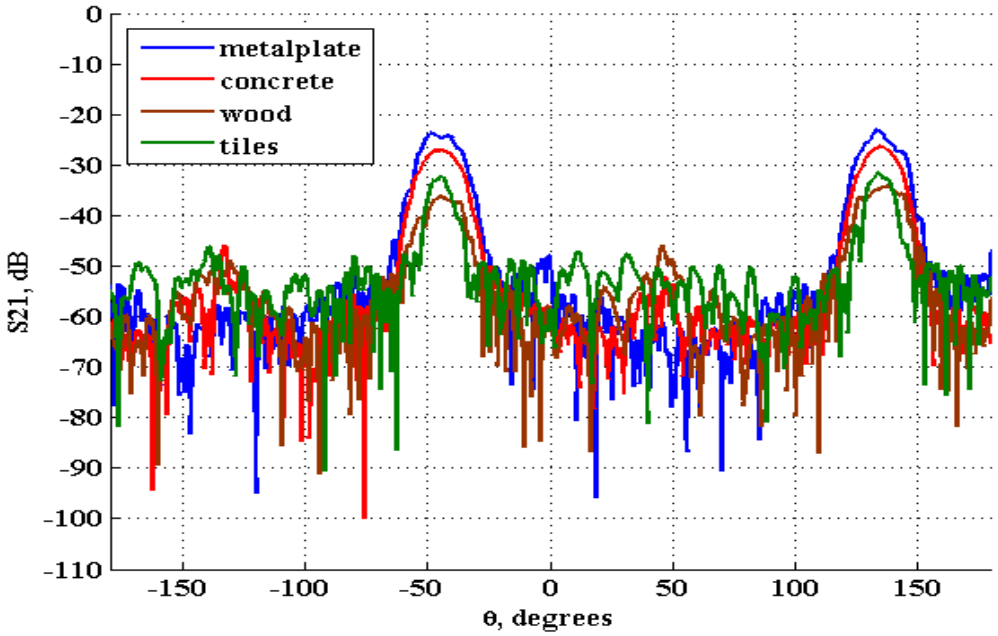

FIGURE 4.12. Short range measurement: Material comparison at 20GHz (raw data)

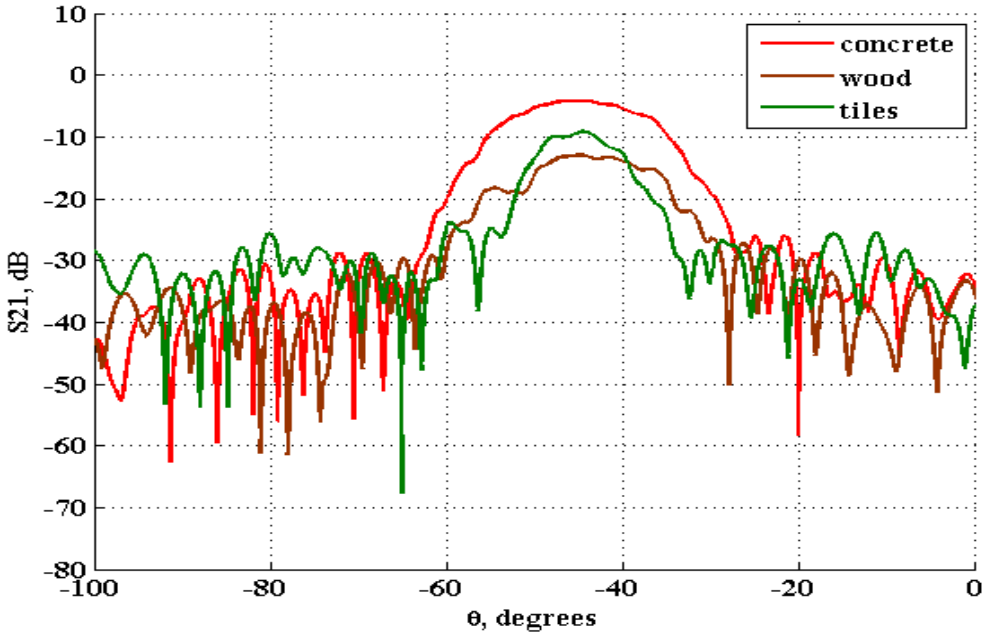

FIGURE 4.13. Short Range Measurement: Material reflectivity at 20GHz (normalised data)

The relative reflectivity is shown in Figure 4.13. Again the maximum values may not be a true outcome of the material reflectivity so the results presented in Table 4.4 show the peak relative values and those average over a 8° range. The concrete is significantly more reflective that the wood, but here the ceramic tiles (not considered before) lie between these two.

Table 4.4: Short Range Measurement: Material Reflectivity Level at 20GHz

Material	**Peak value, dB**	**Average peak value for 8° beamwidth, dB**
Concrete	-3.5	-4.5
Wood	-10.9	-13.6
Tiles	-7.9	-10.6

Although LoS subtraction was performed (a measurement with no material present), the concentrated beams from the antennas mean that the LoS was not identifiable and hence had no impact in this case. For these measurements, the samples were located in a vice below the sample that meant that the 'front' and 'back' of the samples could be observed obscured. This is clear in the data presented with relatively similar responses.

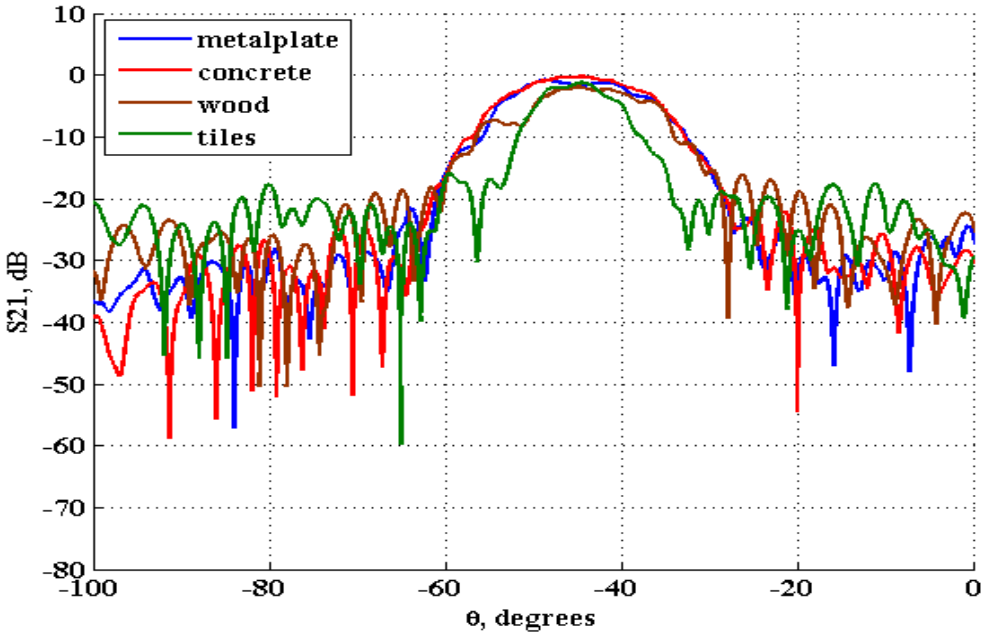

FIGURE 4.14. Short Range Measurement: Material comparison at 20GHz (normalised data)

Figure 4.14 shows the reflected signal in the range of −100° to 0° of rotation. Based on this figure, the beamwidth of each material between the range of −60° to −30° will be further analysed. A metal plate and concrete slab have practically identical beamwidth, while wood has a bit narrower and lower beamwidth. However, tiles tend to have the peak beamwidth at the range of −50° to −30°, therefore the narrowest between all the materials.

The same analysis as in Section 4.1.3 was applied to these material. The diffuse signal levels for the specific range are tabulated in Table 4.5.

Table 4.5: Short range measurement: Average diffraction/diffuse scatter level of materials at 20GHz

Material	**Average Diffraction/Diffuse scatter level at the range (dB):**		**3dB HPBW**
	−100° to −60°	−30° to 0°	
Metal plate	-32.91	-29.58	7°
Concrete	-35.04	-29.15	7°
Wood	-28.88	-28.07	7°
Tiles	-26.32	-24.98	5°

Based on Table 4.5, there are variations of diffuse signal level for both ranges of rotation. Concrete with -32.91dB and -29.58dB have the highest value of attenuation or diffuse signal. This is due to the surface irregularities of concrete that rougher compare to other material.

4.2.2 Metal Plate Size Comparison

In the previous measurements and analysis, the size of the metal plate reference has been fixed. However, in order to better understand the impact of the reference on measurements (reflectivity, illumination etc.) this section considers a number of metal (aluminium) plates of various areas.

In this measurement, metal plate analysis was conducted for various size of the metal plate at 20GHz. Table 4.6 show various sizes of metal plate for measurement.

Table 4.6: Various sizes of metal plate

Metalplate	**Size/cm**
MetalA (reference)	40x40
MetalB	25x25
MetalC	70x70
MetalD	diameter, d=40

Based on Table 4.6, MetalA of 40x40cm acts as a reference. MetalA was chosen as a reference as a continuation of the previous chapter's material characterisation and because the other sample materials are about the same size as this metal plate. MetalA has an area of $1600cm^2$, MetalB is approximately half the size with $625cm^2$ and MetalC is an approximately has a larger area of $4900cm^2$, and MetalD is a circular plate with a cross sectional area of $1256cm^2$.

Figure 4.15 shows the raw data of the metal size comparison. These raw data are essential to observe the trends for reflected signal and diffraction at the edges of materials as it fully rotated from $-180°$ and $180°$. The beamwidth for all the materials have approximately the same maximum value and width at the exact rotation angles.

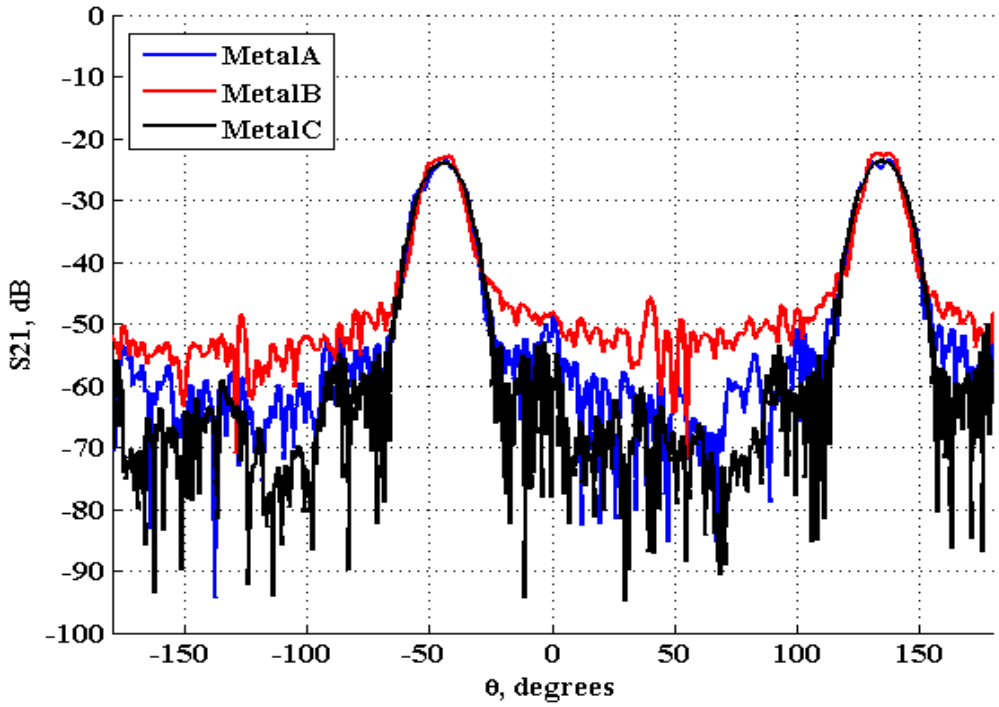

FIGURE 4.15. Short range measurement: Metal size comparison at 20GHz (raw data)

In this figure, MetalB is slightly higher than the MetalA reference, even though the sample size is smaller and hence would be expected to have a lower gain. However, there is actually very little discernible difference in these samples as can be noted with the beamwidth analysis, Figure 4.16. The ripple away from the main beam ('off-axis') clearly show more ripple per degrees for the larger sample (MetalC) but that the smallest sample (MetalB) has the narrower beam but also higher off-axis levels. Therefore, the smaller size of MetalB contributed to higher diffraction effect at the edges compared to the other two materials.

For further analysis, the raw data have been undergoing the two process of calibration to eliminate the path loss with respect to the line of sight, LoS and aligned to the maximum value of the signal received.

Figure 4.16 shows the normalised data to the maximum level of S21 in dB in the range of $-100°$ and $0°$. Based on this figure; the size of the reflected beamwidth signal is increase with the increase of metal plate size. The diffracted signal at the edges decreases with an increase in metal plate size. A diffracted signal level below $-65°$ angle of rotation shows approximately 5dB different in signal level. This trend also can be seen at the angle above $-30°$.

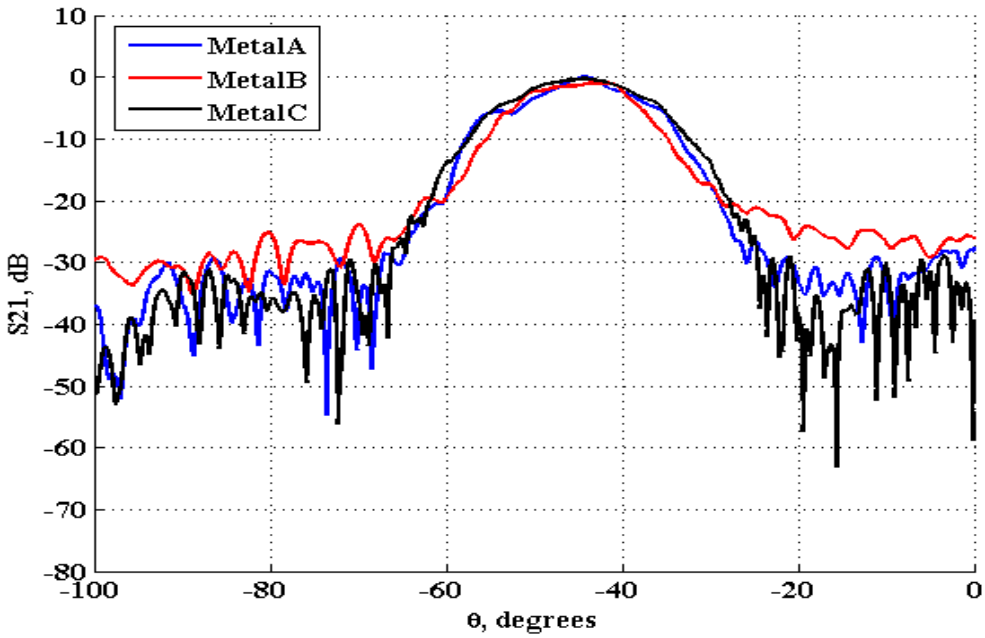

FIGURE 4.16. Short Range Measurement: Metal size comparison at 20GHz (normalised data)

In addition, shape or dimension comparison also being conducted through this measurement.

Approximately the same size but different shape of metal plates has been investigated in Figure 4.17; MetalD is a circular metal plate with a diameter of 0.4m. Based on observation from the raw data, both signals produced the same curve and approximately the exact number of ripples or null points.

Further analysis was conducted by performing the two steps of normalisation. Based on Figure 4.18, Therefore the shape of the material does not contribute to the reflected or diffracted signal.

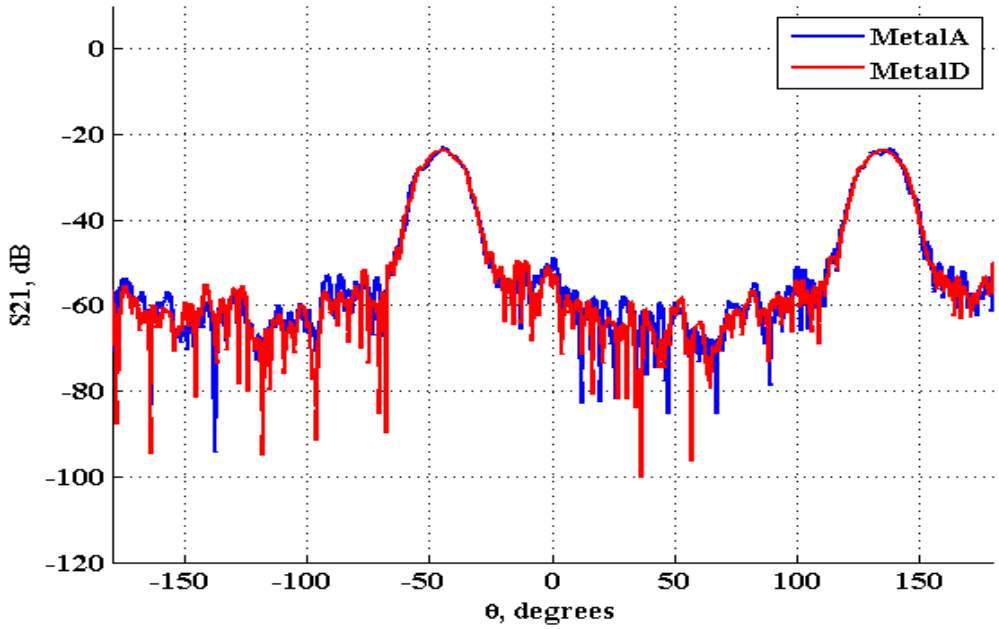

FIGURE 4.17. Short range measurement: Metal shape comparison at 20GHz (raw data)

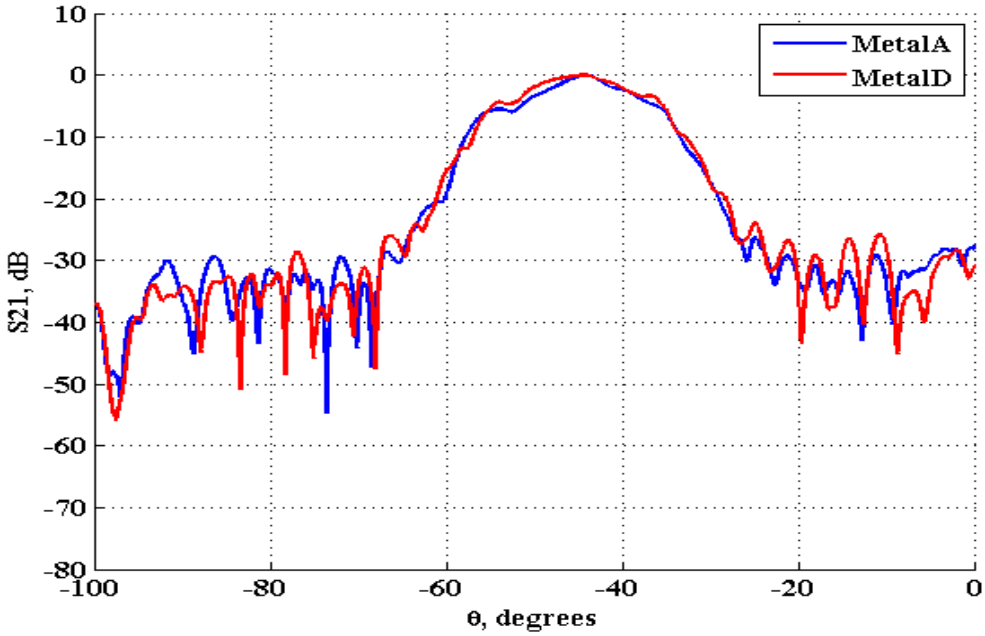

FIGURE 4.18. Short Range Measurement: Metal shape comparison at 20GHz (normalised data)

4.2.3 60GHz Material Comparison in Short-Range Measurement

The same setup was used for 60GHz. Standard gain horn antenna of the frequency range between 49.9GHz to 75.8GHz with a half power beamwidth of 10° approximately and aperture width of 19mm was used for both the transmitter and the receiver.

The same calibration processes have again been applied for these 60GHz data set. The value LoS (measurement when there is no material on the positioner) is so low compared to the other values that the first normalisation process does not demonstrated much different values. In Figure 4.19 the noise floor of the analyser is clearly present though the possible dynamic range of the observed signal is around 30dB.

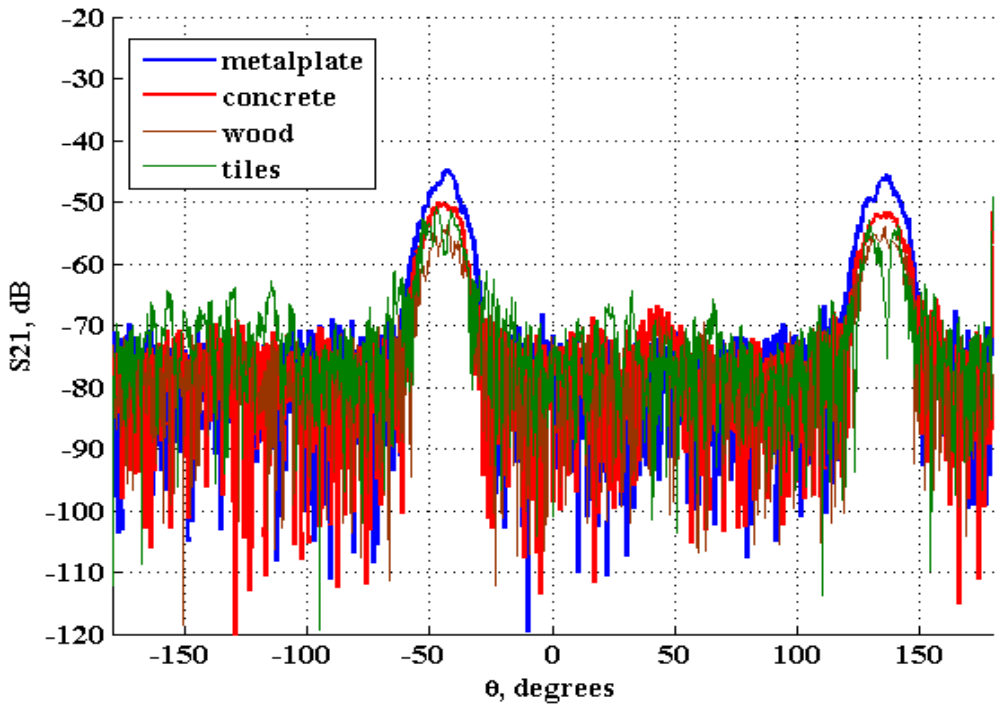

FIGURE 4.19. Short range measurement: Material comparison at 60GHz (raw data)

The analysis of the samples at 60GHz then followed the same process. Comparison of sample levels with respect to the metal plate to yield maximum reflectivity levels was first conducted and then normalisation with respect to each sample maximum to yield beamwidth and diffraction ripple.

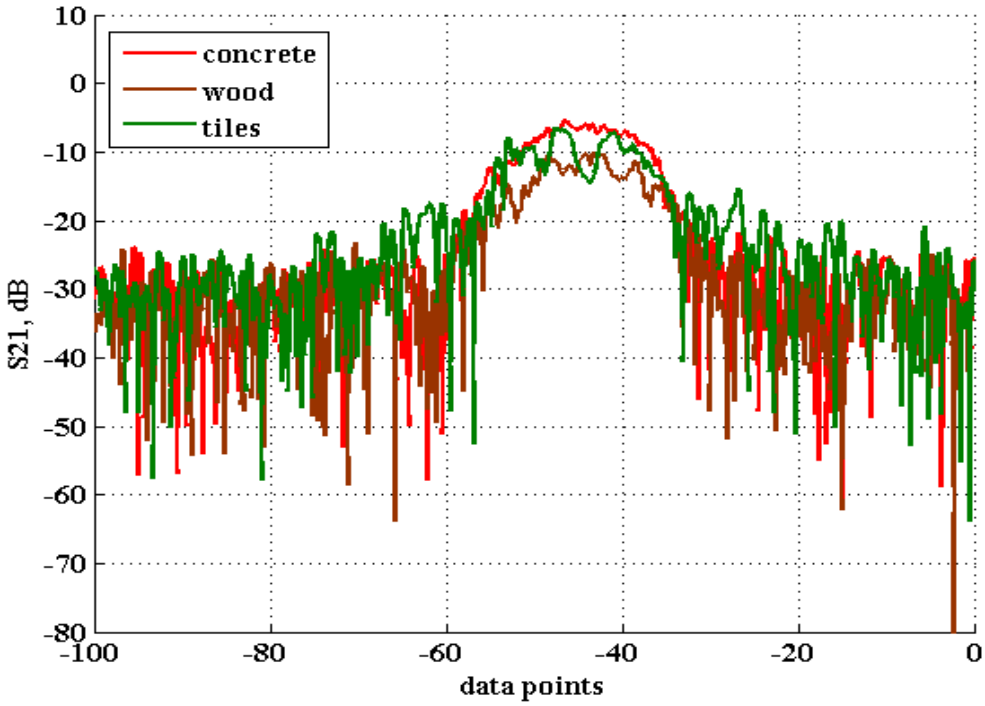

FIGURE 4.20. Short Range Measurement: Material Reflectivity at 60GHz (normalised data)

The relative reflectivity is shown in Figure 4.20. Again the maximum values may not be a true outcome of the material reflectivity so the results presented in Table 4.7 show the peak relative values and those average over a 8° range. The concrete is significantly more reflective that the wood, but here the ceramic tiles have the highest reflectivity.

Table 4.7: Short range measurement: Material Reflectivity Level at 60GHz

Material	**Peak value, dB**	**Average peak value for 8° beamwidth, dB**
Concrete	-2.8	-6.7
Wood	-7.7	-11.7
Tiles	-0.9	-10.43

Figure 4.21 shows material comparison after normalised to the maximum of each data set. Based on this figure, the roll-off from $-60°$ to $-45°$(peaks) are the approximately the same for all materials and it's about 20dB. The beamwidth difference within this range also can be deduced,

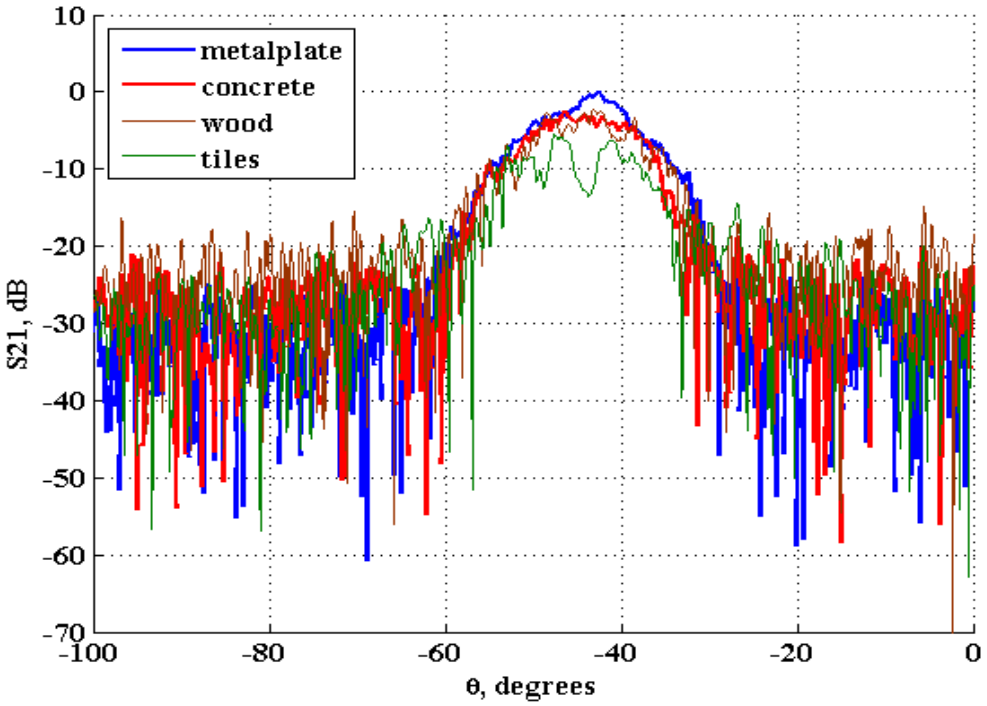

FIGURE 4.21. Short Range Measurement: Material comparison at 60GHz (normalised data)

The next analysis is to observe at the ripples away from the peak and see if they are noise or repetitive ripples, hence try to determine the usable signal level above noise. This has been done by averaging all the normalised data in the range of $-100°$ to $-60°$ and $-35°$ to $-0°$ and 3dB HPBW were carried out and tabulated in Table 4.8.

Table 4.8: Short Range Measurement: Average diffraction/diffuse scatter level of materials at 60GHz

Material	**Average Diffraction/Diffuse scatter level at the range (dB):**		**3dB HPBW**
	$-100°$ to $-60°$	$-35°$ to $0°$	
Metal plate	-32.19	-29.25	5°
Concrete	-27.06	-24.55	7°
Wood	-23.81	-22.14	7°
Tiles	-24.92	-22.65	5°

Based upon these average data, metal apparently have the highest reflection signal, followed with concrete that -6dB below metal, tiles with -7dB different and wood with approximately -12dB below reflected signal of metal. Noted that for tiles, the surface of

the tiles produced high reflectivity, but area where with grouting on tends to reduce the reflectivity. The tiles showed a series of ripples and these tie in with the number of tiles (3 whole of part of tiles with two gaps). After correctly normalised, the tiles give a wider beam spread hence higher scatter, though overall lower reflectivity. The same trends of reflected and diffuse scatter signal can be observed both at 20GHz and 60GHz.

4.3 Conclusion

In this chapter, a method to identify peak reflectivity levels and material scatter has been suggested, and outcomes from practical measurements have been presented. The method depends on the rotation of the sample and the analysis of the resultant data set that shows the main beam and diffraction/diffuse scatter lobes. The main beam occurs at 45° and 135°, and the analysis includes the level of the main beam and the width of the beam. The level is indicating reflectivity (using a metal plate as a reference) and beamwidth an indication of the scatter (though as results have shown this is not always conclusive due to their influence of the illuminating antennas beamwidth). Results were presented for chamber measurements for 5GHz to 22GHz and a shorter range at 20GHz and 60GHz for a number of material samples.

In chamber measurements, the beamwidth and the roll-off increase as frequency increases. The increase in the roll-off represents the increase in the visibility of scatter at a higher frequency. The relative reflectivity of materials at 20GHz with respect to a metal plate showed that a difference of -12dB for concrete and -19dB for wood. Average reflectivity of the peak value for 8° beamwidth also showed how less reflective concrete at -16dB and wood at approximately -26dB.

For short-range measurement, at 20GHz, the relative material reflectivity level showed that a difference of only -3dB for concrete, -7dB for tiles and -10dB for wood. The differences level for concrete and tiles are contras. This because of the frequency (and beamwidth) versus distance range. Subsequently, at 60GHz, the peak value of material reflectivity showed a better value with -0.9dB for tiles and -2.8dB for concrete, while wood has less reflectivity value at -7.7dB.

This chapter provides measurement with respect to the metal plate as a model reference. The calibration process was applied to eliminate the LoS effect and normalisation to the maximum value of the metal plate to obtain the reflectivity values of the materials. This model of metal plates and antenna beam pattern are useful to better understand the diffraction, illumination and gain of materials.

Future works include measurement for metal with corrugations in order to have a better study of surface roughness with ‘known’ level of ‘roughness’.

CHAPTER 5

INDOOR SCANNING; OBJECTS IDENTIFICATION AND PROPAGATION MECHANISM

In the previous chapter, the effect of diffuse scatter was seen in the rotated sample materials as showing up as increased beamwidth with respect to the reference flat metal plate. The distance to the sample has an impact on the data as well as the size of the single, isolated sample. The next stage of analysis was then to consider how the size, orientation, proximity and number of objects might impact on the signal received at a transmitter as opposed to just considering a single sample material.

The thinking behind this was mainly to identify where there was a need to fully characterise a particular material for use in a deterministic model, or whether the combined effects of its position in an environment surrounded by other scatterers would reduce the impact of the diffuse scatter. The work is therefore less to do with diffuse scatter and more to do with object identification and their perceived size as seen at a receiver. For instance, would two closely-spaced reflectors be seen as two separate entities or as one wider entity.

The first part of this chapter presents (3D) azimuth-elevation scan measurements for materials placed inside an anechoic chamber, thus identifying the area of material reflection. This environment allowed total control of placement of objects to study reflection and diffraction. Due to cabling and amplifier constraints, the work here concentrated on the 22GHz measurements to allow suitable dynamic range to be observed and measurements were undertaken for a 5m inside the chamber but also included

some measurements for a transmitter placed outside the chamber (with doors open) as a prelude for a second set of propagation measurements. Here metal and wood poles and plates were used as the sample materials.

The second set of measurements were for the indoor laboratory and adjacent office environment, again at a frequency of 22GHz. Here there is no control of the reflection and diffraction mechanisms but allows identification of the dominant propagation paths, and hence features (in terms of size and material) that have to be included in deterministic modelling tool and those that may be less important or of no significant consequence. This is again uses azimuth-elevation scans to pinpoint these features in space and determine their size and influence.

Section 5.1 therefore describes the radar cross section theory that is relevant to the scenarios being used in this chapter of work and therefore focuses on metal plates and cylinders. The use of a metal cylinder is seen as a particularly good object to allow calibration of the environment. Its rotational symmetry generates and omni-direction reflection pattern for any incident signal angle of arrival. Although azimuth-elevation scans is being used, most angles of arrival at the receiver are predominantly 'azimuth', being mainly within range of $\pm 45^{\circ}$ in elevation. An alternative, such as a metal plate, would give a higher reflection so long as the 'correct' angle of arrival and departure were observed and therefore no reliable.

Section 5.2 details the measurements that were conducted in the anechoic with cylindrical poles and flat plates. A series of measurements allows identification of the location of the samples, reflectivity of the samples and the effect of distance between samples. Calibration for range and removal of the Line of sight path allows better definition of the object and furthermore the use of the known path lengths from transmitter directly to the receiver and the transmitter-to-scatterer-to-receiver allows an estimation of the scattering from objects in terms of 'gain' and radar-cross-section. Also, by placing the transmit antenna outside the chamber (with doors open) the diffraction effects can be observed.

Section 5.3 then considers a series of measurements in the laboratory environment with the receiver position (azimuth-elevation scanner) fixed and the transmit antenna placed at various locations in the laboratory space and adjoining office space. Here reflectivity of object and propagation, through and round walls could now be observed. Range calibration could also be carried out here using a close by transmit reference measurements and hence 'gain' and RCS of the object featured could again be estimated.

5.1 Radar Cross Section of Material

Even though there is a considerable number of publications relating to propagation in indoor and outdoor environments (as has been outlining in Chapter 2, section 2.4), these environments are complex, and hence data is heavily dependent on the amalgamation of reflections, diffraction and other propagation mechanisms.

In order to obtain the best indoor scanning measurement data, the object identification measurements in a controlled environment need to be conducted first. This is to detect or identify which materials will act best as a reflector, diffract or attenuate at 22GHz of frequency. This work aimed to get a basic understanding of the scattering from common shapes and to tie this in with known theory relating mainly to Radar Cross Section. Focusing on the metal poles, this section will also look into another type of materials. From these object identification measurements, the signal strength reflects the radar cross section concept.

The radar cross section (RCS) of a target σ, is defined as the area intercepting that amount of power which, when scattered isotropically, would ppoleuce an echo at the receiver equal to that observed from the target [105]. The basic concept of radar is to detect or track a target and ability to identify the target from the echo signal [106]. Therefore; in the design and operation of radars, the ability to quantify or represent the echo signal in terms of target characteristics (size, shape and orientation) are essential.

The operation of radar also involves the propagation mechanism of the signals [107]. The radar transmitter transmits a signal towards the target or object and upon incident on the target, reflect and scatter in all direction. The reflected and scattered signals propagating in the direction of the receiver are captured and processed by the receiver. The reflected and scattered signal are due to the target properties and the medium surrounding it. Thus, the amount of power reflected and scattered towards the radar is determined by the Radar Cross Section (RCS) of the target [108]. The radar equation is as follows:

$$P_r = \frac{P_t G_t G_r \lambda^2}{4\pi^3 R_t^2 R_r^2} \sigma \tag{5.1}$$

Table 5.1 provide the Radar Cross Section equation, σ for three simple target object.

Table 5.1: Radar Cross Section (RCS) of simple target object [2]

Simple Target Object	Dimension	RCS equation
Sphere	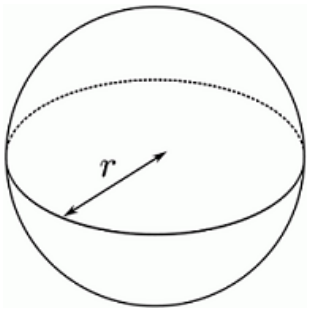	$\sigma = \pi r^2$independent of frequency
Square plate	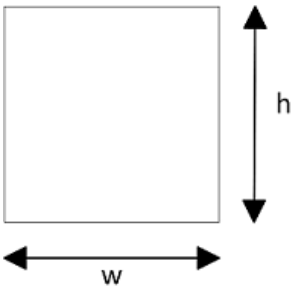	$\sigma_{square} = \frac{4\pi w^2 h^2}{\lambda^2}$
Cylinder	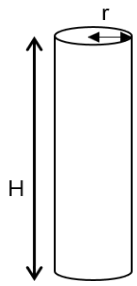	$\sigma_{cylinder} = \frac{2\pi H^2 r}{\lambda}$

5.1.1 Theoretical validation with Radar Cross Section

In order to make the object identifications more precise and assuming metal pole as calibrated references, it is indispensable to investigate and analyse the radar cross section generated by the object. These beamwidth patterns represent the reflection mechanisms in the interaction process of the signal with the object or the dimension of the object.

There are a number of alternative ways that the RCS may be expressed that may also help with the range calibration. Taking Equation 5.1, this can be rearranged in to Equation 5.2 and here expressed in terms of the practical S21 VNA measurements that will be described in Section 5.2.

$$S_{21} = G_t G_r \frac{\lambda^2}{(4\pi)^3} (\frac{1}{R_{TS} R_{SR}})^2 \sigma \tag{5.2}$$

where $G_t G_r$ are the antenna gains, R_{TS} and R_{SR} are the range transmit scatterer and the range scatterer to receiver.

These can be separated out into the product of the two path losses and an object gain, Gs, giving Equation 5.3. Basically this would be like the scatterer acting as an antenna relay that has a gain , Gs.

$$S_{21} = G_t G_r (\frac{\lambda}{4\pi R_{TS}})^2 (\frac{\lambda}{4\pi R_{SR}})^2 G_S^2 \tag{5.3}$$

If the direct path between transmitter and receiver is known, then the standard path loss equation is applicable, Equation 5.4.

$$S_{21(TR)} = G_t G_r (\frac{\lambda}{4\pi R_{TR}})^2 \tag{5.4}$$

This therefore allows the calibration of the system without necessarily having to explicitly know the antenna gains of the transmit and receive antennas. In practice the measurements must also include cabling and any system amplification from/to the VNA ports and hence these too are not needed to be known as Gs can be found by ratioing Equation 5.3 and Equation 5.4. Equation 5.5 is this but written in terms of decibels.

$$G_S^2 = S_{21} - S_{21(TR)} - PL_{TR} + PL_{TS} + PL_{SR} \qquad [dB] \tag{5.5}$$

Comparison of Equation 5.2 and Equation 5.3 together will show the conversion between RCS, GS and also the affective area of the object, Aeff, based upon the relationship of a reflector antenna and it gain, Equation 5.7, [105].

$$\sigma = G_S A = G_S^2 \frac{\lambda^2}{4\pi} = 4\pi (\frac{A}{\lambda})^2 \tag{5.6}$$

$$A_{eff} = G_S \frac{\lambda^2}{4\pi} \tag{5.7}$$

5.2 Object identifications measurement

The object identification measurements were undertaken in the anechoic chamber in order to have total control of the scattering environment, and to allow a direct (unobstructed) path from transmitter to receiver to be used for range calibration. The measurement will first focus on reflections from metal poles. The metal pole is a cylinder with 1.85m high and a radius of 0.03m. The measurement will be conducted at 22GHz with two types of horn antennas as the receiver. Further on, the results will be validated using the radar cross section theory that has been described and calculated based on the said dimension of cylindrical metal pole.

5.2.1 Measurement setup

Figure 5.1 shows the plan of the anechoic chamber and the positions of the azimuth-elevation receive antenna (located at coordinates x=0m, y=0m) and the initial position of the transmit antenna.

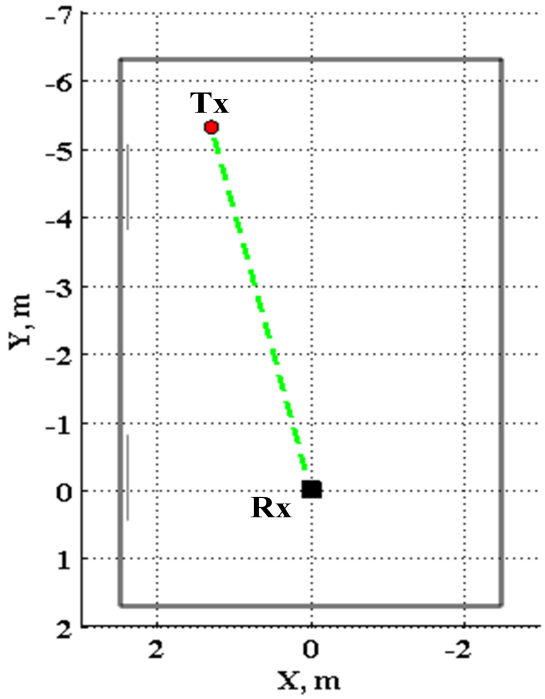

FIGURE 5.1. The schematic diagram of University of Bristol anechoic chamber

The skirt dipole antenna as in Figure 5.2 operating at 22GHz was used as a transmit-

ter. In all these measurements the dipole was placed vertically to give only a vertically-polarised, omni-directional signal in the azimuth plane. This meant that the signal from the transmitter to the receiver for all measurements depended only on the amplifier, cables and path losses, and the directive gain could be assume the same for all azimuth angles. A rectangular aperture horn antennas was used as a receive. The rectangular horn antenna has a half power beamwidth (HPBW) of 18.5°(E-plane) and 17.8°(H-plane) at 22GHz.

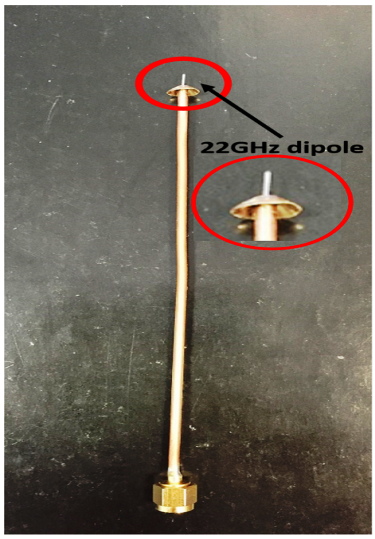

FIGURE 5.2. The skirt dipole antenna

5.2.2 Object Identification: Metal pole

In this measurement, the setup for transmitter and receiver are set to be as Figure 5.4(a). The measurement will start with a single pole to identify the levels of reflections and subsequently with two poles. This is to identify the levels of reflection for two poles with respect to the one pole and the relative level and whether there are two distinct reflections or else merged into one.

The dimension of the cylindrical metal pole is 1.85m high with radius of 0.03m. Therefore, σ can be calculated based on equation in Table 5.1 to be approximately $43m^2$. Based on the measurement in the chamber, the distance between the cylinder metal pole to the transmitter antenna is 6.2m and the distance to the receiver antenna is 2.2m. Noted that the cylindrical metal pole was placed at 125° to the right of the transmitter. Based on these calculation, the comparison between theoretical value versus the measurement values will be discussed after the results analysis.

For this part, there are three configurations involved to place the metal poles as follows and shown in Figure 5.3 and describes as follows:

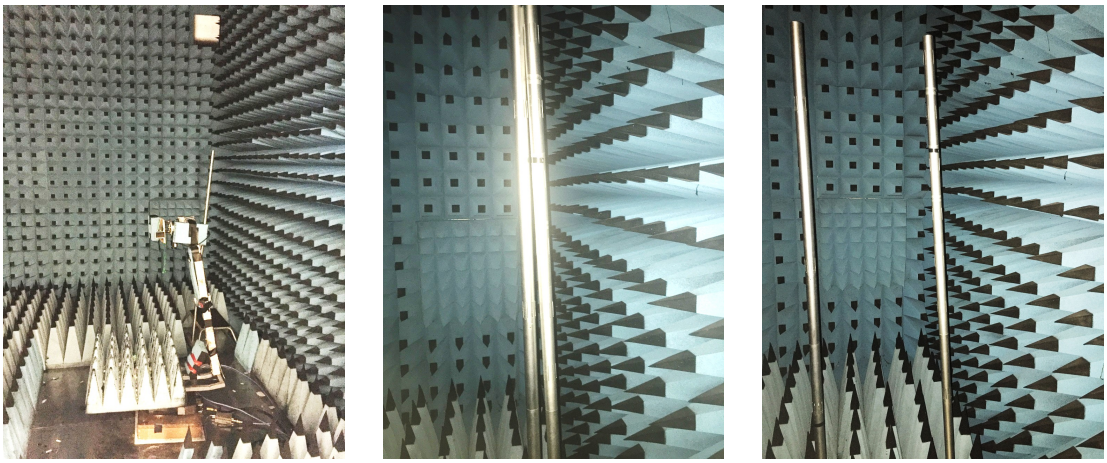

(a) first (b) second (c) third

Figure 5.3: Three configurations of the metal pole in the anechoic chamber

1. The first configuration: one metal pole was placed at 125° with respect of the receiver as in Figure 5.3(a).

2. The second configuration: two metal poles were placed at 125° with respect of the receiver as in Figure 5.3(b); where the two metal poles were placed next to each other.

3. The third configuration: two metal poles are place wider apart (0.45m) as depicted in Figure 5.3(c). This configuration aims to differentiate the reflected signal strength when the surface area increases and when there is an air gap between the two materials.

For this initial analysis only the azimuth plane was chosen (rather than full azimuth-elevation scans) as the poles were all on the same plane and the effect of azimuth separation only was being examined here.

Figure 5.4 shows the schematic diagram of the first configuration in the chamber and the polar plot respective gain with respect to LoS as shown in Figure 5.4(b). Based on the polar plot, the main beam and the reflected lobe are align to the transmitter and the metal pole. The reflected beam gain, as in polar plot is -25dB with respect to the main beam.

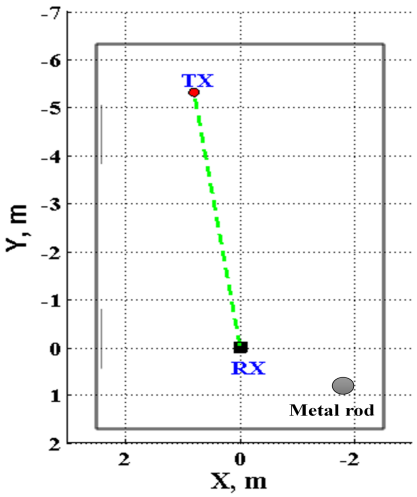

(a) Location of one metal pole

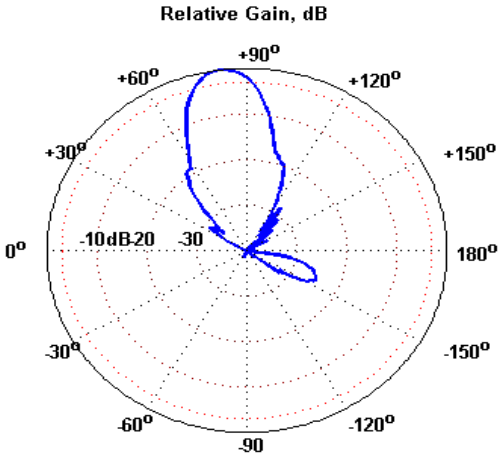

(b) Polar plot of one metal pole at 22GHz

Figure 5.4: Metal pole as reference

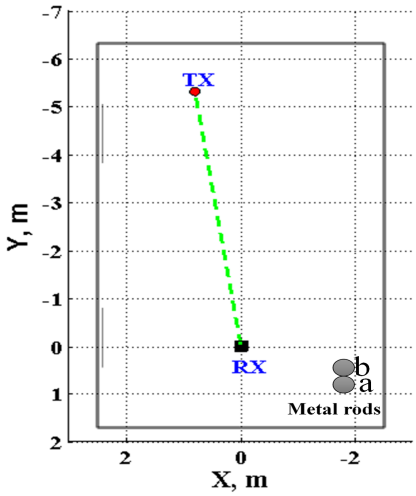

(a) Location of two metal poles

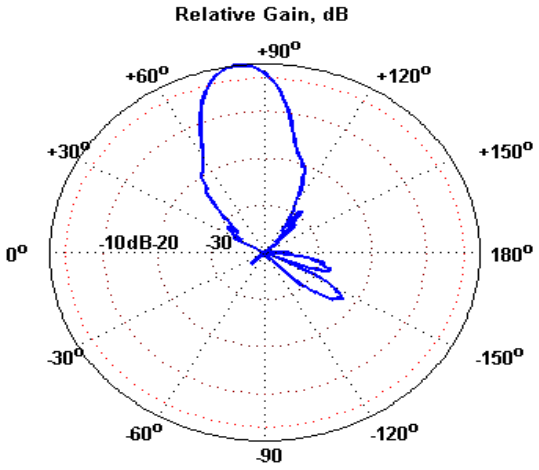

(b) Polar plot of two metal poles at 22GHz

Figure 5.5: Two metal poles configuration

The second and the third configurations as Figure 5.5 and Figure 5.6 produce a distinctive polar plot. When the pole placed next to each other as in Figure 5.5(a), there is a different of 5dB (reflected signal) between the adjacent metal poles. Meanwhile, in Figure 5.6(a) where the two poles are further apart (0.45m), the reflected signals produce

roughly the same reflected value with only approximately 2dB difference. The air gap between the two poles is visible in the polar plot.

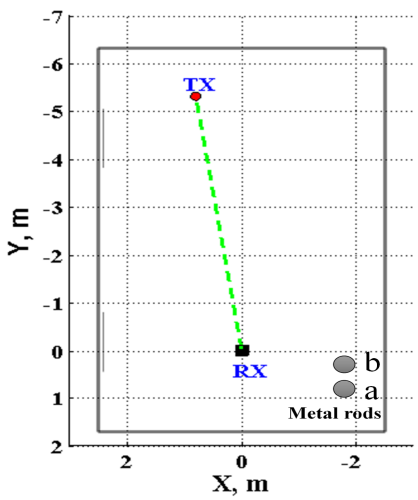

(a) Location of two metal poles (0.45m apart)

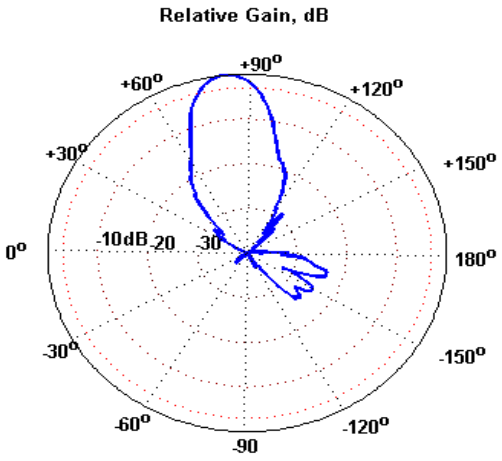

(b) Polar plot of two metal poles (0.45m apart)

Figure 5.6: Two metal poles (wider apart)

Table 5.2 summarised the reflected signal of the metal pole in terms of Equation 5.5. From this equation, RCS, σ of the metal poles as respective position were obtained. Based on earlier calculation of RCS, σ from theoretical, there are a great difference, but with the same figure values.

Table 5.2: Metal poles Gain, Gs and RCS, σ

Metal pole configuration		**Gs, dB**	σ, m^2
1		-25	0.45
2	**a**	-23	0.41
	b	-27	0.48
3	**a**	-25	0.45
	b	-23	0.41

5.2.3 Object identifications analysis; various object classification

The same method was employed to identify positions and reflectivity of a variety of objects. The objects are selected based on the cylinder shape that can cooperate to the theoretical calculation. The frequency of measurement maintained at 22GHz, and the same configuration of transmitter and receiver in the chamber was used to identify reflected signals from various other objects.

The objects selected are a PVC pole, wood pole, metal sheet, metal cylinder and a plastic cylinder. Table 5.3 tabulated the dimension of the selected objects. The same configurations as listed in previous subsection were used for this object identification measurement. This configuration is intended to examine the effects of an other type and dimension of an object in the presence of a dominant incoming signal. PVC and wood poles are the same dimension as metal poles, however both are with different material and composition. Metal and plastic cylinder in this case, are larger in diameter.

Table 5.3: List of objects for identification measurement

Objects	Dimension (m)
PVC pole	1.85(H) x 0.06(D)
Wood pole	1.85(H) x 0.06(D)
Metal cylinder	0.5(H) x 0.5(D)
Plastic cylinder	0.5(H) x 0.5(D)

Based on the polar plot as in Figure 5.7, PVC and wood poles have a lower reflected values of -30dB and -36dB even with same dimension. The theoretical calculation of RCS, σ did not consider this parameters. There was approximately 10dB difference for different type of materials.

Table 5.4 summarised the object gain for these four materials. Larger dimension of metal cylinder and plastic cylinder reflected gain showed not much different from the metal pole, but it clearly visible that the beams are wider as it illuminate wider area.

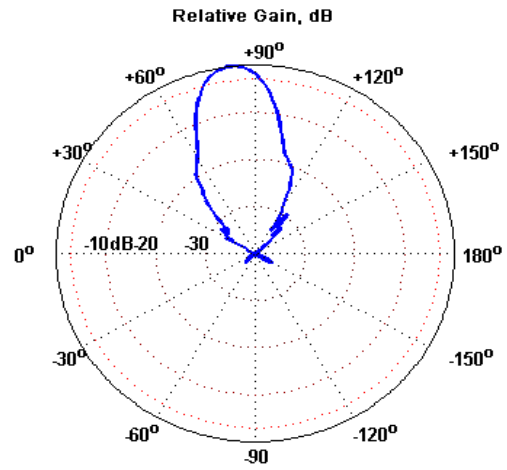

(a) Wood pole

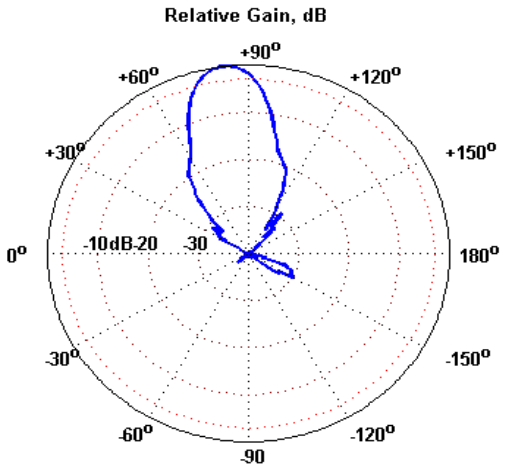

(b) PVC pole

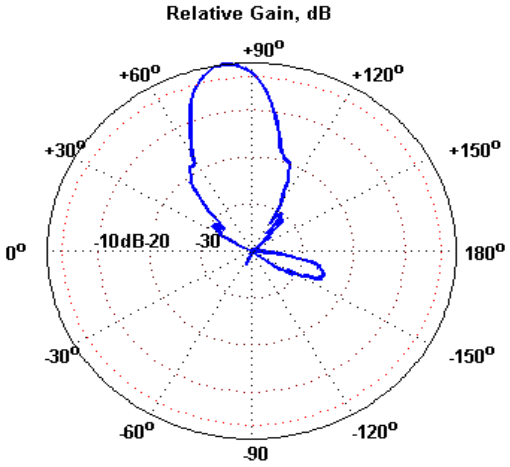

(c) Metal cylinder

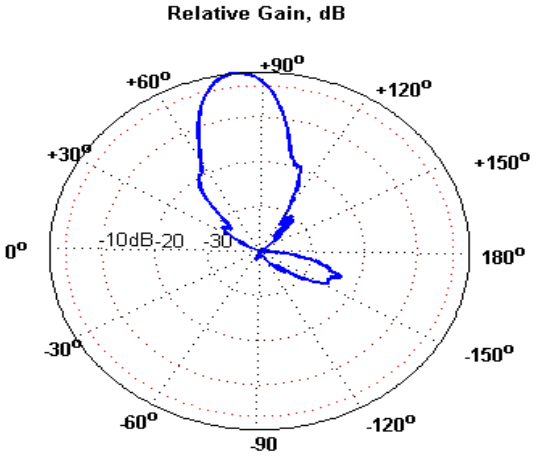

(d) Plastic cylinder

Figure 5.7: Azimuth scans at 22GHz for the four reflective materials

Table 5.4: Object Gain, Gs and RCS, σ

Objects	**Gs, dB**	σ, m^2
PVC pole	-30	0.54
Wood pole	-36	0.64
Metal cylinder	-27	0.48
Plastic cylinder	-23	0.41

5.2.4 Beamwidth refinement

The beamwidth of the receive antenna impacts on the ability to angularly resolve closely-space objects. In this section measurements a Flann dual polarised circular horn antenna (see Section 4.1.1 for details) is used instead of the standard gain horn as it produces a more directive main beam.

Figure 5.8 represents the all three configurations. Considering the directional antenna used, the difference between these two configurations are very distinct. The placement of the two metal poles even a few centimetres influenced the reflected signal. The main beam of these plots were not observable at 1dB since its pointed downwards slightly (-5dB to be exact). For first configuration as in Figure 5.8(a), the reflected signal is -26dB. There are about -8dB different between the first reflected and the second reflected signal as shown in Figure 5.8(b) for the second configuration. Subsequently, approximately the same signal drop for the third configuration as in Figure 5.8(c) (the beam seems narrowest).

Table 5.5 summarised the object gain and σ for this measurement. Generally, the same values of object gain and RCS were obtained, but the beams were narrower compared to the previous measurement.

Table 5.5: Metal poles Gain, Gs and RCS, σ

Metal pole configuration		**Gs, dB**	σ, m^2
1		-26	0.46
2	**a**	-23	0.41
	b	-33	0.6
3	**a**	-27	0.48
	b	-32	0.57

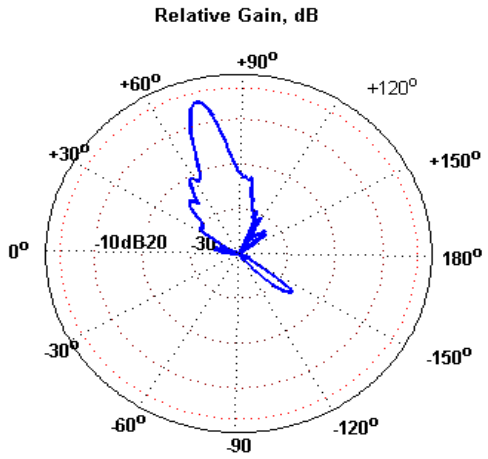

(a) 1st Configuration; single pole

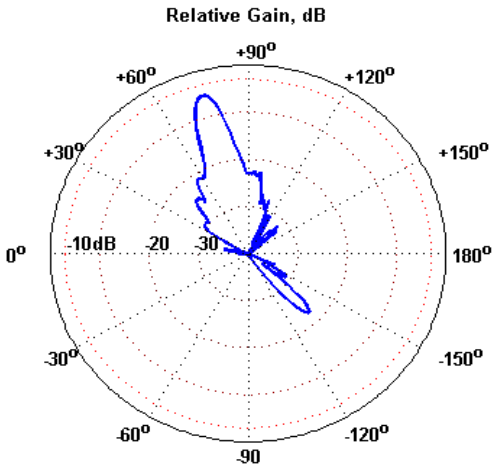

(b) 2nd Configuration; Two metal poles (0.3m apart)

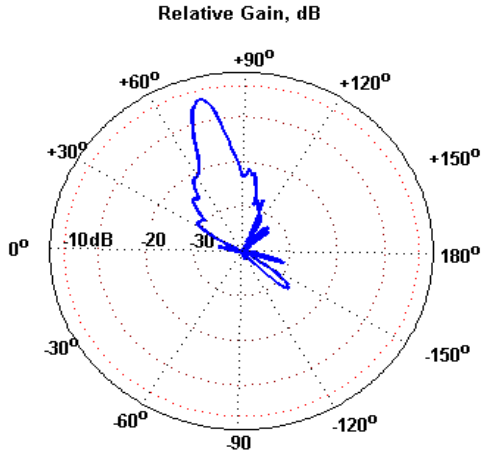

(c) 2nd Configuration; Two metal poles (0.45m apart)

Figure 5.8: All 3 configurations: beam refinement at 22GHz

In a typical environment, there will be both curved and flat surfaces. The emphasis so far has been directed towards the metal pole, but here consideration is given to flat surface (in this case metal discs with 0.4m radius). The orientation of the disc is important since only when the angle of arrival from the transmitter and departure to the receiver are the same about the normal to the disc surface will the signal be a maximum and away from this the signal reduces and ripples as seen in Chapter 4 results. Two angles, 0° and 90°, Figure 5.9, were therefore chosen as examples of plate reflectivity.

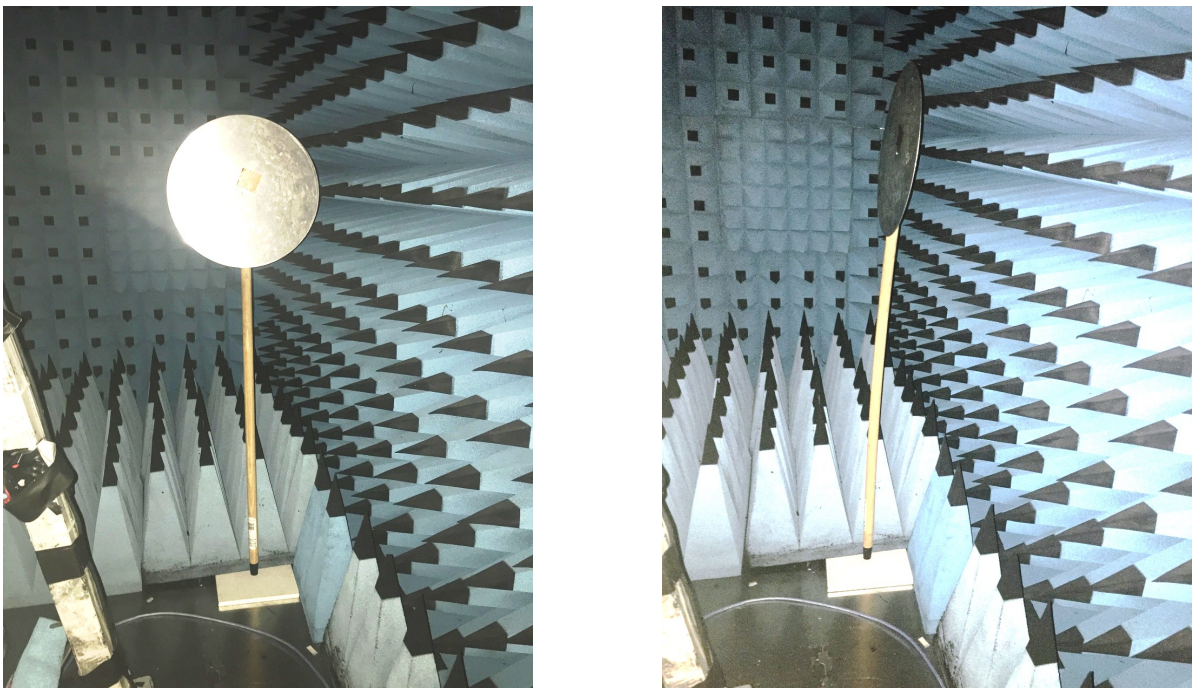

(a) circular metal sheet at 0° (b) circular metal sheet at 90°

Figure 5.9: Circular metal sheet with different angle of configuration

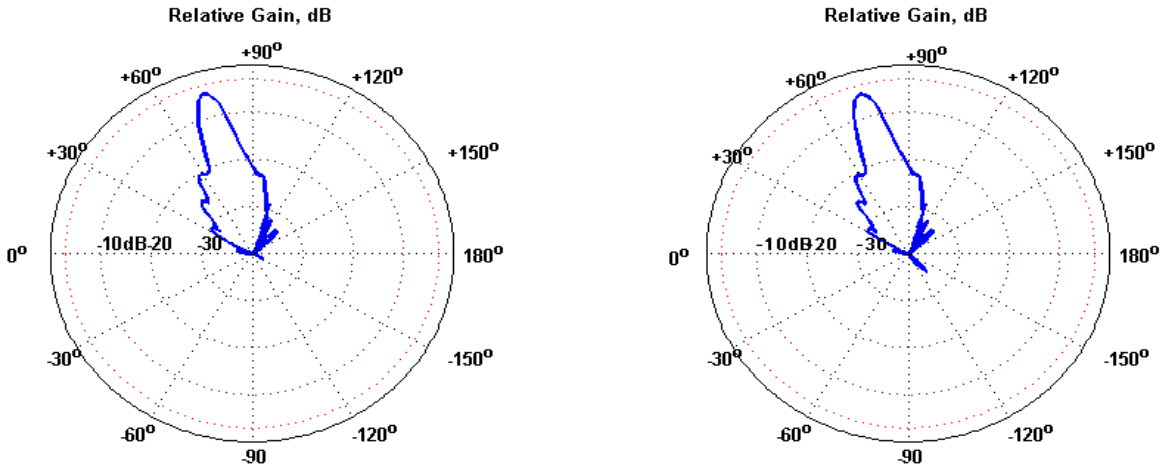

(a) circular metal sheet at 0° (b) circular metal sheet at 90°

Figure 5.10: Polar plot of circular metal sheet with different angle configuration at 22GHz

Figure 5.10 show the polar plots of the two configuration of the metal sheet. The

reflected signal of Figure 5.9(a) configuration only produced quite small reflection (-38dB) as shown in Figure 5.10(a) compared to the configuration in Figure 5.9(b) with the polar plot as shown in Figure 5.10(b) (-35dB).

The illumination angles and placement or configurations of the object in the chamber affect the reflected signal strength.

5.2.5 Outside Anechoic Chamber

The previous measurements have all had the benefit of having visibility of the transmitter and hence can use the directly LoS for signal reference. Here, the chamber doors were open and the transmitter was placed outside the chamber so there was no directly LoS signal path. In this measurement setup, there are two positions of transmitter antennas for discussion, as shown in Figure 5.11.

The anechoic chamber has two doors. One at the same horizontal line of the receiver, approximately 2.5m to the left of the receiver antenna. The "far" door is 4m away from the first door and approximately 60° from the receiver. Position A is 1m away from the door or the anechoic chamber, while position B is at the chamber door. .

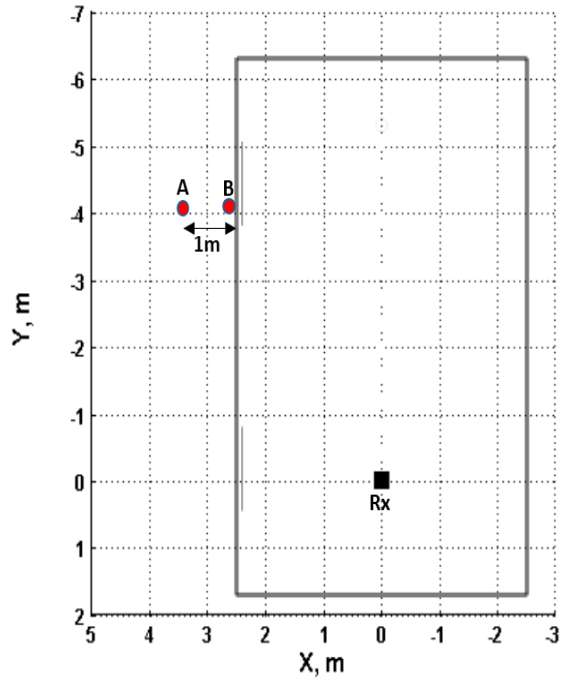

FIGURE 5.11. Dipole antenna configurations

The results indicate both configurations at position A and position B. For position A when both doors are open; there are two main peaks at approximately 25° and 60° with -5dB and -12dB reflective signal respectively. At a 60° angle, there is a direct line of sight between the transmitter and the receiver antenna, but there is an attenuation at a 25° angle because its transmitted through the chamber wall. When only the far door open, the direct line of sight signal at 60° angle is a dominant signal with -5dB.

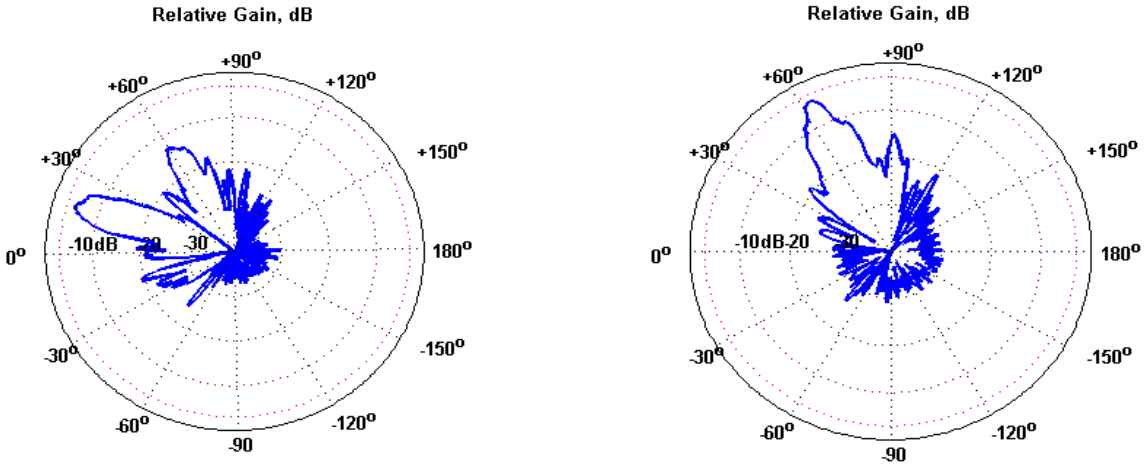

(a) A; both door open

(b) A; far door open

Figure 5.12: Dipole at position A for both configurations at 22GHz

At position B, the transmitter antenna is at the chamber door. Results in Figure 5.13 when both the doors open showing several peaks at 0°, 25°, 60° and 90°. The value of the reflected signal when only the far door opens lower than in position A.

These set of results are important in order to introduce the effect of uncontrolled environment towards the measurements of a real indoor and outdoor scenarios.

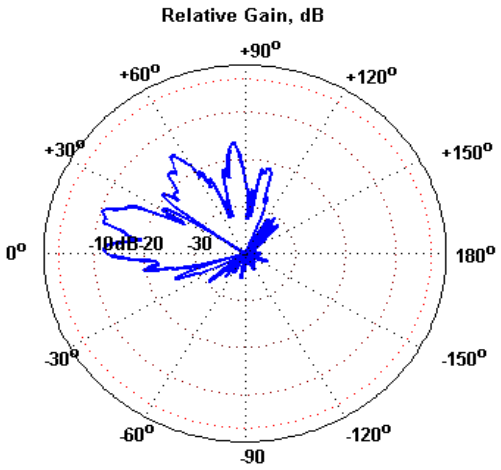

(a) B; both door open

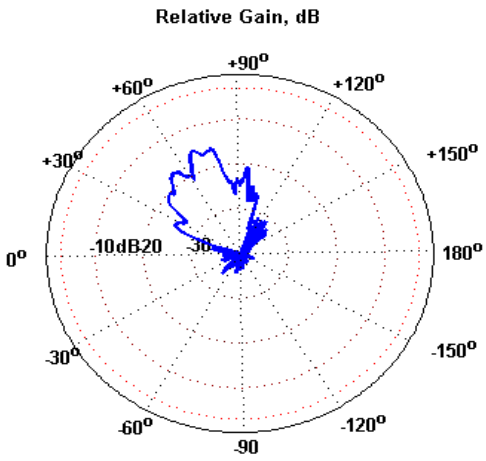

(b) B; far door open

Figure 5.13: Dipole at position B for both configurations at 22GHz

5.3 Indoor Laboratory Environment Measurements

In this section the ability to distinguish between objects (amongst the general signal clutter) and the main mechanisms for signals reaching the receiver are examined. The indoor measurement was conducted in a laboratory and adjacent office environment.

The laboratory is furnished with multiple bench and desks. Also, the room is equipped with several computers and electronic devices. The walls are typical plasterboard walls, and the suspended ceiling and floors. The floor contains metal, and above ceiling tiles are air conditioning ducts that are wrapped in aluminium foil. Hence all highly reflective materials. In addition, the adjacent office area is a common area with sofa and small kitchen appliances.

The receiver antenna was a dual polarised Flann horn antenna mounted on the positioner at the height of 1.5m. The receiver performed full azimuthal scans of all elevations for vertical and horizontal polarisation. The transmitter is a skirt dipole antenna as shown in Figure 5.2 of 22GHz. The measurements reported here are only for vertical transmit polarisation at 20GHz. Both transmit and receive antenna was connected to Anritsu 37397C vector network analyser. In all cases the amplification cabling and antennas are the same and hence and differences in signal levels must be due to differences in path loss and environment. Hence both relative levels and absolute levels (with range calibration) can be determined.

The aim for this scanning measurement is to relate the clutter identification measurement as the previous section with the actual environment. The location signal identification analysis also will relate to how the signal affected by the propagation mechanism such as reflection, diffraction and attenuation.

A layout of laboratory and adjacent office space where the measurement was conducted is shown in Figure 5.14. The fixed receiver (RX) position and six chosen transmitter (TX) locations, as well as benching in the laboratory, anechoic chamber and adjacent office space, are indicated in Table 5.6. Of interest in this study are position 4 (in the laboratory and direct lines of sight), position 5 (in the laboratory with diffraction of the wall) and position 6 (in kitchen area with no visible line of sight).

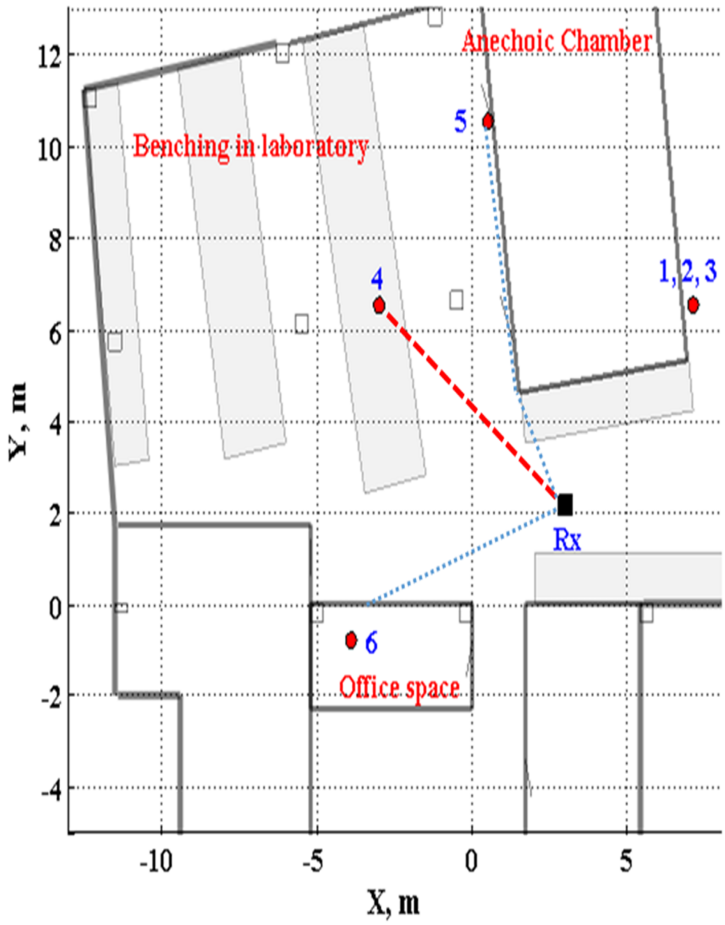

FIGURE 5.14. Layout of the laboratory and adjacent office space

Table 5.6: Measurement in the laboratory configurations

Configuration	Description
Location 1, 2 and 3	At these locations, the antenna was located at the same coordinate with different height. The coordinate for these locations is [7m 6.5m] with the height of 0.6m, 1.25m and 2.4m.
Location 4	At this location, the transmitter at at the height of 2.4m (on top of the laboratory bench). This higher up location, produce the line of sight signal and hence useful as reference.
Location 5	The transmitter is located at the "far" door of the anechoic chamber. The distance from the receiver to the transmitter is approximately 8m apart. There is a corner of the chamber wall that separated between these two. The height of the transmitter is 1.5m.
Location 6	The adjacent office space is a small room beside the laboratory area. There are two connecting doors at the end of the room, separating the transmitter and the receiver.

5.3.1 AoA Measurement Results for the Laboratory Environment

Full azimuth and elevation scan data for received vertical polarisation with respect to vertical transmit polarisation have been collected, and each set of data is normalised to the maximum received signal at each location respectively. Observation and analysis will be based on the 3D indoor laboratory plots and the respective relative power level and AoA plots.

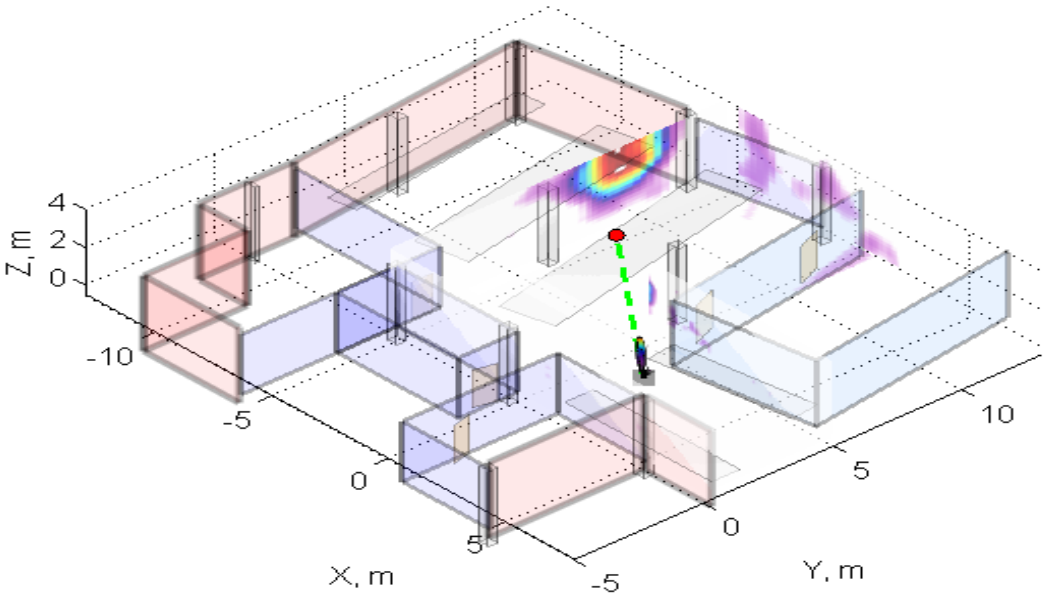

FIGURE 5.15. 3D: Location 4

Location 4: at this location, the transmitter was at the height of 2.4m above the floor with no obstruction, and therefore there is a strong signal of the line of sight (LOS). Figure 5.15 showed the 3D plot with a lot of details on projections on the screen. The 3D plot was useful because it showed where the signal came from and pointed to and how the signal related to the indoor laboratory environment. The colours represent the signal strength; red is showing the main beam while the purple is generally noise of the system. However, this 3D plot did not show the fine details of the beam.

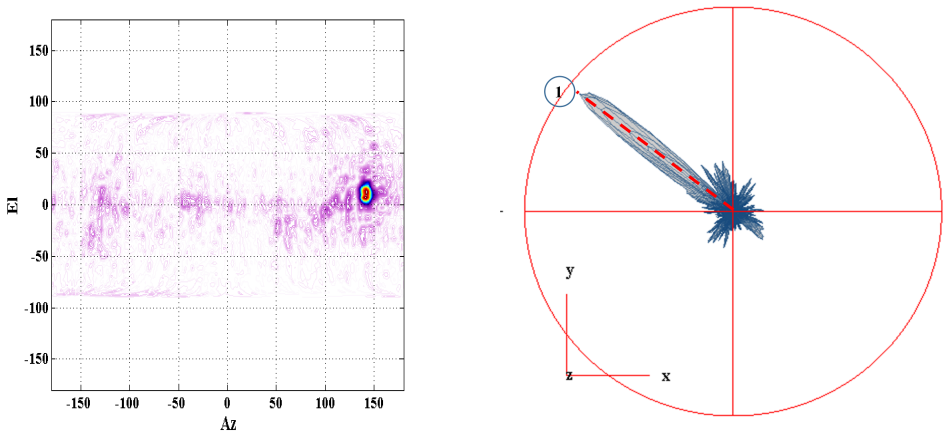

(a) relative power level (b) AoA

Figure 5.16: Location 4

Figure 5.16(a) showed a relative power level of the system. In here, a high density signal can be seen at the specific place and clutters of noise around it. Moreover, Figure 5.16(b) showed more details in AoA form for one plane. The strongest signal of the line of sight (LOS) was observed (bold red line).

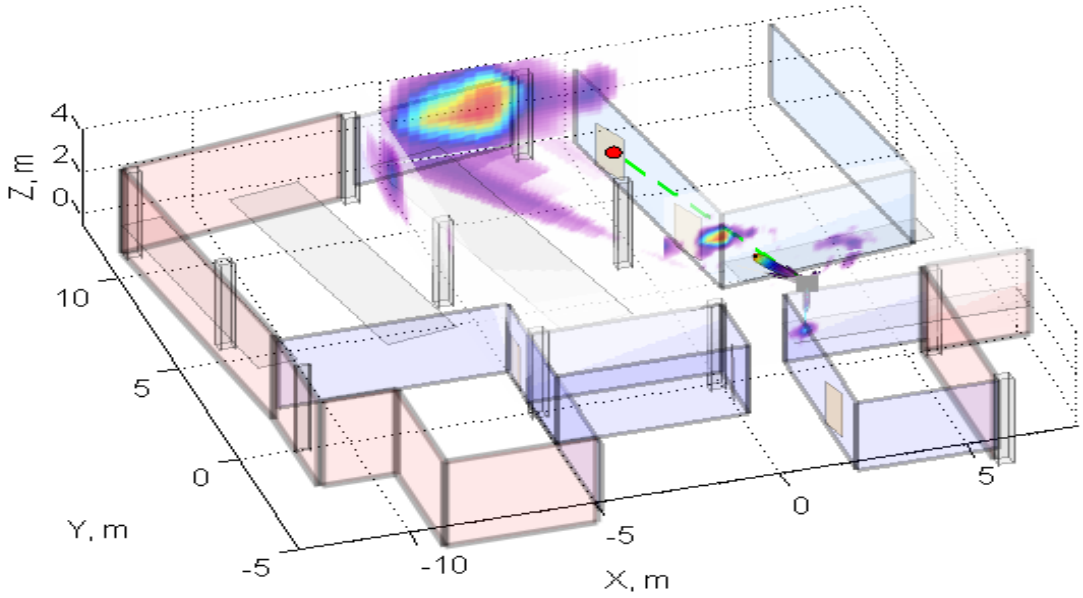

FIGURE 5.17. 3D: Location 5

Location 5: Figure 5.17 shows the 3D plot in the same indoor laboratory environment. The transmitter antenna is at the "far" door of the anechoic chamber, resulting in a diffraction effect from the edge of the chamber's wall. This can be clearly visible in the plot.

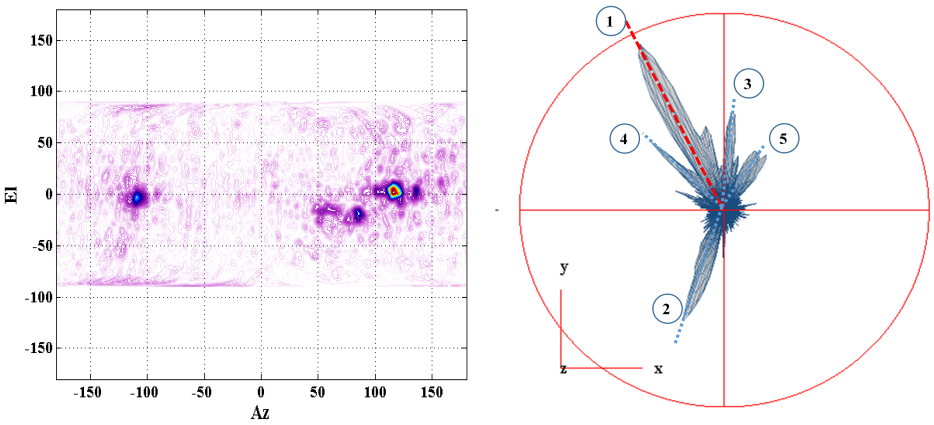

(a) relative power level (b) AoA

Figure 5.18: Location 5

The power level plot, Figure 5.18(a) also show a high density for both the radiated beam from the transmitter and at the edge of the chamber. Figure 5.18(b) shows the AoA of location 5. It is noted that there are five main peaks observed. The highest peak came from the transmitter antenna with a diffraction effect from the right-hand-side with respect to the chamber's wall. The second peak came from the metal pole that was placed at the bench near the receiver antenna. The third and fifth peaks came from the clutters from the main table near the measurement area. A few scattered signal also being observed as a table is against the anechoic chamber wall.

Location 6: For position 6, there is a signal concentrated towards the adjacent office space (wall penetration), and there are weak signals from diffraction around a door and signal that scattered around the receiver itself as shows in Figure 5.19. The higher density coming from the diffraction and attenuation also can be visible in Figure 5.20(a). The AoA in Figure 5.20(b) clearly showed the attenuation from the wall and some reflection from the ground as numbered of 1, 3 and 4. There was also a clutter in the laboratory that contributed to the signal as numbered (2).

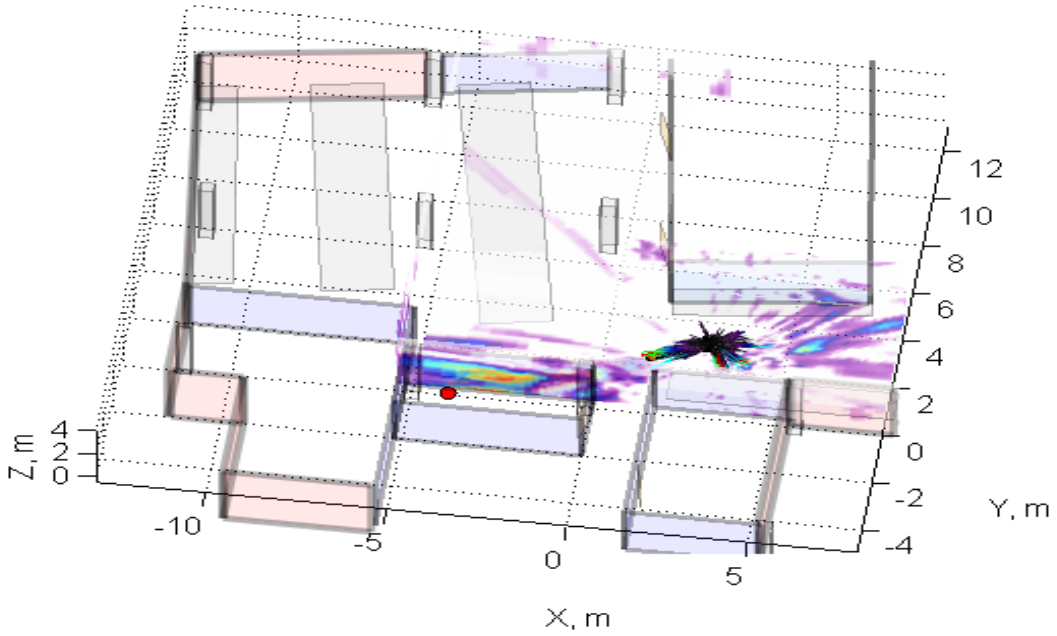

FIGURE 5.19. 3D: Location 6

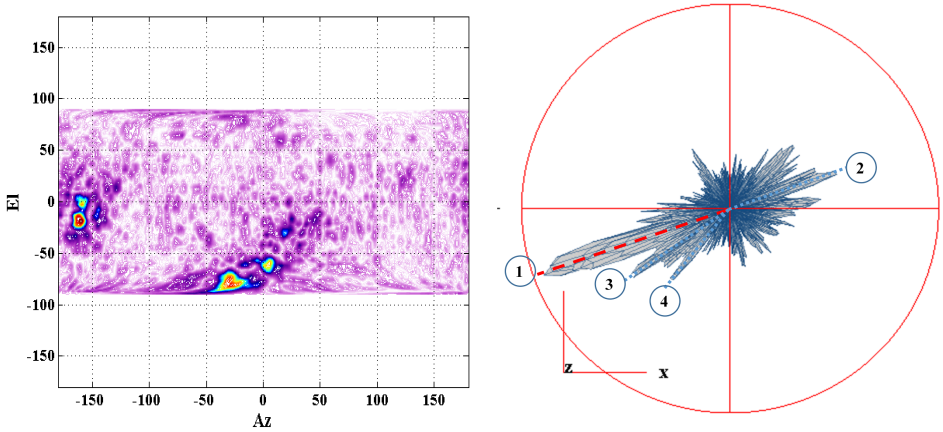

(a) relative power level (b) AoA

Figure 5.20: Location 6

Results for position 1, 2 and 3 are not presented here, however the 3D plots are available in Appendix B.

These measurement results demonstrate a strong correlation between the propagation environments and the multipath signal detected. Table 5.7 shows the summary

of the propagation mechanism involved with respect to the location assigned. Location 4 have the highest received signal since its the direct line of sight. For location 5, the received signals were mainly from duffraction and reflection, therefore the highest signal received only -5.07 dB and location 6 was the lowest received signal because of attenuation through the wall and diffraction from the laboratory door.

Table 5.7: Summary of propagation mechanism involved

Location	Propagation mechanism	Signal strength/AoA, dB
4	direct line of sight	-1.26
5	diffraction, reflection	-5.07
6	attenuation, diffraction	-5.6

5.4 Conclusion

This chapter presents investigation measurements of indoor scan for both azimuth and elevation plane. The measurements were conducted both in an anechoic chamber and indoor laboratory environment.

The first set of measurement emphasises the identification of the object in terms of the reflected signal at 22GHz. Based on the data set, the use of cylindrical poles to identify the location of the samples based on the reflected signal and for two poles whether these were able to be identified as separate reflections, even when there was an only a 0.45m gap between the two poles. There was an approximately 2dB difference of signal gain for that small gap distance. The S21 from the measurement were also compared with the theoretical value of the radar cross section, σ of materials to determine the effect of illumination towards the received reflection signal. The value σ of the metal pole was calculated at $43m^2$, whereas from measurements, the σ establish at $45m^2$; not much different because radar cross section only concentrates on how much area being seen by the antennas.

Additionally, in this chamber measurement, two types of antennas (rectangular horn and cylindrical horn antennas) were used. The circularly polarised horn antenna produced a more directive signal compared to the rectangular horn antenna. Therefore the reflected beams were narrower and distinctive. The effect of the outdoor environment also being introduced in this chapter, there was a 7dB different of two main peaks detected when the transmitter was placed outside the chamber (in front of the chamber door).

The second set of measurements were conducted in an indoor laboratory and adjacent office area. This again used the azimuth-elevation scans to identify the dominant signal based on 3 locations of interest. The operating frequency was 20GHz. The results were presented in 3D plots with respective relative power level and the AoA plots. With the 3D plots, projections on the screen showed where the signal came from and pointed to with noise from the surrounding clutter. Finer details of the propagated signal, showing the dominant and secondary signals with density and the specific place of the signal were presented using the relative power level and AoA plots. The dominant propagation path is a line of sight based on position 4 with a signal strength of -1.26dB. However, diffraction (with a signal strength of -5.07dB) also contributed to the propagation as the signal hit the edge of the chamber's wall in position 5. Attenuation through the wall also produced -5.6dB that need to be considered as one of the important propagation paths.

Further works should include more measurements on object identifications with different dimensions of materials at various locations from the actual indoor or outdoor scenario. Full azimuth and elevation scan measurements also need to be expanded with the existence of the human body and with frequent time-lapse to observe the received signal with a slight change of environment.

CHAPTER 6

CONCLUSION AND FUTURE WORKS

6.1 Thesis overview

The research presented in this thesis has considered electromagnetic propagation mechanism, mainly in K-band (18GHz to 27GHz) and millimetre wave (28GHz to 60GHz) band. More specifically this has involved the development of methodologies for the characterisation of materials in order to obtain a better understanding of the reflection, scattering, diffraction and attenuation of materials and how this knowledge may then be applied to deterministic models for EM propagation. The analysis presented has covered the calibration process and highlighting the main issue for practical measurements such as the repeatability of the measurements and the easiness of data collections. A number of materials have been considered in this study with emphasis on metal, wood, concrete and ceramic tiles - all materials commonly found in buildings.

In Chapter 2, a background review of various measurement campaign, and propagation mechanism based on the positions of a transmitter (Tx) and receiver (Rx) with respect to a material surface were presented. Based on the reviews, three main chapters were delivered by extended and modified the methodology to suit the research of this thesis. The three practical measurements cover firstly, the transmission measurement, this has been used in Chapter 3 to prove the diffraction analysis for small sample materials and extended in terms of repeatability of measurement to improve the resolution and proficiently to detect the reflection from the surface materials. Secondly, it is clear that the full characterisation of materials is extremely complex since single angles of

arrival, angles of departure, polarisation, material bulk properties, material scatter (surface) properties, material area and thickness, layers etc. that all may vary with frequency are all characteristic variables. One single method can, therefore, be applied to extract the useful information, and this has been discussed in Chapter 4 by fixed the materials and moves the antennas. Finally, the azimuth and elevation scan. The challenges in this area are how the clutters and human blockage in the environment affect the propagation mechanism. Therefore, Chapter 5 will rectify this measurement by initially conducted an object identification measurement in the controlled environment before further investigation of the propagation path in larger scenarios.

In Chapter 3, the (normal) reflection, and attenuation measurements of sample materials with a dimension of 40x40cm were conducted initially. Based on this transverse measurement it was found that it is not worth looking at attenuation until further understanding of reflection of the materials were studied. The resolution of 20mm was too coarse and this led to the development of a comprehensive model of the normal reflection of a material taking into account the transmit antenna, path between the material and antenna and the thickness of the sample, with the method of system calibration in the latter part of Chapter 3. This method undertaken the repeatable wideband measurements using an automated test set up with 2mm resolution. Measurements in this chapter have a distance limitation since the automated track is 1m long and the distance between the transmitter and receiver were also limited.

In Chapter 4 the angular spread (scatter) characteristics are examined and is an extension of the work from Chapter 3. The measurements of signal AoD from a material for every possible AoA (in both azimuth and elevation) would require very complex position control and considerable resources in time. A method has therefore been suggested that would allow a subset of this data to be acquired and possibly sufficient to process for inclusion into a deterministic model. This practical method solved the AoA and AoD problems by keeping the antennas fixed and moving the sample. Using this method, the AoA (illumination) normal to the material surface and the AoD of the 'main' signal normal to the surface add up to the 90° orientation of the two antennas. Maximum reflectivity of materials was successfully obtained by normalisation to the maximum value of metal plate. This methodology only focus on small sample materials, using a larger materials might caused some problem in fixing the material onto the rotating stand and might need a longer processing time.

While Chapter 3 and Chapter 4 have considered mounting small-scale samples for measurements and analysis, Chapter 5 has considered a method to determine material

characteristics from large samples and artefacts of the environment (walls, corners etc.). Features such as LoS, diffracted paths, reflection, scatter and attenuation through the wall have all been conserved in a number of measurements carried out in an anechoic chamber (where there is precise control of scatterers) and a laboratory environment (where there is not). The object identification in the chamber measurements was compared with RCS to investigate the relation between the received reflected signal with an area of illumination. The illumination from antennas was compared by using both the rectangular horn antenna and circularly polarised antenna, where circularly polarised horn antenna produced a more directive signal compared to the rectangular horn antenna. The investigation of dominant and secondary propagation path were also conducted for six locations in an indoor laboratory and adjacent office area. Even though this measurement yield good observation and results based on propagation paths, but the azimuth and elevation because some details might not being captured clearly.

6.2 Material Characteristic

The main findings obtained from this thesis based upon the material tested are:

- Metal (plate and cylinder): This material has been assumed to be the reference throughout the thesis because of the highest reflectivity value. In Chapter 3, measurement for wideband frequency, a metal plate of 40x40cm was used and even it is a good reflector, the 'diffraction curve' at the edge of the metal plate was still be detected (3dB difference). In Chapter 4, the larger size of 70x70cm of metal plate was used for the angular measurement in the chamber for frequency comparison (5GHz, 15GHz, 20GHz and 22GHz). This resulted in a wider beam at a lower frequency compared at a higher frequency. In the same chapter for short range measurement at 20GHz and 60GHz, metal plate sizes and shapes were compared. These size of the reflected beamwidth signal is increase with the increase of metal plate size and for the shape of the metal, not visible different observed. The metal poles were used in object identification measurement in Chapter 5. The calculated RCS, σ of this cylindrical metal poles were compared with the measurement results and produced almost identical values.

- Concrete: In the transverse measurement, comparison for diffraction gain for concrete based on the measurement results and KED have shown agreeable results at the edge/penumbra region (-6dB signal drop). The difference in surface roughness

for both sides of concrete is also noticeable. There was a 0.6dB different of M11 values. In the angular measurement, the reflectivity of concrete with respect to metal plate produce approximately 12dB different of peak values for chamber measurement but only 3dB different for a short-range measurement at 20GHz and 60GHz.

- Wood: Two different types of wood (surface different) with the same dimension have been presented in transverse measurement and produce approximately 2dB different in diffraction analysis. In Chapter 4, the reflectivity of wood compared with metal plate produced a different of approximately 19dB. In Chapter 5, wood pole reflected signal was tested in the chamber and produced the lowest reflected signal of -36dB even with the same dimension as a metal pole.

- Tiles: Ceramic tiles that have been used in all measurement in this thesis consist of four tiles (plus two strips) are pasted onto 1cm thick plasterboard. The reflective surface and grout between the tiles can be clearly observed in both transverse and angular measurements. In the transverse measurement, -5dB different with respect to the metal plate of reflectivity level was recorded. In the angular measurement, the reflectivity peak values were -7.9dB at 20GHz and only -0.9dB at 60GHz for short-range measurement. It shows that there were not much different reflectivity parameters compared to metal.

6.3 Future Works

The thesis has been concentrated on three different practical methods; transverse measurement (normal reflection), angular and indoor scan (azimuth and elevation). In this section, the limitation based on the three methods will be discussed first in order to identify future works to improve these matters. Even though the practical measurement presented in this thesis adequate for small sample materials, but there were some limitations that can be improved for better results finding.

In Chapter 3, a single dimension scan has been successfully conducted, resulted with reflection and diffraction path with the attention of distance, illumination and antenna types. However, there is a need for comprehensive measurement studies based on this consideration. The distance between the sample to the antennas and the distance travel across the sample materials need to be increased. The size of the sample and thickness with respect to the wavelength of the signal. The resolution to scan over single plane scan - ideally, 2D scan for diffraction analysis is needed to observe the effect for both sides of edges with the top and bottom of materials too.

In Chapter 4, the same parameters need to be further analysed, such as distances, size of sample, illumination and angle of incident and reflected. For AoA and AoD consideration, the development of a mathematical model that illustrated both angles and gains are essential.

In Chapter 5, azimuth and elevation scan, the polarisation of antennas only set to be vertical Tx to vertical Rx (V-V) in this measurement. Polarisation for another co-polar and cross-polar also need. Gathering more data for consistency of results also needed. In the chamber measurement, additional reflectors that rotates are beneficial to identify the angular effect.

Other future works considerations are:

- Other indoor scenarios: Measurement at various indoor environment should be conducted in order to highlight or identify other objects/clutters in that specific environment. The reflection from the ceiling particularly should be considered
- Cabling issues: this problem for connections between transmitter and receiver antenna to VNA have been resolved for the angular measurement by fixing the antennas and rotated the material under test. However, measurement at a higher frequency (60GHz) still produces a high level of cabling noise as in Chapter 4. Therefore, the used of a specific cable at higher frequency is crucial even though it will increase the cost of measurement tremendously. The usage of cable for 60GHz

is not practical. Using separate Tx n Rx and being able to synchronize the Tx oscillator and Rx isolator and phase reference data are more beneficial. Sufficient dynamic range of approximately 40dB is needed for better understanding.

- Materials: Limitation of the materials used in this thesis should be extended in terms of dimension (size), thickness and distance between the materials to the transmitter and receiver antennas. Most of the sample is 40x40cm and comparable with the wavelength of the signal. However, usage of larger sample not really produced a different in results.

  Various type of building materials (indoor and outdoor) should be used. Other building materials that need to be considered are: bricks, plasterboard, insulation materials (brick with air gap), double skinned wall, single skinned wall.

  Surface roughness of material: a systematic approach to identify the surface roughness of materials. Rougher materials such as Portland stone.

- Propagation Model: The results from the measurements in this thesis should be useful for the existing ray tracing model's parameters and to improve the channel model indirectly. Surface materials should be taken into consideration. Based on the measurement for both side of the concrete slab in Chapter 3, there is a significant value even the roughness of the surface it's not visible. Combination of the different surface in one material also important for example the set of tiles with grouting in between.

Overall, material characterisation is the first steps to achieve a close alignment between measured and theoretical channel models. The methodologies developed in this thesis for small sample materials is a practical way to determine the significant power changes in the reflected energy for varies material surface types. The angular measurement setup for instance, will take into account the varying reflective properties of different materials on a surface.

Finally, the work done in this thesis has motivated some discussion on further measurement/testing for characterising materials at higher frequency band in order to provide acceptable input parameters for deterministic channel model (ray tracing) specifically in indoor scenarios.

APPENDIX A

APPENDIX A: ANTENNA RADIATION PATTERNS

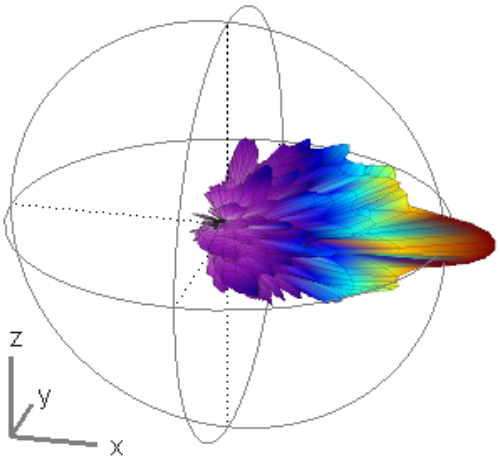

FIGURE A.1. Radiation pattern of rectangular horn antenna at 22GHz

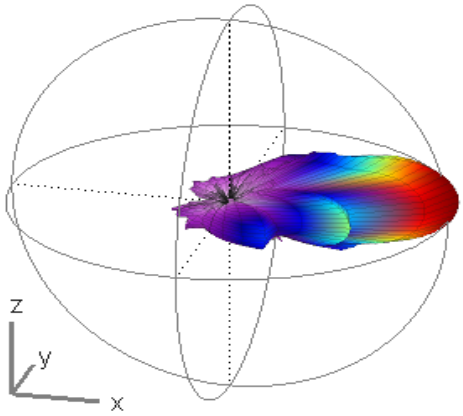

FIGURE A.2. Radiation pattern of circularly polarised antenna at 22GHz

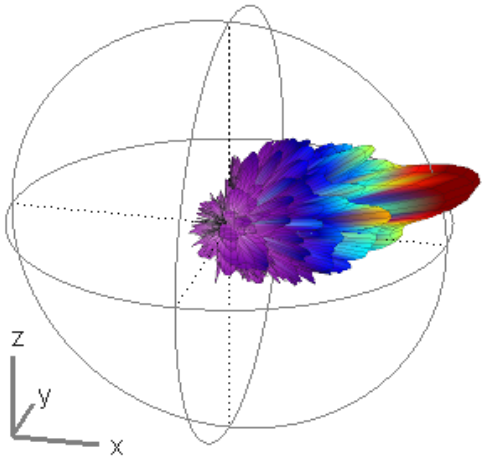

FIGURE A.3. Radiation pattern of dipole antenna at 22GHz

APPENDIX B

APPENDIX B: 3D INDOOR LABORATORY PLOTS

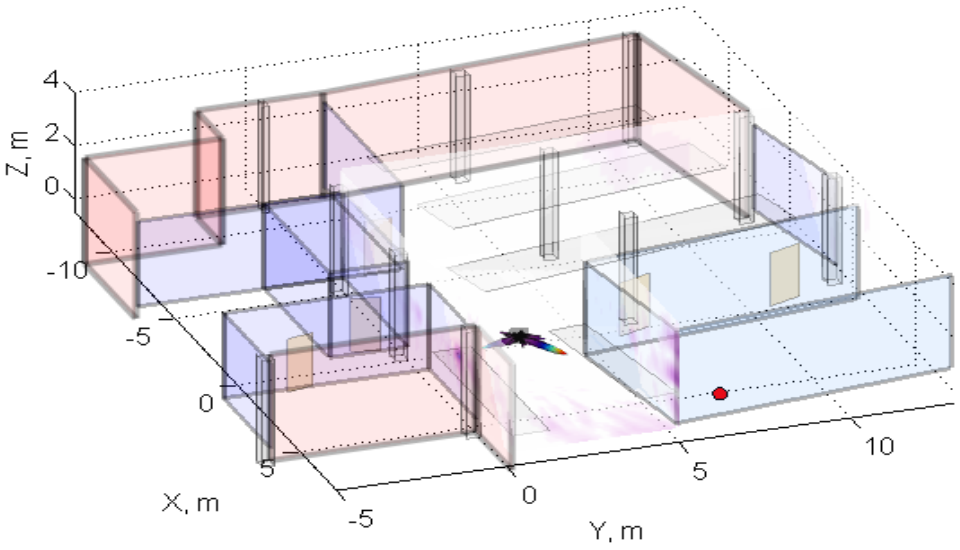

FIGURE B.1. 3D: Location 1

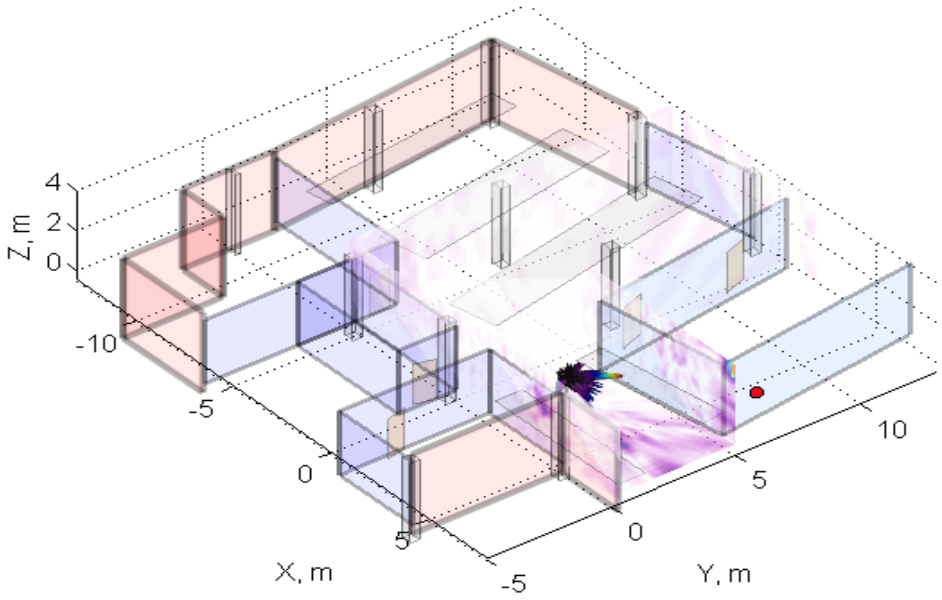

FIGURE B.2. 3D: Location 2

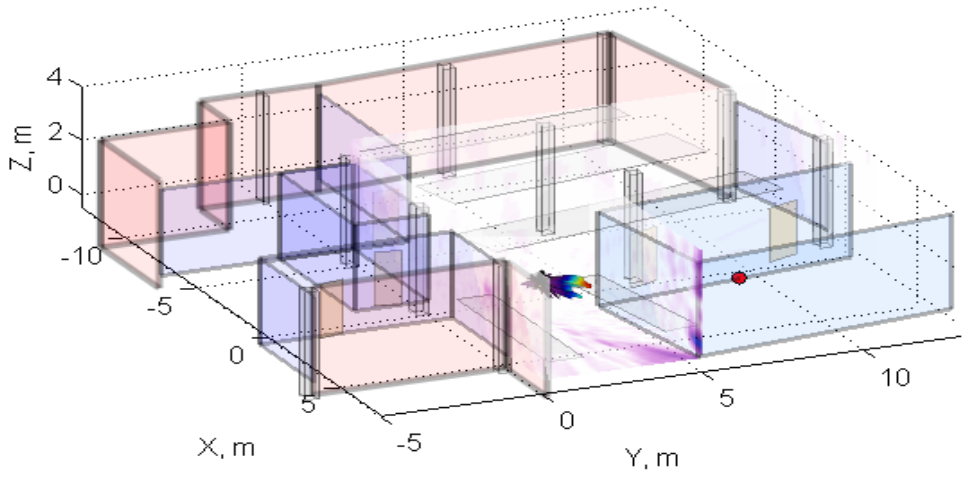

FIGURE B.3. 3D: Location 3

BIBLIOGRAPHY

[1] Z. Hang, R. Mayzus, S. Shu, M. Samimi, J. K. Schulz, Y. Azar, K. Wang, G. N. Wong, F. Gutierrez, and T. S. Rappaport, "28 GHz millimeter wave cellular communication measurements for reflection and penetration loss in and around buildings in New York city," in *Communications (ICC), 2013 IEEE International Conference on*, pp. 5163–5167.

[2] M. A. S. Miacci, E. L. A.-s. Nohara, I. A. M. Martin, G. G. Peixoto, and M. C. Rezende, "Indoor Radar Cross Section Measurements of Simple Targets," *Journal of Aerospace Technology and Management*, vol. 4, pp. 25 – 32, 03 2012.

[3] R. W. Heath, *Introduction to wireless digital communication a signal processing perspective*.
Prentice Hall, 2017.

[4] "Propagation by diffraction," 2018.
`https://www.itu.int/rec/R-REC-P.526/en`.

[5] S. Geng, J. Kivinen, X. Zhao, and P. Vainikainen, "Millimeter-wave propagation channel characterization for short-range wireless communications," *Vehicular Technology, IEEE Transactions on*, vol. 58, no. 1, pp. 3–13, 2009.

[6] I. A. Hemadeh, K. Satyanarayana, M. El-Hajjar, and L. Hanzo, "Millimeter-Wave Communications: Physical Channel Models, Design Considerations, Antenna Constructions, and Link-Budget," *IEEE Communications Surveys Tutorials*, vol. 20, pp. 870–913, Secondquarter 2018.

[7] J. W. McKown and R. L. Hamilton, "Ray tracing as a design tool for radio networks," *IEEE Network*, vol. 5, pp. 27–30, Nov 1991.

[8] P. Charriere, K. H. Craig, and A. Seville, "A ray-based, millimetre wave urban propagation tool," in *1995 Ninth International Conference on Antennas and*

Propagation, ICAP '95 (Conf. Publ. No. 407), vol. 2, pp. 258–261 vol.2, April 1995.

[9] S. Hur, S. Baek, B. Kim, Y. Chang, A. F. Molisch, T. S. Rappaport, K. Haneda, and J. Park, "Proposal on Millimeter-Wave Channel Modeling for 5G Cellular System," *IEEE Journal of Selected Topics in Signal Processing*, vol. 10, pp. 454–469, April 2016.

[10] P. Almers, E. Bonek, A. Burr, N. Czink, M. Debbah, V. Degli-Esposti, H. Hofstetter, P. Kyosti, D. Laurenson, G. Matz, and et al., "Survey of Channel and Radio Propagation Models for Wireless MIMO Systems," *EURASIP Journal on Wireless Communications and Networking*, vol. 2007, no. 1, p. 019070, 2007.

[11] J. Jurveluinen and K. Haneda, "Sixty gigahertz indoor radio wave propagation prediction method based on full scattering model," *Radio Science*, vol. 49, no. 4, pp. 293–305, 2014.

[12] S. Y. Seidel and T. S. Rappaport, "Site-specific propagation prediction for wireless in-building personal communication system design," *IEEE Transactions on Vehicular Technology*, vol. 43, pp. 879–891, Nov 1994.

[13] H. C. Nguyen, G. R. MacCartney, T. Thomas, T. S. Rappaport, B. Vejlgaard, and P. Mogensen, "Evaluation of Empirical Ray-Tracing Model for an Urban Outdoor Scenario at 73 GHz E-Band," in *2014 IEEE 80th Vehicular Technology Conference (VTC2014-Fall)*, pp. 1–6, Sep. 2014.

[14] D. Ferreira, I. Cuinas, R. F. S. Caldeirinha, and T. R. Fernandes, "A review on the electromagnetic characterisation of building materials at micro- and millimetre wave frequencies," in *The 8th European Conference on Antennas and Propagation (EuCAP 2014)*, pp. 145–149.

[15] P. Jaturatussanai, M. Chamchoy, and S. Promwong, "Characteristics of UWB propagation through building materials," in *IEEE International Symposium on Communications and Information Technology, 2005. ISCIT 2005.*, vol. 2, pp. 987–990, Oct 2005.

[16] J. W. Wallace, R. Mehmood, and M. A. Jensen, "4,Äì40 GHz Transmission Measurement of Indoor Building Materials at Normal Incidence," in *2018 IEEE International Symposium on Antennas and Propagation USNC/URSI National Radio Science Meeting*, pp. 2483–2484, July 2018.

[17] B. Langen, G. Lober, and W. Herzig, "Reflection and transmission behaviour of building materials at 60 GHz," in *Personal, Indoor and Mobile Radio Communications, 1994. Wireless Networks - Catching the Mobile Future., 5th IEEE International Symposium on*, pp. 505–509 vol.2.

[18] F. Sagnard and G. E. Zein, "In situ characterization of building materials for propagation modeling: frequency and time responses," *IEEE Transactions on Antennas and Propagation*, vol. 53, pp. 3166–3173, Oct 2005.

[19] T. S. Rappaport, G. R. MacCartney, S. Sun, H. Yan, and S. Deng, "Small-Scale, Local Area, and Transitional Millimeter Wave Propagation for 5G Communications," *IEEE Transactions on Antennas and Propagation*, vol. 65, pp. 6474–6490, Dec 2017.

[20] T. S. Rappaport, G. R. MacCartney, M. K. Samimi, and S. Sun, "Wideband millimeter-wave propagation measurements and channel models for future wireless communication system design," *IEEE Transactions on Communications*, vol. 63, pp. 3029–3056, Sep. 2015.

[21] T. S. Rappaport, Y. Xing, G. R. MacCartney, A. F. Molisch, E. Mellios, and J. Zhang, "Overview of Millimeter Wave Communications for Fifth-Generation (5G) Wireless Networks - With a Focus on Propagation Models," *IEEE Transactions on Antennas and Propagation*, vol. 65, pp. 6213–6230, Dec 2017.

[22] T. S. Rappaport, S. Sun, R. Mayzus, H. Zhao, Y. Azar, K. Wang, G. N. Wong, J. K. Schulz, M. Samimi, and F. Gutierrez, "Millimeter Wave Mobile Communications for 5G Cellular: It Will Work!," *IEEE Access*, vol. 1, pp. 335–349, 2013.

[23] N. Al-Falahy and O. Y. Alani, "Millimetre wave frequency band as a candidate spectrum for 5G network architecture: A survey," *Physical Communication*, vol. 32, pp. 120–144, 2019.

[24] J. Walfisch and H. L. Bertoni, "A theoretical model of UHF propagation in urban environments," *IEEE Transactions on Antennas and Propagation*, vol. 36, pp. 1788–1796, Dec 1988.

[25] L. M. Correia and P. O. Frances, "Estimation of materials characteristics from power measurements at 60GHz," in *5th IEEE International Symposium on Per-*

sonal, Indoor and Mobile Radio Communications, Wireless Networks - Catching the Mobile Future., pp. 510–513 vol.2.

[26] J. Lu, D. Steinbach, P. Cabrol, P. Pietraski, and R. V. Pragada, "Propagation characterization of an office building in the 60 GHz band," in *Antennas and Propagation (EuCAP), 2014 8th European Conference on*, pp. 809–813.

[27] N. Tran, T. Imai, and Y. Okumura, "Outdoor-to-indoor channel characteristics at 20 GHz," in *2016 International Symposium on Antennas and Propagation (ISAP)*, pp. 612–613.

[28] C. Larsson, F. Harrysson, B. E. Olsson, and J. E. Berg, "An outdoor-to-indoor propagation scenario at 28 GHz," in *The 8th European Conference on Antennas and Propagation (EuCAP 2014)*, pp. 3301–3304, April 2014.

[29] A. Alejos, M. Sanchez, and I. Cuinas, "Measurement and Analysis of Propagation Mechanisms at 40 GHz: Viability of Site Shielding Forced by Obstacles," *Vehicular Technology, IEEE Transactions on*, vol. 57, no. 6, pp. 3369–3380, 2008.

[30] A. V. Alejos, M. G. Sanchez, and I. Cuinas, "Improvement of material characterization in the 40GHz band," in *2006 IEEE Antennas and Propagation Society International Symposium*, pp. 3191–3194.

[31] S. Salous and Y. Gao, "Wideband measurements in indoor and outdoor environments in the 30 GHz and 60 GHz bands," in *2016 10th European Conference on Antennas and Propagation (EuCAP)*, pp. 1–3.

[32] C. A. L. Diakhate, J. M. Conrat, J. C. Cousin, and A. Sibille, "Millimeter-wave outdoor-to-indoor channel measurements at 3, 10, 17 and 60 GHz," in *2017 11th European Conference on Antennas and Propagation (EUCAP)*, pp. 1798–1802, March 2017.

[33] E. Semaan and F. Harrysson and A. Furuskar and H. Asplund, "Outdoor-to-indoor coverage in high frequency bands," in *2014 IEEE Globecom Workshops (GC Wkshps)*, pp. 393–398, Dec 2014.

[34] Y. Du, C. Cao, X. Zou, J. He, H. Yan, G. Wang, and D. Steer, "Measurement and Modeling of Penetration Loss in the Range from 2 GHz to 74 GHz," in *2016 IEEE Globecom Workshops (GC Wkshps)*, pp. 1–6.

[35] I. Rodriguez, H. C. Nguyen, N. T. K. Jorgensen, T. B. Sorensen, and P. Mogensen, "Radio Propagation into Modern Buildings: Attenuation Measurements in the Range from 800 MHz to 18 GHz," in *2014 IEEE 80th Vehicular Technology Conference (VTC2014-Fall)*, pp. 1–5, Sept 2014.

[36] M. Inomata, W. Yamada, M. Sasaki, and T. Onizawa, "Outdoor-to-indoor path loss model for 8 to 37 GHz band," in *2015 International Symposium on Antennas and Propagation (ISAP)*, pp. 1–4.

[37] I. Rodriguez, H. C. Nguyen, T. B. Sorensen, J. Elling, J. A. Holm, P. Mogensen, P. Mogensen, and B. Vejlgaard, "Analysis of 38 GHz mmWave Propagation Characteristics of Urban Scenarios," in *European Wireless 2015; 21th European Wireless Conference; Proceedings of*, pp. 1–8.

[38] M. Jacob, S. Priebe, R. Dickhoff, T. Kleine-Ostmann, T. Schrader, and T. Kurner, "Diffraction in mm and Sub-mm Wave Indoor Propagation Channels," *Microwave Theory and Techniques, IEEE Transactions on*, vol. 60, no. 3, pp. 833–844, 2012.

[39] G. A. Andreev, D. A. Korbakov, and A. V. Yudaev, "Edge diffraction of a narrow beam of millimeter waves in the shadow zone of an obstacle," *Journal of Communications Technology and Electronics*, vol. 52, no. 10, pp. 1089–1094, 2007.

[40] A. Maltsev, R. Maslennikov, A. Sevastyanov, A. Lomayev, A. Khoryaev, A. Davydov, and V. Ssorin, "Characteristics of indoor millimeter-wave channel at 60 GHz in application to perspective WLAN system," in *Proceedings of the Fourth European Conference on Antennas and Propagation*, pp. 1–5, April 2010.

[41] M. T. Martinez-Ingles, J. V. Rodriguez, J. M. Molina-Garcia-Pardo, J. Pascual-Garcia, and L. Juan-Llacer, "Experimental and Theoretical Comparison of Cylindrical Against Rectangular Obstacles in mm-Wave Multiple Diffraction," *Antennas and Propagation, IEEE Transactions on*, vol. 61, no. 10, pp. 5347–5350, 2013.

[42] M. Ghaddar, L. Talbi, G. Y. Delisle, and J. LeBel, "Deflecting-Obstacle Effects on Signal Propagation in the 60 GHz Band," *Antennas and Propagation, IEEE Transactions on*, vol. 61, no. 1, pp. 403–414, 2013.

[43] Y. L. Xingrong Li and B. Li, "The Diffraction Research of Cylindrical Block Effect Based on Indoor 45GHz Millimeter Wave Measurements," *Information*, vol. 8, no. 2, p. 50, 2017.

[44] G. R. Maccartney, T. S. Rappaport, S. Sun, and S. Deng, "Indoor Office Wideband Millimeter-Wave Propagation Measurements and Channel Models at 28 and 73 GHz for Ultra-Dense 5G Wireless Networks," *IEEE Access*, vol. 3, pp. 2388–2424, 2015.

[45] S. Deng, G. R. MacCartney, and T. S. Rappaport, "Indoor and Outdoor 5G Diffraction Measurements and Models at 10, 20, and 26 GHz," in *2016 IEEE Global Communications Conference (GLOBECOM)*, pp. 1–7, Dec 2016.

[46] P. A. Tenerelli and C. W. Bostian, "Measurements of 28 GHz diffraction loss by building corners," in *Personal, Indoor and Mobile Radio Communications, 1998. The Ninth IEEE International Symposium on*, vol. 3, pp. 1166–1169 vol.3.

[47] M. Kvicera, P. Valtr, T. Korinek, P. Pechac, M. Grabner, V. Kvicera, and A. Martellucci, "Short-term terrain diffraction measurements: Preliminary results," in *2013 7th European Conference on Antennas and Propagation (EuCAP)*, pp. 52–55, April 2013.

[48] K. W. Kim, M. D. Kim, J. J. Park, J. Lee, J. Liang, and K. C. Lee, "Diffraction Loss Model Based on 28GHz Over-Rooftop Propagation Measurements," in *2017 IEEE 86th Vehicular Technology Conference (VTC-Fall)*, pp. 1–5, Sept 2017.

[49] T. H. Barratt, E. Mellios, P. Cain, A. R. Nix, and M. A. Beach, "Measured and modelled corner diffraction at millimetre wave frequencies," in *2016 IEEE 27th Annual International Symposium on Personal, Indoor, and Mobile Radio Communications (PIMRC)*, pp. 1–5.

[50] J. S. Lu, P. Cabrol, D. Steinbach, and R. V. Pragada, "Measurement and Characterization of Various Outdoor 60 GHz Diffracted and Scattered Paths," in *MILCOM 2013 - 2013 IEEE Military Communications Conference*, pp. 1238–1243.

[51] J. S. Lu, H. L. Bertoni, and V. Degli-Esposti, "Scale Model Investigation of Mechanisms for Scattering From Office Buildings at 2 GHz," *Antennas and Propagation, IEEE Transactions on*, vol. 62, no. 12, pp. 6435–6442, 2014.

[52] L. Zhou, L. Xiao, J. Li, Z. Yang, J. Lian, and S. Zhou, "Path Loss Model Based on Cluster at 28GHz in the Office and Corridor Environments," in *2016 IEEE 84th Vehicular Technology Conference (VTC-Fall)*, pp. 1–5, Sep. 2016.

[53] M. Kim, J. Liang, Y. K. Yoon, and J. H. Kim, "28GHz path loss measurements in urban environments using wideband channel sounder," in *2015 IEEE International Symposium on Antennas and Propagation USNC/URSI National Radio Science Meeting*, pp. 1798–1799, July 2015.

[54] J. H. Kim, Y. Yoon, Y. J. Chong, and M. Kim, "28GHz Wideband Characteristics at Urban Area," in *2015 IEEE 82nd Vehicular Technology Conference (VTC2015-Fall)*, pp. 1–3, Sep. 2015.

[55] B. Guo, Y. Wu, M. Yang, and J. Li, "28GHz millimeter wave propagation models based on ray-tracing in urban scenario," in *2015 IEEE 26th Annual International Symposium on Personal, Indoor, and Mobile Radio Communications (PIMRC)*, pp. 2209–2213, Aug 2015.

[56] S. Li, Y. Liu, L. Lin, M. Wang, Z. Sheng, and D. Sun, "Millimeter-Wave Propagation Measurement and Simulation in a Indoor Office Environment at 28 GHz," in *2017 Sixth Asia-Pacific Conference on Antennas and Propagation (APCAP)*, pp. 1–3, Oct 2017.

[57] S. Kawasaki, Y. Ito, H. Iwai, S. Nakano, Y. Suegara, M. Sibayama, and M. Umehara, "Analysis of Diffraction Characteristics at 28GHz Band in a Vehicular Communication Environment," in *2018 International Symposium on Antennas and Propagation (ISAP)*, pp. 1–2, Oct 2018.

[58] J. pascual Garcia, J. Molina-Garcia-Pardo, M. Martinez-Ingles, J. Rodriguez, and N. Saurin-Serrano, "On the Importance of Diffuse Scattering Model Parameterization in Indoor Wireless Channels at mm-Wave Frequencies," *IEEE Access*, vol. 4, pp. 688–701, 2016.

[59] J. Pascual-Garcia, M. T. Martinez-Ingles, J. M. Molina-Garcia-Pardo, J. V. Rodriguez, and V. Degli-Esposti, "Experimental parameterization of a diffuse scattering model at 60 GHz," in *2015 IEEE-APS Topical Conference on Antennas and Propagation in Wireless Communications (APWC)*, pp. 734–737.

[60] E. M. Vitucci, J. Chen, V. Degli-Esposti, J. S. Lu, H. L. Bertoni, and X. Yin, "Analyzing Radio Scattering Caused by Various Building Elements Using Millimeter-Wave Scale Model Measurements and Ray Tracing," *IEEE Transactions on Antennas and Propagation*, vol. 67, pp. 665–669, Jan 2019.

[61] L. Minghini, R. D'Errico, V. Degli Esposti, and E. M. Vitucci, "Electromagnetic simulation and measurement of diffuse scattering from building walls," in *Antennas and Propagation (EuCAP), 2014 8th European Conference on*, pp. 1298–1302.

[62] J. Ahmadi-Shokouh, S. Noghanian, E. Hossain, M. Ostadrahimi, and J. Dietrich, "Reflection Coefficient Measurement for House Flooring Materials at 57-64 GHz," in *GLOBECOM 2009 - 2009 IEEE Global Telecommunications Conference*, pp. 1–6, Nov 2009.

[63] N. Tran, T. Imai, and Y. Okumura, "Measurement of indoor channel characteristics at 20 GHz band," in *2015 International Symposium on Antennas and Propagation (ISAP)*, pp. 1–4.

[64] Q. Wang, S. Li, X. Zhao, M. Wang, and S. Sun, "Wideband Millimeter-Wave Channel Characterization Based on LOS Measurements in an Open Office at 26GHz," in *2016 IEEE 83rd Vehicular Technology Conference (VTC Spring)*, pp. 1–5.

[65] X. Wu, Y. Zhang, C. X. Wang, G. Goussetis, H. M. A. e, and M. M. Alwakeel, "28 GHz indoor channel measurements and modelling in laboratory environment using directional antennas," in *2015 9th European Conference on Antennas and Propagation (EuCAP)*, pp. 1–5.

[66] M. D. Kim, J. Liang, H. K. Kwon, and J. Lee, "Directional delay spread characteristics based on indoor channel measurements at 28GHz," in *Personal, Indoor, and Mobile Radio Communications (PIMRC), 2015 IEEE 26th Annual International Symposium on*, pp. 403–407.

[67] F. Wei, I. Carton, and G. F. Pedersen, "Comparative study of centimetric and millimetric propagation channels in indoor environments," in *2016 10th European Conference on Antennas and Propagation (EuCAP)*, pp. 1–5.

[68] J. H. Kim, M. W. Jung, Y. K. Yoon, Y. J. Chong, and M. S. Song, "60 and 28GHz delay spread measurements and simulation at indoor," in *2014 International Con-*

ference on Information and Communication Technology Convergence (ICTC), pp. 148–150.

[69] J. Lee, J. Liang, J. J. Park, and M. D. Kim, "Directional path loss characteristics of large indoor environments with 28 GHz measurements," in *Personal, Indoor, and Mobile Radio Communications (PIMRC), 2015 IEEE 26th Annual International Symposium on*, pp. 2204–2208.

[70] M. Lei, J. Zhang, T. Lei, and D. Du, "28-GHz indoor channel measurements and analysis of propagation characteristics," in *2014 IEEE 25th Annual International Symposium on Personal, Indoor, and Mobile Radio Communication (PIMRC)*, pp. 208–212.

[71] G. R. MacCartney, S. Deng, and T. S. Rappaport, "Indoor Office Plan Environment and Layout-Based mmWave Path Loss Models for 28 GHz and 73 GHz," in *2016 IEEE 83rd Vehicular Technology Conference (VTC Spring)*, pp. 1–6.

[72] S. Li, Y. Liu, Z. Chen, X. Sun, and L. Lin, "Measurements and modelling of millimeter-wave channel at 28 GHz in the indoor complex environment for 5G radio systems," in *2017 9th International Conference on Wireless Communications and Signal Processing (WCSP)*, pp. 1–6, Oct 2017.

[73] S. Li, Y. Liu, X. Zhang, and X. Qi, "Measurement and simulation of 28 GHz millimeter-wave propagation characteristics in the corridor environment," in *2016 IEEE 9th UK-Europe-China Workshop on Millimetre Waves and Terahertz Technologies (UCMMT)*, pp. 134–137, Sept 2016.

[74] X. Yin, C. Ling, and M. D. Kim, "Experimental Multipath-Cluster Characteristics of 28-GHz Propagation Channel," *IEEE Access*, vol. 3, pp. 3138–3150, 2015.

[75] X. Gao, L. Tian, P. Tang, T. Jiang, B. Liu, and J. Zhang, "Channel Characteristics Analysis of Angle and Clustering in Indoor Office Environment at 28 GHz," in *2016 IEEE 84th Vehicular Technology Conference (VTC-Fall)*, pp. 1–5, Sep. 2016.

[76] Ma, Yuanyuan and Hogstad, Bjorn Olav and Patzold, Matthias and Crespo, Pedro M., "Statistical Modeling, Simulation, and Experimental Verification of Wideband Indoor Mobile Radio Channels," *Wireless Communications and Mobile Computing*, vol. 2018, pp. 1–13, 2018.

[77] M. Kim, T. Iwata, K. Umeki, J. Takada, and S. Sasaki, "Indoor channel characteristics in atrium entrance hall environment at millimeter-wave band," in *2017 11th European Conference on Antennas and Propagation (EUCAP)*, pp. 707–710, March 2017.

[78] T. Mantoro, M. A. Ayu, and M. R. Nugroho, "NLOS and LOS of the 28 GHz bands millimeter-wave in 5G cellular networks," in *2017 International Conference on Computing, Engineering, and Design (ICCED)*, pp. 1–5, Nov 2017.

[79] S. Geng, J. Kivinen, and P. Vainikainen, "Propagation characterization of wideband indoor radio channels at 60 GHz," in *2005 IEEE International Symposium on Microwave, Antenna, Propagation and EMC Technologies for Wireless Communications*, vol. 1, pp. 314–317 Vol. 1, Aug 2005.

[80] H. Sawada, H. Nakase, S. Kato, M. Umehira, K. Sato, and H. Harada, "Polarization dependence in double directional propagation channel at 60GHz," in *2009 IEEE 20th International Symposium on Personal, Indoor and Mobile Radio Communications*, pp. 3010–3014, Sept 2009.

[81] J. Jarvelainen and M. Kurkela and K. Haneda, "Impacts of Room Structure Models on the Accuracy of 60GHz Indoor Radio Propagation Prediction," *IEEE Antennas and Wireless Propagation Letters*, vol. 14, pp. 1137–1140, 2015.

[82] N. Moraitis, D. Vouyioukas, and P. Constantinou, "Indoor angular profile measurements and channel characterization at the millimeter-wave band," in *Proceedings of the 5th European Conference on Antennas and Propagation (EUCAP)*, pp. 155–159.

[83] B. Neekzad, K. Sayrafian-Pour, and J. S. Baras, "Clustering Characteristics of Millimeter Wave Indoor Channels," in *2008 IEEE Wireless Communications and Networking Conference*, pp. 1217–1222.

[84] X. Hao, V. Kukshya, and T. S. Rappaport, "Spatial and temporal characterization of 60 GHz indoor channels," in *Vehicular Technology Conference, 2000. IEEE-VTS Fall VTC 2000. 52nd*, vol. 1, pp. 6–13 vol.1.

[85] N. Moraitis and A. D. Panagopoulos, "Millimeter wave channel measurements and modeling for indoor femtocell applications," in *2015 9th European Conference on Antennas and Propagation (EuCAP)*, pp. 1–6, May 2015.

[86] S. Guerin, “Indoor wideband and narrowband propagation measurements around 60.5 GHz in an empty and furnished room,” in *Proceedings of Vehicular Technology Conference - VTC*, vol. 1, pp. 160–164 vol.1.

[87] C. DeVries, J. B. Deforge, and D. Badiere, “Predicting indoor performance of a 60 GHz WPAN,” in *2013 IEEE Radio and Wireless Symposium*, pp. 157–159.

[88] T. Manabe, Y. Miura, and T. Ihara, “Effects of antenna directivity and polarization on indoor multipath propagation characteristics at 60 GHz,” *IEEE Journal on Selected Areas in Communications*, vol. 14, pp. 441–448, April 1996.

[89] K. Haneda, J. Jarvelainen, A. Karttunen, M. Kyro, and J. Putkonen, “Indoor short-range radio propagation measurements at 60 and 70 GHz,” in *The 8th European Conference on Antennas and Propagation (EuCAP 2014)*, pp. 634–638, April 2014.

[90] O. H. Koymen, A. Partyka, S. Subramanian, and J. Li, “Indoor mm-Wave Channel Measurements: Comparative Study of 2.9 GHz and 29 GHz,” in *2015 IEEE Global Communications Conference (GLOBECOM)*, pp. 1–6.

[91] N. O. Oyie and T. J. O. Afullo, “Measurements and Analysis of Large-Scale Path Loss Model at 14 and 22 GHz in Indoor Corridor,” *IEEE Access*, vol. 6, pp. 17205–17214, 2018.

[92] S. Deng, M. K. Samimi, and T. S. Rappaport, “28 GHz and 73 GHz millimeter-wave indoor propagation measurements and path loss models,” in *2015 IEEE International Conference on Communication Workshop (ICCW)*, pp. 1244–1250.

[93] A. A. AlAbdullah, N. Ali, H. Obeidat, R. A. Abd-Alhmeed, and S. Jones, “Indoor millimetre-wave propagation channel simulations at 28, 39, 60 and 73 GHz for 5G wireless networks,” in *2017 Internet Technologies and Applications (ITA)*, pp. 235–239, Sept 2017.

[94] Al-Samman, Ahmed M. and Rahman, Tharek Abd and Azmi, Marwan Hadri, “Indoor Corridor Wideband Radio Propagation Measurements and Channel Models for 5G Millimeter Wave Wireless Communications at 19GHz, 28GHz, and 38GHz Bands,” *Wireless Communications and Mobile Computing*, vol. 2018, pp. 1–12, 2018.

[95] Al-Samman, A. M. and Rahman, T. A. and Azmi, M. H. and Hindia, M. N. and Khan, I. and Hanafi, E., "Statistical Modelling and Characterization of Experimental mm-Wave Indoor Channels for Future 5G Wireless Communication Networks," *Plos One*, vol. 11, no. 9, 2016.

[96] K. Myung-Don, L. Jinyi, L. Juyul, P. Jaejoon, and P. Bonghyuk, "Directional multipath propagation characteristics based on 28GHz outdoor channel measurements," in *2016 10th European Conference on Antennas and Propagation (EuCAP)*, pp. 1–5.

[97] J. J. Park, J. Liang, J. Lee, H. K. Kwon, M. D. Kim, and B. Park, "millimeter-wave channel model parameters for urban microcellular environment based on 28 and 38 ghz measurements," in *2016 IEEE 27th Annual International Symposium on Personal, Indoor, and Mobile Radio Communications (PIMRC)*.

[98] M. Samimi, K. Wang, Y. Azar, G. N. Wong, R. Mayzus, Z. Hang, J. K. Schulz, S. Shu, F. Gutierrez, and T. S. Rappaport, "28 GHz Angle of Arrival and Angle of Departure Analysis for Outdoor Cellular Communications Using Steerable Beam Antennas in New York City," in *Vehicular Technology Conference (VTC Spring), 2013 IEEE 77th*, pp. 1–6.

[99] A. I. Sulyman, A. T. Nassar, M. K. Samimi, G. R. Maccartney, T. S. Rappaport, and A. Alsanie, "Radio propagation path loss models for 5G cellular networks in the 28 GHZ and 38 GHZ millimeter-wave bands," *IEEE Communications Magazine*, vol. 52, no. 9, pp. 78–86, 2014.

[100] T. S. Rappaport, E. Ben-Dor, J. N. Murdock, and Y. Qiao, "38GHz and 60GHz angle-dependent propagation for cellular peer-to-peer wireless communications," in *2012 IEEE International Conference on Communications (ICC)*, pp. 4568–4573.

[101] Sana Salous and Degli Esposti, Vittorio and Franco Fuschini and Diego Dupleich and Robert Müller and Thomä, Reiner S. and Katsuyuki Haneda and Molina Garcia-Pardo, Jose-Maria and Pascual Garcia, Juan and Gaillot, Davy P. and Maziar Nekovee and Sooyoung Hur, "Millimeter-wave propagation characterization and modelling towards 5G systems," *IEEE Antennas and Propagation Magazine*, vol. 58, pp. 115–127, 12 2016.

[102] T. Rappaport, *Wireless Communications: Principles and Practice*. Upper Saddle River, NJ, USA: Prentice Hall PTR, 2nd ed., 2001.

[103] D. M. Pozar, *Microwave engineering; 3rd ed.*
Hoboken, NJ: Wiley, 2005.

[104] University of Bristol, *Communication Systems and Networks Research Group*.
`http://www.bristol.ac.uk/engineering/research/csn/facilities.html`.

[105] C. A. Balanis, *Antenna theory: analysis and design*.
Wiley-Interscience, 2005.

[106] K. B. R. Cafe, "Electronic Warfare and Radar Systems Engineering Handbook."
`http://www.rfcafe.com/references/electrical/ew-radar-handbook/ew-radar-handbook-toc.htm`.

[107] Tarig Ibrahim Osman Ahmed, Moutaman Mirghani, "Estimation of Radar Cross Sectional Area of Target using Simulation Algorithm," *International Journal of Research Studies in Electrical and Electronics Engineering 2018*, vol. 4, no. 2, 2018.

[108] C. Nguyen and J. Park, *Stepped-Frequency Radar Sensors*.
Springer International Publishing, 2016.